

DISS. ETH Nr. 20975

**Transport across lipid bilayers:
Permeation and fusion studies using microfluidic devices**

ABHANDLUNG
zur Erlangung des Titels

DOKTOR DER WISSENSCHAFTEN

der

ETH ZÜRICH

vorgelegt von

Phillip Kuhn

Dipl. Ing. Mikrosystemtechnik, Albert-Ludwigs-Universität Freiburg

geboren am 22.12.1982

aus

Deutschland

Angenommen auf Antrag von

Prof. Petra S. Dittrich

Prof. Peter J. Walde

2013



Eidgenössische Technische Hochschule Zürich
Swiss Federal Institute of Technology Zurich

Dissertation

**Transport across lipid bilayers:
Permeation and fusion studies using
microfluidic devices**

Phillip Kuhn

Author Phillip Kuhn
phillip.kuhn@org.chem.ethz.ch

Editing time September, 2009 to January, 2013

Assessors Prof. Dr. Petra S. Dittrich, D-CHAB, ETH Zurich
Prof. Dr. Peter J. Walde, D-MATL, ETH Zurich

Tutors Prof. Dr. Petra S. Dittrich, D-CHAB, ETH Zurich

Abstract

The cell membrane represents the boundary between the cytosol and the extracellular environment. It maintains the integrity of the cell by forming a barrier for most substances while it controls the transduction of information and the exchange of molecules. Microfluidic devices are under current investigation as platforms for cell membrane research because experimental conditions can be controlled much more precisely as in bulk assays. However, the integration of cell models, like liposomes, for these studies into microfluidic devices is still challenging and thereby not many devices have been used for studying the transport across lipid bilayers.

The work presented herein discusses the development and fabrication of microfluidic devices with integrated lipid membranes and their use for permeation and fusion studies. Such integration of membranes usually involves an immobilization step, therefore protocols were developed which allow the tethering of artificial liposomes inside microchannels either by tagging the liposome or by a newly developed strategy based on hydrophobic interactions with a modified surface. Three applications of such devices for membrane transport studies are discussed in this work.

First, a microfluidic platform was used to study the kinetics of drug permeation across liposome membranes. Drugs of the tetracycline family were used because these molecules form a fluorescent drug-europium complex inside the liposomes. The permeation rates of various tetracyclines were investigated and the results were compared to conventional methods. The microfluidic method was fast enough to study the permeation of unstable tetracyclines and also allowed the investigation of the influence of membrane composition on the permeation rate.

Second, in order to study the transport of molecules by membrane fusion, single cells were positioned above immobilized liposomes. Fusion was triggered by low pH, simulating the fusion of pH-sensitive liposomes with endosomal membranes. The setup was tested with fluorescent dyes and also used to deliver β -galactosidase enzymes into the cytosol of the cells.

In a third set of experiments, a similar microfluidic device was used to study viral fusion. The acid-dependent fusion of single virions on individual cells was analyzed to obtain more information about the fusion mechanism of vaccinia virus particles. The kinetics of single hemifusion events initiated by a fast low-pH trigger could be measured and revealed unexpectedly long lag phases between pH change and hemifusion.

Besides a more fundamental understanding of the permeation and fusion processes, microfluidic-based studies were shown to be suitable for screening of permeation rates and lipofection efficiency.

Keywords: microfluidics, liposomes, immobilization, permeation, fusion

Zusammenfassung

Die Zellmembran ist die Begrenzung zwischen Zytosol und der extrazellulären Umgebung. Während die Weiterleitung von Informationen und den Austausch von Molekülen kontrolliert wird, hält die Membran die Unversehrtheit der Zelle aufrecht indem sie eine Barriere für die meisten Substanzen bildet. Mikrofluidische Systeme werden momentan als Plattformen für die Zellmembranforschung untersucht, weil experimentelle Bedingungen viel präziser kontrolliert werden können, als in konventionellen Experimenten. Die Integration von Zellmodellen, wie zum Beispiel Liposomen, in mikrofluidische Systeme ist allerdings immer noch sehr anspruchsvoll und somit wurden bis jetzt nicht viele mikrofluidische Chips für Transportstudien eingesetzt. Diese Doktorarbeit diskutiert in diesem Zusammenhang die Entwicklung und die Herstellung von Mikrofluidiken, und deren Anwendung in Permeations- und Fusionsstudien. Da eine solche Integration von Membranen normalerweise mit einem Immobilisierungsschritt verbunden ist, wurden Protokolle entwickelt die es erlauben Liposomen in Mikrokanälen anzubinden. Dies wurde entweder durch eine gezielte Veränderung der Liposomen erreicht oder mit einer neuartigen Strategie die auf hydrophoben Interaktionen mit einer behandelten Oberfläche beruht. Drei Anwendungen von solchen mikrofluidischen Systemen für Transportstudien werden in dieser Arbeit vorgestellt. Als erstes wurde die mikrofluidische Plattform eingesetzt um die Kinetik der Permeation von Medikamenten über Lipidmembranen zu untersuchen. Moleküle der Tetracyclinfamilie wurden dabei benutzt, weil diese einen fluoreszierenden Komplex mit Europium formen. Die Permeationsraten verschiedener Tetracycline wurden untersucht und die Ergebnisse mit konventionellen Methoden verglichen. Die mikrofluidische Methode war schnell genug um Permeation von instabilen Tetracyclinen zu messen, und erlaubte zusätzlich die Untersuchung des Einflusses der Membranzusammensetzung auf das Permeationsverhalten. Zweitens wurden einzelne Zellen über immobilisierten Liposomen positioniert um den Transport von Molekülen durch Membranfusion zu erforschen. Die Fusion wurde durch niedrigen pH ausgelöst, was die Fusion von pH-sensitiven Liposomen im Endosom simuliert. Das System wurde mit Fluoreszenzfarbstoffen getestet und danach dazu verwendet Enzyme in das Zytosol der Zellen zu bringen. In einem dritten Experiment wurde ein ähnliches mikrofluidisches System verwendet um virale Fusion zu untersuchen. Es wurde die Protonen-abhängige Fusion von einzelnen Virionen auf individuellen Zellen analysiert um mehr Informationen über den Fusionsmechanismus von Vaccinia Virus Partikeln zu erhalten. Die Kinetik von einzelnen Hemifusionsereignissen, die durch niedrigen pH ausgelöst wurden, konnte gemessen werden und enthüllte unerwartet lange Verzögerungen zwischen der pH Änderung und der Hemifusion. Es wurde gezeigt dass Studien die auf Mikrofluidik basieren, neben einem grundsätzlichen Verständnis der Permeations- und Fusionsprozesse auch dazu verwendet werden können um Permeationsraten und Lipofektionseffizienzen zu überprüfen.

Stichwörter: Mikrofluidik, Liposom, Immobilisierung, Permeation, Fusion

Contents

1	Introduction	1
1.1	Cell membranes	1
1.1.1	Lipid bilayers	1
1.1.2	Liposomes as model systems for biological membranes	2
1.2	Transport across membranes	3
1.2.1	Permeation	3
1.2.2	Active and passive transport by proteins	6
1.2.3	Fusion of lipid bilayers	6
1.3	Microfluidics	9
1.3.1	Physics at the micro-scale	10
1.4	Microfluidic devices for cell membrane analysis	11
1.4.1	Platforms for lipid bilayer studies	13
1.4.2	Applications of microfluidic platforms for membrane analysis	17
1.4.3	Cell-based platforms	23
1.5	Scope of this thesis	24
2	Materials and Methods	27
2.1	Materials	27
2.2	Microfabrication	29
2.3	Microfluidic device fabrication	30
2.3.1	PDMS top part	30
2.3.2	Microcontact printing	31
2.3.3	Device assembly	31
2.3.4	Further surface modifications	32
2.4	Liposome formation	33
2.5	Microscopy	35
2.6	Microfluidic device operation	35
2.6.1	Pump mode	35
2.6.2	Withdrawal mode	37
3	Immobilization of liposomes, virus particles, bacteria and yeast cells in microfluidic devices	39
3.1	Introduction	39
3.2	Materials and methods	40
3.2.1	Chip fabrication	40
3.2.2	Cell culturing	41
3.2.3	Vaccinia virus preparation	41

3.2.4	Vesicle preparation	41
3.2.5	Giant unilamellar vesicle preparation	42
3.2.6	Immobilization	42
3.2.7	Imaging	42
3.3	Results and discussion	43
3.3.1	Description of the immobilization assay	43
3.3.2	Immobilization of artificial lipid vesicles	43
3.3.3	Immobilization of native vesicles	45
3.3.4	Immobilization of biological objects	47
3.3.5	Summary and outlook	47
4	Permeation of tetracyclines across lipid bilayers	51
4.1	Introduction	51
4.2	Materials and methods	53
4.2.1	Microfluidic chips with immobilized liposomes	53
4.2.2	Permeation kinetics experiments	54
4.2.3	Data acquisition	54
4.2.4	Data processing	54
4.2.5	Stopped-flow measurements	57
4.2.6	Octanol-water partitioning	57
4.3	Results	58
4.3.1	Vesicle immobilization and device operation	58
4.3.2	Quantitative structure-permeation analysis of tetracycline derivatives	60
4.3.3	Permeation rates for unstable compounds	64
4.3.4	Influence of Cholesterol on Permeation Kinetics	66
4.4	Conclusion and outlook	67
5	Delivery of enzymes into single cells by liposome fusion	69
5.1	Introduction	69
5.2	Methods	71
5.2.1	Cell lines	71
5.2.2	Microfabrication	71
5.2.3	Liposome preparation	71
5.2.4	Immobilization of liposomes and cells	72
5.2.5	Fusion of liposomes and cells	72
5.2.6	Image acquisition	72
5.3	Results and discussion	72
5.3.1	Cell and liposome immobilization	72
5.3.2	Fusion observed by dequenching	73
5.3.3	Delivery of enzymes into cells by acid induced fusion	76
5.4	Conclusion and Outlook	81
6	Acid-induced fusion of single vaccinia virus particles with immobilized cells	83
6.1	Introduction	83

6.2	Methods	85
6.2.1	Cell lines	85
6.2.2	Viruses	85
6.2.3	Microfluidic chips with pH sensors	87
6.2.4	Bulk fusion experiments	87
6.2.5	Single virus particle fusion experiment	87
6.2.6	pH-dependent fluorescence of virus particles	88
6.2.7	Image acquisition	88
6.2.8	Data analysis	88
6.3	Results	89
6.3.1	Bulk fusion experiments	89
6.3.2	Microfluidic devices to detect single particle fusion	89
6.3.3	Hemifusion and dequenching rate for individual virus particles	92
6.3.4	Acidification of EGFP-containing cores	96
6.3.5	pH-dependent EGFP fluorescence of immobilized MVs	98
6.3.6	Recovery of EGFP-A5 fluorescence after fusion	98
6.4	Discussion	102
6.5	Conclusion	103
7	Conclusions and outlook	105

Nomenclature

Abbreviations

Abbreviation	Description
ABC	ATP-binding cassette
AC	Alternating current
ASLV	Avian sarcoma leukosis virus
ATP	Adenosine triphosphate
bBSA	Biotinylated BSA
BLM	Black lipid membrane
BSA	Bovine serum albumin
cDNA	Complementary DNA
DIB	Droplet interface bilayer
DLPC	1,2-dilauroyl- <i>sn</i> -glycero-3-phosphocholine
DLS	Dynamic light scattering
DMSO	Dimethylsulfoxid
DNA	Deoxyribonucleic acid
DOPC	1,2-dioleoyl- <i>sn</i> -glycero-3-phosphocholine
DOPE	1,2-dioleoyl- <i>sn</i> -glycero-3-phosphoethanolamine
DOPG	1,2-dioleoyl- <i>sn</i> -glycero-3-phospho-(1'- <i>rac</i> -glycerol)
DPPC	1,2-dipalmitoyl- <i>sn</i> -glycero-3-phosphocholine
DSPE	1,2-dioctadecanoyl- <i>sn</i> -glycero-3-phosphoethanolamine
EDTA	Ethylenediaminetetraacetic acid
EGFP	Enhanced green fluorescent protein
ELISA	Enzyme-linked immunosorbent assay
FCS	Fluorescence correlation spectroscopy
EGFP	Enhanced green fluorescent protein
FITC	Fluorescein isothiocyanate
FRAP	Fluorescence recovery after photobleaching
GluR	Glutamate receptor
GPCR	G protein-coupled receptor
GUV	Giant unilamellar vesicle
HIV	Human immunodeficiency virus
HDMS	hexamethyldisilazane
HPLC	High-performance liquid chromatography
HPTS	8-Hydroxypyrene-1,3,6-trisulfonic acid, trisodium salt
ITO	Indium tin oxide

Abbreviation	Description
LPS	Lipopolysaccharide
LUV	Large unilamellar vesicle
MEMS	Microelectromechanical systems
MES	2-(N-morpholino)ethanesulfonic acid
MOI	Multiples of infection
MV	Mature virion
NA	Numerical aperture
NTA	Nitrilotriacetic acid
OA	Oleic acid
OD	Optical density
OmpF	Outer membrane protein F
PAMPA	Parallel artificial membrane permeability assay
PBS	Phosphate buffered saline
PDMS	Polydimethylsiloxane
PEB	Post exposure bake
PEG	Polyethylene glycol
PgP	P-glycoprotein
POPG	1-palmitoyl-2-oleoyl- <i>sn</i> -glycero-3-phospho-(1'-rac-glycerol)
R18	Octadecylrhodamine B
SLB	Supported lipid bilayer
SM	Sphingomyelin
SNARE	Soluble NSF attachment protein receptor
SPR	Surface plasmon resonance
SUV	Small unilamellar vesicle
TEM	Transmission electron microscopy
TIRF	Total internal reflection fluorescence
μ TAS	Micro total analysis systems
UV	Ultraviolet
UWL	Unstirred water layer
VACV	Vaccinia virus
VSV	Vesicular stomatitis virus
WR	Western reserve
YFP	Yellow fluorescent protein

List of Figures

1.1	Schematic of a liposome	3
1.2	Models of permeation through lipid bilayers	4
1.3	Cholesterol in lipid bilayers	5
1.4	Cholesterol in lipid bilayers	6
1.5	Membrane fusion	7
1.6	Fusion of liposomes in the endosome	8
1.7	Difference between flow in macro-and microsystems	12
1.8	Different immobilization techniques for liposomes	14
1.9	Microfluidic platforms for suspended lipid membranes	16
1.10	Microfluidic platforms for supported lipid bilayers	17
1.11	Channel and transporter studies in microfluidic devices	20
1.12	Lipid bilayer fusion studies in microfluidic devices	22
2.1	Schematic of the microfabrication of a negative resist.	30
2.2	Schematic of the fabrication of a microfluidic device from PDMS.	31
2.3	Schematic of microcontact printing.	32
2.4	Plasma bonding of microcontact printed glass and a microfluidic device.	33
2.5	Schematic of liposome preparation with thin-film rehydration.	34
2.6	Cryo-TEM image of unilamellar liposomes.	34
2.7	Schematic representation of microfluidic chip operation.	36
3.1	Schematic of the immobilization method.	44
3.2	Immobilization of artificial liposomes in a microfluidic channel	45
3.3	Immobilization of native vesicles derived from cell membranes.	46
3.4	Immobilization of different organisms.	48
3.5	Staining of yeast cell membranes.	49
4.1	Structure of tetracyclines	53
4.2	Schematic of the experimental setup	55
4.3	Illustration of the experiment for drug permeation kinetics.	56
4.4	Raw data from a permeation experiment with oxytetracycline	57
4.5	Stability of the interface over time	59
4.6	Stability of liposomes over time	60
4.7	Comparison between kinetics measured on different microfluidic chips	61
4.8	Fluorescent intensity measurements for several tetracyclines	62
4.9	Correlation of the kinetic data with lipophilicity values obtained by the octanol-buffer partition system	63
4.10	Rolitetracycline decomposes into tetracycline.	65

4.11	Comparison of the kinetic curves of tetracycline solutions at different times after sample preparation.	66
4.12	Influence of cholesterol on membrane permeability of oxytetracycline.	67
5.1	Schematics of cell-liposome trapping	74
5.2	Co-immobilization of cells and liposomes	75
5.3	Kinetics of acid-induced fusion observed with dequenching assay	77
5.4	Delivery of β -galactosidase into single U937 cells	79
5.5	Influence of lipid composition on fusion efficiency	80
6.1	Illustration of the microfluidic device used for cell-virus fusion.	86
6.2	Bulk fusion experiments.	90
6.3	Microcontact printed BSA-FITC spots as pH sensor.	91
6.4	Images from a typical microfluidic virus fusion experiment.	93
6.5	Fluorescence of cell-bound virions at physiological pH and after a pH drop.	94
6.6	R18 dequenching of single virus particles.	95
6.7	GFP recovery after fusion pore opening.	97
6.8	EGFP-A5 fluorescence in virions at acidic and neutral pH without fusion.	99
6.9	Model of acid-induced fusion VACV MV with the plasma membrane.	100
6.10	Bulk fusion experiments.	101

1 Introduction

This chapter starts with a short discussion of the most important characteristics of cell membranes and why liposomes are ideal model membranes. It is explained how the various components of cell membranes influence the permeation of molecules, and how fusion is established in nature and in model systems. After an introduction of microfluidic systems and the interesting phenomena occurring at these length scales, a special focus is made on a literature review on microfluidic systems to study lipid membranes.

1.1 Cell membranes

The cell membrane represents the boundary between the cytosol and the extracellular environment. It maintains the integrity of the cell by forming a barrier for most substances. Compartments inside the cell, like the golgi apparatus, the endoplasmatic reticulum and other organelles, are organized by membrane enclosure. The approximately 5 – 6 nm thick membranes are composed mainly of a variety of lipids and proteins. These constituents are dynamic and are therefore not fixed to a certain position. Lipids compose the main structure of the membrane and predominately provide a barrier for hydrophilic molecules, while membrane proteins or membrane-bound proteins fulfill many different highly specialized functions (transduction of signals, transport of molecules, catalysis, etc.).

1.1.1 Lipid bilayers

Lipids are hydrophobic or amphiphilic molecules. The amphiphilic lipids self-assemble spontaneously into lipid bilayers or into micelles (depending on the shape of the lipid) in an aqueous environment. Hydrophobic side-chains of lipids are sandwiched between the hydrophilic heads in these nano-structures. In the case of lipid bilayers, it is energetically unfavorable for the sheets to have edges, since this would mean that uncovered tails are in contact with the aqueous phase. Hence, sheets self-assemble into closed compartments (also called liposomes or lipid vesicles) [1]. Lipid membranes are fluidic and individual molecules can diffuse inside the bilayer in two dimensions. An exchange of lipids between the bilayers is also possible but happens only rarely (compared to normal diffusion) in a process called flip-flop movement. The fluidity of the membrane depends on its composition and the temperature. Synthetic bilayers, e.g. in liposomes, change from a fluidic state to a gel-like (crystalline) state at their phase transition temperature. This temperature depends on the length and composition of the hydrophobic side chains and is lower if they are shorter and have unsaturated bonds due to less packaging.

In the membrane of eukaryotic cells, phospholipids are the most abundant lipids. They are composed of a hydrophilic head group and two hydrophobic chains, which are usually

fatty acids. The length of the tails varies between 14 to 24 carbon atoms usually with one chain unsaturated and one chain saturated. The most common group of phospholipids are the phosphoglycerides which are glycerol derivatives. Besides this group, cell membranes are also composed of spingomyelin, cholesterol and glycolipids. Glycolipids are mainly found on the outside of the cell membrane and possess a negative charge. The influence of cholesterol on the behavior of the membrane will be described later.

The membrane of the cell predominantly receives its various characteristic properties from the myriad of membrane proteins that are associated to the lipid bilayer. Transmembrane proteins reach through the lipid bilayer with their hydrophobic parts conserved inside the hydrophobic interior and with the hydrophilic parts outside. This family of membrane proteins is probably the most interesting because they can transport ions, molecules and information across the lipid bilayer. Other membrane proteins are bound to one part of the bilayer by either insertion, covalent attachment to a lipid anchor molecule or by other interactions.

1.1.2 Liposomes as model systems for biological membranes

Liposomes, or lipid vesicles, were first described in 1965 in a seminal publication by Bangham and coworkers [2]. In this work, it was shown that liposomes formed after the addition of an aqueous solution to dried lipids and that these liposomes exhibited similar properties as cell membranes. Since this discovery, liposomes have been used extensively as models for cell membranes.

For most experiments unilamellar liposomes are preferred as the results are easier to interpret than for multilamellar liposomes where for example an analyte would need to cross several membranes in a permeation experiment. Unilamellar liposomes are categorized into three groups depending on their size: (*i*) small (less than 100 nm), (*ii*) large (between 100 nm and 1 μm) and (*iii*) giant (more than 1 μm) liposomes. They are usually abbreviated as SUVs, LUVs and GUVs. Various different preparation methods are available to produce lipid vesicles. Many of these methods still rely on the original approach from Bangham where a dried lipid film is hydrated with an aqueous solution. However, it is still very difficult to produce unilamellar and homogeneously sized liposomes with all currently available methods [1]. Liposome formulations are therefore typically a heterogeneous mixture of liposomes with a given mean diameter.

The most intriguing feature of liposomes is the possibility to tailor their properties exactly to the specified needs. Figure 1.1 shows the various different possibilities of how a liposome can be modified.

Liposomes have been used extensively for biophysical and bioanalytical studies because they are ideal model systems for biological membranes [4–6]. To give two examples, experiments based on liposomes have yielded important insights in the understanding of the underlying biophysics of membrane fusion [7] and the interaction of analytes and membranes is routinely studied with liquid chromatography with liposomes as the stationary phase [8].

Besides the use of liposomes as cell mimics they have been widely used as drug carriers [3] as they are able to transport hydrophilic substances to a given target inside the body, for example doxorubicin in cancer therapy [9]. They are also used as complexes together

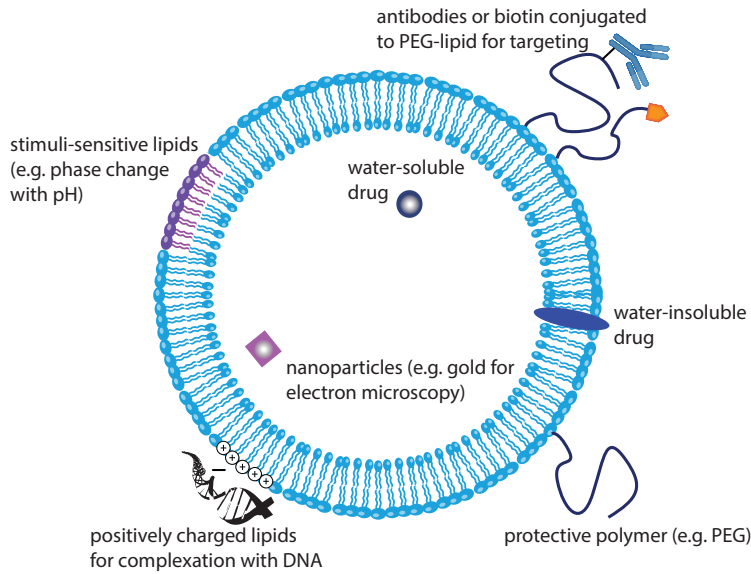


Figure 1.1: Schematic of a liposome showing some of the various possibilities to tailor the properties to a given application. (adapted from [3])

with DNA (called lipoplexes) for cell transfection, and in immunoassays and biosensors to amplify signals [5].

1.2 Transport across membranes

The lipid bilayer prevents most transport of molecules due to its hydrophobic interior. Only small and hydrophobic molecules can pass this barrier on a significant time scale. In order to exchange larger and hydrophilic molecules, the cell membrane contains proteins to mediate or drive this permeation entirely. To transport large amounts of molecules quickly, e.g. the release of neurotransmitters into the synaptic cleft, vesicles can fuse with membranes to release their content. These processes will be explained here in detail with more emphasis on passive permeation and membrane fusion as they are within scope of the experiments discussed in this thesis.

1.2.1 Permeation

Passive permeation is the primary route of absorption of most drugs in the human body, especially in the intestine [10]. Here, the biological membrane is mainly a physical (hydrophobic) barrier for permeating molecules. Hence, the rate of diffusion through a lipid bilayer depends on the charge, size and the polarity of the molecule. An uncharged, small and hydrophobic molecule like carbon dioxide can therefore quickly cross the membrane while DNA and proteins can not.

1.2.1.1 Permeation models

The classic description of permeation through a lipid bilayer assumes that the lipid leaflets can be simplified as a hydrophobic membrane with a given thickness (shown in figure 1.2 a)). By using this assumption, *Fick's* first law of diffusion can be used to derive an equation that describes the permeation of an uncharged molecule [11]:

$$Perm = \frac{D \cdot P}{h} \quad (1.1)$$

where $Perm$ [$\text{cm} \cdot \text{s}^{-1}$] is the permeation coefficient, D [$\text{cm}^2 \cdot \text{s}^{-1}$] is the diffusion coefficient of the molecule inside the membrane, P the partition coefficient of the molecule and h [cm] the thickness of the membrane. The partition coefficient is defined as the ratio of solved molecules of a compound in the hydrophobic and in the aqueous phase at equilibrium, i.e. is an indicator for the lipophilicity of a substance. For practical reasons it is usually given in logarithmic form $\log P$. From equation 1.1 it follows that a drug with high lipophilicity permeates a membrane quickly. However, most drugs are amphiphilic molecules and their permeation is better described by the *flip-flop* model (see figure 1.2 b)) [11]. In this model, drug molecules are arranged similar to lipids in the membrane. The permeation is thus a three step process, consisting of (i) a partitioning into the outer leaflet, (ii) a flip-flop movement into the inner leaflet and (iii) another partitioning from the inner leaflet into the aqueous phase. This model greatly helped to explain experimentally derived permeation kinetics that were of second or third order and not mono-exponential functions (as would be expected from the diffusion model) [11].

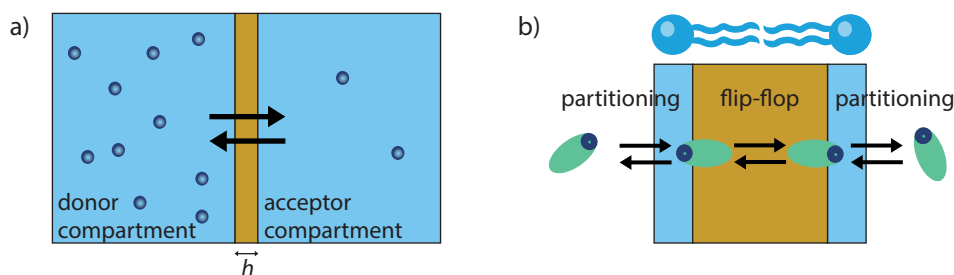


Figure 1.2: Models of permeation through lipid bilayers. a) Diffusion model. The lipid membrane is simplified as a hydrophobic membrane with a thickness h which separates two compartments from each other. b) Flip-flop model. (adapted from [11])

1.2.1.2 Influences on permeation

One of the most important indicators for the ability of the molecule to permeate a lipid bilayer is the partition coefficient $\log P$. It was already postulated more than 100 years ago by Overton that permeability correlates with the $\log P$ of a molecule. There is an optimal range for partitioning coefficients for drugs, which can not be too high, nor too low. Otherwise the drug would either not cross a membrane, as it is too hydrophilic, or would simply stay in the

membrane, as it is too lipophilic. The $\log P$ of a solute can be determined by using standard octanol-water partitioning. Besides the lipophilicity, other properties of molecules influence their permeation behavior. These are summarized in the so-called *Lipinski's rule of five* [12] and will not be discussed here. Additionally, it is also very important for the administration that the drug is soluble in the aqueous phase in concentrations needed for the therapy.

The properties of the lipid membrane also influence the permeation of drug molecules, the cholesterol content is especially important in this context. Cholesterol enhances the permeability barrier of the bilayer by filling the space between phospholipids (see figure 1.3).

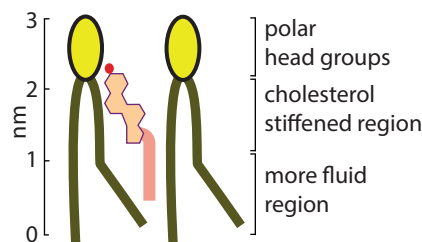


Figure 1.3: Configuration of cholesterol in a bilayer of phospholipids. (Figure adapted from [13])

1.2.1.3 Methods to measure permeation

Different methods are routinely used to measure permeation of molecules across lipid bilayers. The most prominent ones are either based on so-called black-lipid membranes or liposomes (see figure 1.4 for schematics). In the former, a lipid membrane spans over an orifice thus separating two compartments [14–16]. The advantage of this method is that both compartments are easily accessible and thus many different analysis techniques (e.g. electrodes for electrochemical detection [16]) can be used. However, due to the fragility of the membrane rigorous stirring of the solutions is not possible which leads to a state where the permeation is limited by mass transport towards the bilayer.

Therefore, liposomes have been used for permeation experiments [17]. As discussed above, liposomes can be easily prepared, are physically stable and can be modified in various ways. An obvious problem is that probes like electrodes can not be included in the aqueous interior of the vesicle. However, chemical sensors inside the liposome solve this problem. Thomae *et al.* [17] used the lanthanide terbium inside the liposome which forms a luminescent complex with aromatic carboxylic acids. Liposome suspensions and drug solutions were mixed in a stopped flow instrument to obtain a high time resolution of permeation kinetics.

Because these two methods are both not suited for high-throughput experiments, the pharmaceutical industry uses another method which is not based on a lipid membrane. Parallel artificial membrane permeation assays (PAMPA) [18] have become the gold standard in industry settings because this assay format is compatible with multiwell plates. In PAMPA, a hydrophobic filter separates two compartments (donor and acceptor). The pores inside this filter are filled with an organic solvent (in the original publication, dodecane) with solved lipids. The lipid-dodecane mixture thus simulates a lipid membrane, however, with a very

thick organic part between the lipids. PAMPA also suffers from mass transport limitations if solutions are not stirred [19].

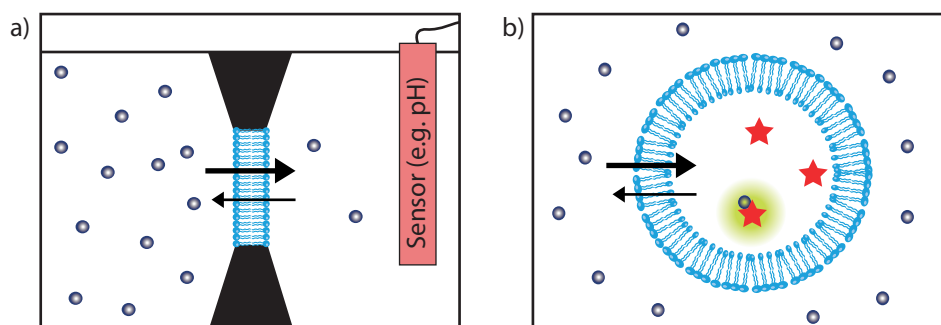


Figure 1.4: Different methods to measure permeation across lipid bilayers. a) Black lipid membrane. A lipid membrane is spanned across an aperture between two compartments. Integration of sensing elements is straightforward and pH can be measured for example to monitor the permeation of molecules. b) Liposomes. Chemical sensors are embedded inside or in the membrane and the permeation is monitored by optical means.

1.2.2 Active and passive transport by proteins

As mentioned before, all transport of hydrophilic molecules (e.g. sugars, amino acids, nucleotides) and ions is facilitated by membrane proteins. They are needed to excrete waste, regulate ion concentrations, for signaling and many other functions. They can be divided into two main classes: transporters and channels. Transporters can undergo conformational changes which facilitate the transfer of molecules to the other side. When coupled to an energy source, e.g. ATP, transporters can also move molecules against concentration gradients. Channels are openings for specific molecules. Since only passive transport is possible through channels, molecules are only transported along a concentration gradient.

1.2.3 Fusion of lipid bilayers

Membrane fusion is an ubiquitous process in nature. In the biosynthetic-secretory pathway new lipids and proteins are delivered to the plasma membrane by exocytosis (fusion of vesicles with the membrane). Intracellular transport between organelles is based on the budding and fusion of vesicles. Moreover, enveloped viruses use fusion to gain entry into the cell cytoplasm.

1.2.3.1 Prerequisites for membrane fusion

Generally, membrane fusion is defined as a merging of two membranes with a mixing of the aqueous content of the two organelles. Membrane fusion is illustrated in figure 1.5. First, fusion requires the lipid bilayers to be brought into close proximity. When they are

adjacent within 1.5 nm [7], they can join and lipids are able to diffuse from one membrane into the other. To bring lipid bilayers this close together, strong hydration forces have to be overcome, i.e. the tightly bound water needs to be removed from the polar heads of the lipids. This process is energetically very unfavorable and in consequence fusion does not occur spontaneously in biological systems.

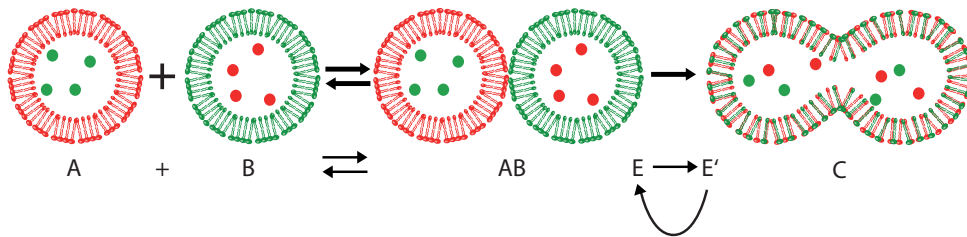


Figure 1.5: Membrane fusion. Two membrane-enclosed compartments (here liposomes A and B) bind together in a process termed 'docking' to form a complex AB. Then a trigger (usually a fusion protein E) catalyses the last reaction step yielding the fused product C. The catalyst can be recycled in some systems (e.g. SNAREs) and used again. (Figure adapted from Blumenthal *et al.* [7])

1.2.3.2 Liposomes as fusion models and carriers

Important insights into the mechanism of how chemical and physical properties of lipids influence the membrane fusion process can be obtained with liposome-based studies [20]. Polyethylene glycol (PEG) was used in many of these early works as a fusogenic agent [21] because of its ability to bind and structure water. PEG can thus remove the hydration shell from the polar lipid heads. In a typical experiment, two differently labeled liposomes are mixed together with PEG in a cuvette while monitoring changes in fluorescence of lipids [22] and/or content markers [23]. It is critical that these two mixing events are imaged separately because lipid mixing can occur without content exchange [24]. It is generally accepted today that the so-called hemifusion (only lipid mixing) always precedes content mixing in all fusion of lipid bilayers [24]. It is hypothesized that a diaphragm grows from the hemifused state. Small pores then open in this diaphragm at defects or at regions under high tension and full fusion is then initiated from these fusion pores [25].

In studies with liposomes it was found that lipid curvature plays an important role in the initiation of hemifusion. An inverted cone-shaped lipids like lysophosphatidylcholine (LPC) inhibits hemifusion [26] while lipids with the opposite curvature like phosphatidylethanolamine (PE) promote this state [27]. This fusogenic character of PE is due to the low degree of hydration of the headgroup which allows the membranes to come close together [28].

This finding is very important for the design of liposomes as pH-responsive carriers because PE can be used to create membranes under tension. pH-responsive liposomes are especially interesting as drug carriers *in vivo* [3, 29] or as a tool to introduce foreign substances into

cells *in vitro*. The concept of pH sensitive liposomes was first introduced by Yatvin *et al.* [30]. They proposed to release the cargo at tumor tissues where the pH differs slightly from physiological pH. It became clear that if certain types of liposomes can fuse under mildly acidic conditions, they could also undergo fusion inside the endosome, where the pH is lowered to pH 5, and release their cargo inside the target cell (see figure 1.6 a) [31, 32].

Liposomes could be tailored to be pH sensitive and fusogenic by incorporation of PE into the membrane as the main constituent. Besides the before mentioned low degree of hydration, PE undergoes a phase structure transition from a stable lamellar phase structure to an unstable hexagonal phase structure with a change in pH. In this hexagonal phase structure the hydrophobic part is larger and the curvature of the bilayer changes accordingly. In most cases dioleoyl phosphatidylethanolamine (DOPE) is used which has to be stabilized by another lipid to stay in the lamellar phase structure at physiological pH. The other lipid in the bilayer is usually acidic, for example DOPG [33] or oleic acid (OA) [34], which become protonated at low pH and hence lose their charge of the headgroup which reduces hydration (see figure 1.6 b)). The loss of hydration reduces the size of the headgroup and leads to the loss of the overall lamellar structure.

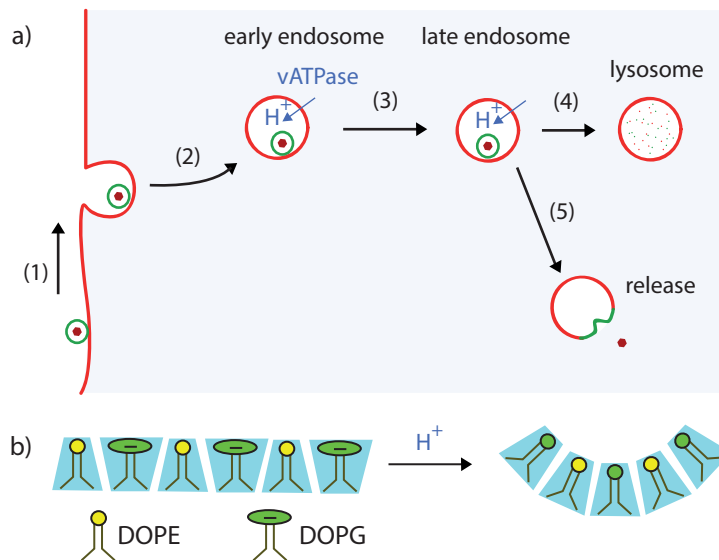


Figure 1.6: Fusion of liposomes in the endosome. a) Nanometer sized liposomes that are in the vicinity of the cell membrane (1) are taken up by the cell in vesicles by endocytosis (2). Proton pumps lower the pH inside the endosome while it is transported into the cell (3). Usually, the interior of the endosome would be digested by enzymes (4), but pH sensitive liposomes can escape the endosome by destabilizing the membrane (5), releasing the cargo into the cytosol. b) Phase transition of a DOPE/DOPG lipid bilayer after a pH drop. The lipid bilayer loses its lamellar structure due to the protonation of DOPG and becomes hexagonal. This configuration is highly fusogenic and will lead to the escape of the liposome cargo from the endosome.

1.2.3.3 Membrane fusion in nature

Fusion in nature is facilitated by highly specialized membrane proteins. In the biosynthetic-secretory pathway, SNARE proteins (soluble *N*-ethyl maleimide sensitive factor attachment protein receptors) [35] mediate the fusion of cargo vesicles with the target membrane. A coiled-coil bundle forms during the fusion process between the SNARE proteins in both bilayers. There are more than 35 different SNARE proteins, a diversity that is needed to add specificity to the fusion process. Hence, vesicles only fuse at the site where they are needed, e.g. a synaptic vesicle only fuses at the synaptic cleft. SNARE proteins have recently been investigated with microfluidic platforms [36] which will be discussed later in more detail.

In viral fusion, also a structural change of membrane proteins establishes the proximity of the membranes [37]. However, compared to SNARE mediated fusion, virus fusion is only established by proteins in the viral membrane. Fusion is usually triggered by a specific factor, e.g. the binding of HIV to CD4 receptors leads to the initiation of fusion. The mechanism of membrane fusion of influenza virus is the best understood of all viruses, mostly because of its simplicity. Influenza virus uses endocytosis to enter the cell and fuses in the endosome with the membrane initiated by a low pH trigger. The trigger leads to a conformational change that exposes a hydrophobic region of the membrane fusion protein (called fusion peptide).

Viral fusion kinetics are traditionally experimentally obtained by using self-quenched lipophilic dyes that dilute upon fusion which is followed by an increase of fluorescence [38]. Octadecyl rhodamine B (or R18) is incorporated into the viral membrane before the virus particles are bound at low temperature to the target cells (to inhibit endocytosis). Fusion is then initiated in a stopped-flow instrument with a low pH trigger (for viruses like influenza that take the endosomal route) [39].

1.3 Microfluidics

Microfluidic systems are characterized by typical sizes on the order of micrometers. The miniaturization of channel dimensions leads to the possibility to manipulate fluids much more precisely than in macrofluidic systems. This is mostly due to the phenomena of laminar flow which will be discussed later.

The concept of microfluidics originated in the 1970s when Terry *et al.* presented the first gas chromatograph based on micrometer-sized etched channels in a silicon wafer [40]. The popularity of these systems increased rapidly in the 1990s when Manz *et al.* introduced the concept of micro total analysis systems (μ TAS) [41]. They proposed that it should be possible to perform complex analytical experiments in microchannels with advantages due to scaling effects. This led to numerous publications covering many different analytical techniques. Electrophoretic separation [42], DNA amplifiers [43] and cytometers [44] are just some examples.

The early microfluidic systems were all made of silicon and glass due to the already available techniques from the MEMS industry, like etching and bonding. But due to the high costs to process these materials and the need for a cleanroom environment only few groups were able to use microfluidic systems for their experiments. This rapidly changed with the introduction of softlithography by the Whitesides group [45]. Here, a microstructure

can be replicated repeatedly with a polymer, poly(dimethylsiloxane) (PDMS). This enabled devices to be replicated from a master form cheaply in any laboratory.

Today, microfluidic systems can be found in many research areas such as material sciences [46, 47], energy generation [48], the development of point-of-care devices [49] and cell analysis [50, 51]. In the following section, the physical phenomena that are most important for the experiments in this thesis will be discussed. After this discussion, microfluidic systems for lipid membrane research are reviewed.

1.3.1 Physics at the micro-scale

When channels are downscaled to micrometer size, interesting and unexpected phenomena occur compared to those in the macro-world. Surface effects become very important because of the high surface-to-volume ratios, flows are laminar not turbulent, and gravitation has negligible effect [52].

1.3.1.1 Fluid flow

Fluid flows are described in macro-and in microsystems with the Navier-Stokes equation:

$$\rho \left[\frac{\partial \mathbf{v}}{\partial t} + \mathbf{v} \cdot \nabla \mathbf{v} \right] = \mathbf{f}_{pressure} + \mathbf{f}_{friction} + \mathbf{f}_{volume} \quad (1.2)$$

where ρ is the density, v the velocity of the fluid, t the time and f the force acting on the fluid. The left-hand side of equation 1.2, with the inertial related terms, describes the change in momentum of the fluid. This could be a change in velocity or an acceleration of the fluid (e.g. due to a flow constriction). The right-hand side takes the forces acting on the fluid into account. $f_{pressure}$ describes a force acting on the fluid due to a pressure gradient and can be written as:

$$\mathbf{f}_{pressure} = -\nabla p \quad (1.3)$$

The volume force f_{volume} is the sum of centrifugal, gravitational and electrostatic forces:

$$\mathbf{f}_{volume} = \mathbf{f}_{volume,\omega} + \mathbf{f}_{volume,g} + \mathbf{f}_{volume,q} = \rho\omega^2\mathbf{r} + \rho\mathbf{g} + \rho_q(\mathbf{x})\mathbf{E}(\mathbf{x}) \quad (1.4)$$

with the rotational speed ω , the radius r , the gravitational field strength g , the charge density ρ_q and the electric field $E(x)$. The gravitation force is very small and can therefore be neglected. Hence, the volume force is zero in microfluidic systems where no centrifugal or electrostatic forces are present.

The friction force $f_{friction}$ can be written as

$$\mathbf{f}_{friction} = \eta\nabla^2\mathbf{v} \quad (1.5)$$

with η being the viscosity of the fluid. The motion of the fluid is changed by friction.

Without gravitational forces, the assumption that there is no convection at the micro-scale and in a system with stationary flow (the flow does not change over time at one point in the channel), the complex Navier-Stokes equation becomes simplified to:

$$\nabla p = \eta \nabla^2 \mathbf{v} \quad (1.6)$$

This equation shows that driving pressure and friction are balanced in a laminar, stationary flow.

1.3.1.2 Reynolds number

The Reynolds number is an important dimensionless number in fluid mechanics and describes whether a fluid is influenced more by viscous or by inertial forces. It can be written as:

$$\text{Re} = \frac{\rho l v}{\eta} \quad (1.7)$$

with the length scale l and the velocity v . When the Reynolds number is low, which is always the case in microfluidic systems, viscous forces are stronger than inertial forces. This leads to the absence of turbulences in microchannels. Figure 1.7 illustrates the differences between turbulent flow in macrosystems and laminar flow in microsystems. The critical Reynolds number where turbulences start to occur is between 2000 and 3000 [52]. In microfluidic channels, Reynolds numbers are usually lower than 10, so no turbulence is expected.

1.3.1.3 Diffusion

Due to the low Reynolds numbers and therefore the absence of turbulence in microfluidic channels, diffusion is the main transport mechanism to mix fluids. The characteristic diffusion time can be written as

$$t_D = \frac{l_D^2}{2D} \quad (1.8)$$

with l_D being the diffusion distance and D the diffusion coefficient. Because of the small length scales in microchannels, the diffusion time t_D is short compared to larger volumes. However, for larger biomolecules, like DNA or proteins, it still takes minutes to cross a distance of 100 μm .

1.4 Microfluidic devices for cell membrane analysis

As discussed before, the cell membrane controls all transduction of information and exchange of molecules between the cytosol and the environment. Hence, it is not surprising that more than half of all drug targets are membrane proteins [53]. Additionally, every drug molecule needs to cross several lipid bilayers to reach its target which makes its permeation and transport behavior very important. For these reasons, research on cell membranes is highly significant for the pharmaceutical industry.

Due to the relatively low sample volumes of newly synthesized drug molecules and the need to perform high-throughput screening in a parallel format, microfluidic devices are under current investigation as platforms for cell membrane research [54]. The use of microfluidic devices and thereby the down-scaling of experiments has lead to less sample consumption

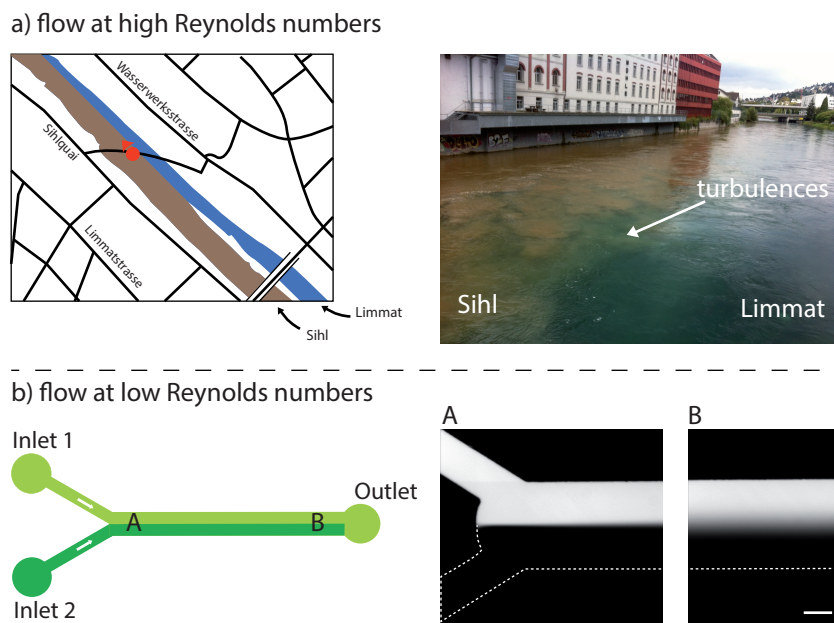


Figure 1.7: Difference between flow in macro- and microsystems. a) The merging of the two rivers Limmat and Sihl in Zurich. The Sihl has a brownish color due to rainfall, the Limmat is clean because it originates from Lake Zurich. The picture on the left was taken a few meters after the rivers met (see also map on the right where the red dot indicated where the image was taken). At the interface of both flows, turbulences are clearly visible. Both fluids mix much faster due to the turbulences. b) In a microfluidic system no turbulences occur. Flows are strictly laminar and fluids can only mix by diffusion. The right pictures show two fluids co-flowing through a channel which is $70\ \mu\text{m}$ high and $300\ \mu\text{m}$ wide. The interface between the two flows becomes less distinct $3.5\ \text{cm}$ downstream due to diffusion (B). Scale bar $100\ \mu\text{m}$.

due to the small dimensions. Fluids can be controlled much more precisely compared to bulk assays. Laminar flows allow precise chemical environments and control over shear forces. Especially when mass-transport limitations would occur due to concentration gradients in bulk systems, a constant fluid supply in microchannels leads to a simplification of experiments.

In the following, microfluidic devices will be discussed that have been used to study characteristics of cell membranes or artificial lipid bilayers. First, the methods to handle lipid bilayers inside microfluidic devices will be elaborated. Afterwards, applications in membrane research will be discussed.

1.4.1 Platforms for lipid bilayer studies

Microfluidic platforms for lipid membrane studies can be divided into four categories: (*i*) liposome-based, (*ii*) suspended lipid bilayers (also called black lipid membranes), (*iii*) supported lipid bilayers and (*iv*) whole cell experiments. The first three platforms types make use of artificial bilayers to test membrane properties and are discussed in the following. A separate section will discuss whole cell experiments in the end of this chapter.

Liposome-based systems are best for membrane protein integration as the available techniques all rely on a transfer of the membrane protein into a liposome. However, liposomes lack the possibility to access the interior with most analytical techniques. Therefore, black-lipid membranes (BLM) can be used where both sides of the membrane are accessible for measurements and solution exchange. The membrane often lacks stability and microfluidic devices have been developed to enhance the durability of the membrane. Supported lipid bilayers (SLBs) are on the other hand much more stable, easy to produce and compatible with surface-based detection techniques. The disadvantage is that they are not mimicking the naturally occurring membrane as closely as the BLMs, which means that proteins might behave differently than in their natural environment, and only one side of the membrane is accessible.

1.4.1.1 Liposome-based platforms

Liposomes in microfluidic devices are usually immobilized on a solid support [55, 56]. This is due to the possibility of arraying liposomes for high-throughput experiments and the option to use surface-sensitive techniques for detection. The combination with microfluidics enables fast solution exchange for kinetic studies and reduction in sample volume.

Many different methods to tether liposomes to solid supports have been developed in the last decade, some of them also in combination with microfluidic channels. The most important immobilization techniques are shown in figure 1.8. Biotin and streptavidin as linkers between surface and vesicle were first used by Stamou *et al.* [57] for single vesicle studies. Because it is not possible to array different vesicles at desired locations with this techniques, other groups used DNA-labeled vesicles that can bind to immobilized complementary strands [58, 59]. The use of histidine-tags in vesicle membranes enabled the immobilization on surfaces with nitriloacetic acid (NTA) in the presence of Ni^{2+} [60], with the advantage that the binding is reversible when Ni^{2+} is complexed by EDTA.

Furthermore, vesicles were also immobilized in microwells in an impressively large array [61] which is potentially ready to be integrated with glass fiber optics for individual detection

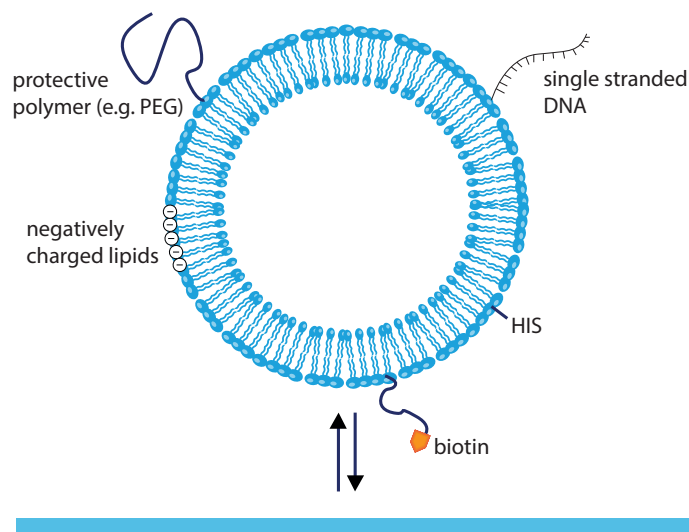


Figure 1.8: Immobilization techniques for liposomes. Lipid vesicles can be tethered to the surface via interactions of biotin-streptavidin, DNA/cDNA and histidine/NTA. Charged lipids or polymers like PEG are often used to repel the liposome from the surface if it is not immobilized and thus reduce unspecific binding. Figure reproduced from [55].

of each vesicle. Other approaches to pattern liposomes on surfaces include the use of micro-contact printing to pattern the linker molecule on the surface [57] and the use of laminar flows in microchannels to pattern different types of liposomes next to each other [62].

Only few examples have been reported where liposomes are not tethered to the surface in the channel. For example, Tan *et al.* presented a microfluidic chip to study weak protein interactions of claudin-2 in vesicles [63]. The travel distance of vesicles in a microchannel was measured between two electrodes and could be correlated to the dispersion of the vesicles and hence the interaction between claudin-2 proteins in vesicle membranes.

1.4.1.2 Suspended lipid membranes

Suspended lipid bilayers, or black lipid membranes, were first used by Mueller *et al.* in the 1960s [64]. In their original experiment, a lipid mixture was painted on a teflon orifice between two buffer-containing reservoirs. Since then, this setup has been widely used for many different transport studies over lipid membranes. However, the setup lacks structural stability and the membrane is usually only stable for hours [65], which prevents long and repetitive experiments with the same membrane and also hinders commercialization. Microfluidic technology has greatly helped to increase the stability and integration of BLMs in the last years [54], especially to study transport with membrane proteins.

The first report of a suspended lipid bilayer in a microfluidic chip was from Takeuchi and coworkers in 2004 [66]. The membrane spanned an aperture of 100 – 200 μm between two

channels with integrated electrodes. The same group showed later that this setup can be used to study individual ion channels [67] and others showed the possibility to fabricate arrays of bilayers with individual electrical read-out [68]. Membrane proteins and ion channels can either be integrated into the bilayer by self assembly from solution (only possible for some channels like gramicidin and α -hemolysin) or by fusion of proteoliposomes with the bilayer [69].

More recently, the aperture size was dramatically decreased by using nanofabrication techniques. Han *et al.* prepared lipid bilayers on nanopore chips which were fabricated in silicon/siliconnitride [70]. They could show that the reduction in size increased the durability of the membrane significantly up to several days. Kawano *et al.* advanced the system to use nanometer-sized pores in combination with microfluidics when they changed the material to parylene [71]. Because silicon materials suffer from electrical noise due to leakage currents, parylene and its high level of isolation is advantageous. In this work, which is illustrated in figure 1.9 a), several milestones for BLM integration into microfluidic devices were accomplished. First, a low-cost fabrication technique was presented, second, the stability of the membrane was several days and third, solution exchange was possible without rupture of the membrane. In a follow-up work, the same group reported that the device can be upscaled to an array of pores for small molecule detection [72].

Another approach to create BLMs inside microfluidics is based on the contact of lipid monolayers at the interface of water and organic phases. Again, the Takeuchi group pioneered this technique by creating bilayers that were permeable for ions when gramicidin was added (see figure 1.9 b)). Stanley *et al.* showed that droplet interface bilayers (DIBs) can be made in high-throughput by storing droplets in a capillary adjacent to each other [75]. Bilayer formation was successfully proved with a fluorescein permeation assay.

Another creative approach to form a BLM inside a channel was based on solvent extraction and presented by Malmstadt *et al.* [74] (shown in figure 1.9 c)). It is also possible to seal micrometer- and nanometer-sized compartments in microfluidic channels and thus create black lipid membranes [76]. Hook and co-workers showed that a supported lipid bilayer (which will be explained later in more detail) can be driven by shear flow over the surface of a channel to seal submicrometer-sized wells.

1.4.1.3 Supported lipid bilayers

Supported lipid bilayers (SLBs) are fixed on a solid support for more stability of the membrane. Many different methods to create SLBs were developed since they were first reported by Tamm *et al.* in the 1980s [77] and they have been reviewed in the literature [65, 78–80]. Here, only the method is described which is most compatible with microfluidic devices. For this, small unilamellar vesicles are prepared in the desired lipid composition and they are added into the channel of the device. It should be noted that this preparation method has some limitations in lipids and cholesterol content that can be used [81]. If surfaces are properly cleaned, vesicles adhere to the glass and fuse creating a bilayer on the glass (see figure 1.10 a)). Without spacers between the glass and the lipid bilayer, a 1 – 2 nm water layer fills the gap and facilitates the free movement of lipids in the bilayer. However, as illustrated in figure 1.10 b), membrane proteins protrude more than this distance from the bilayer. Hence, these proteins might be limited in free diffusion or even denature. Polymer-supported mem-

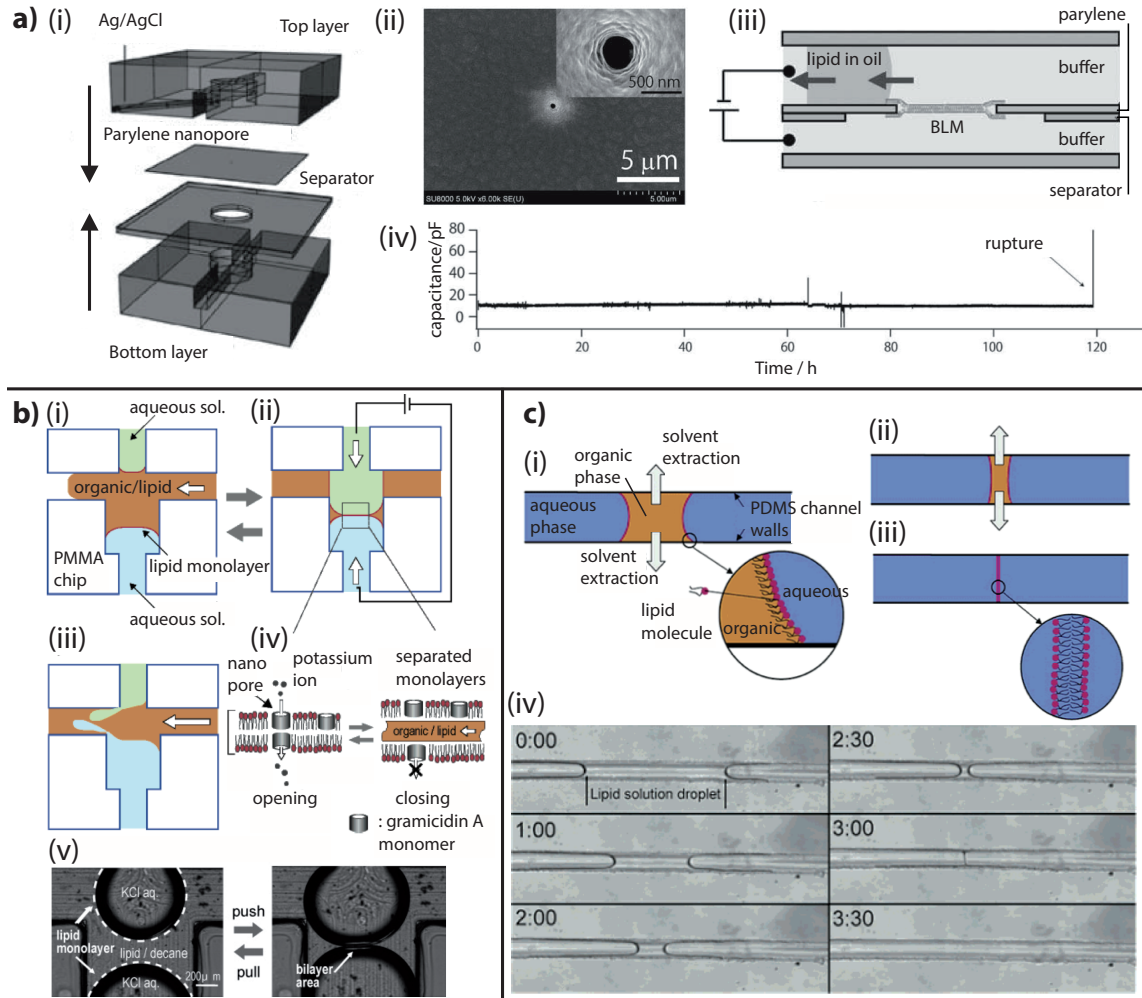


Figure 1.9: Microfluidic platforms for suspended lipid membranes. a) Platform presented by Kawano *et al.* [71]. (i) Illustration of the device assembly. Two fluidic layers are connected by a 400 nm pore in parylene (ii). (iii) The lipid bilayer is created by a moving oil droplet with solvated lipids. (iv) Capacitance of the membrane over time. The membrane was stable for almost 120 h. b) Droplet interface bilayer chip from Funakoshi *et al.* [73]. Illustration of the formation process. (i) Two aqueous solutions are injected into the top and bottom channels and are separated by an organic phase containing the lipids. (ii) By pressurizing the aqueous inlets, the interfaces are connected and a bilayer is formed. (iii) The bilayer can be opened again by flushing with organic phase. (iv) Illustration of the assay that was used to test for bilayer presence. Gramicidin can only transport potassium ions when the bilayer is intact and oil-free. (v) Images from the formation of the bilayer. c) Automated bilayer formation from Malmstadt *et al.* [74]. (i-ii) The mechanism of the BLM formation relies on the evaporation of solvent through PDMS. (iii) After all solvent is evaporated, a BLM forms inside the channel. (iv) Microscopic images of the formation process. The bilayer forms within 3.30 min inside the 100 μm wide channel.

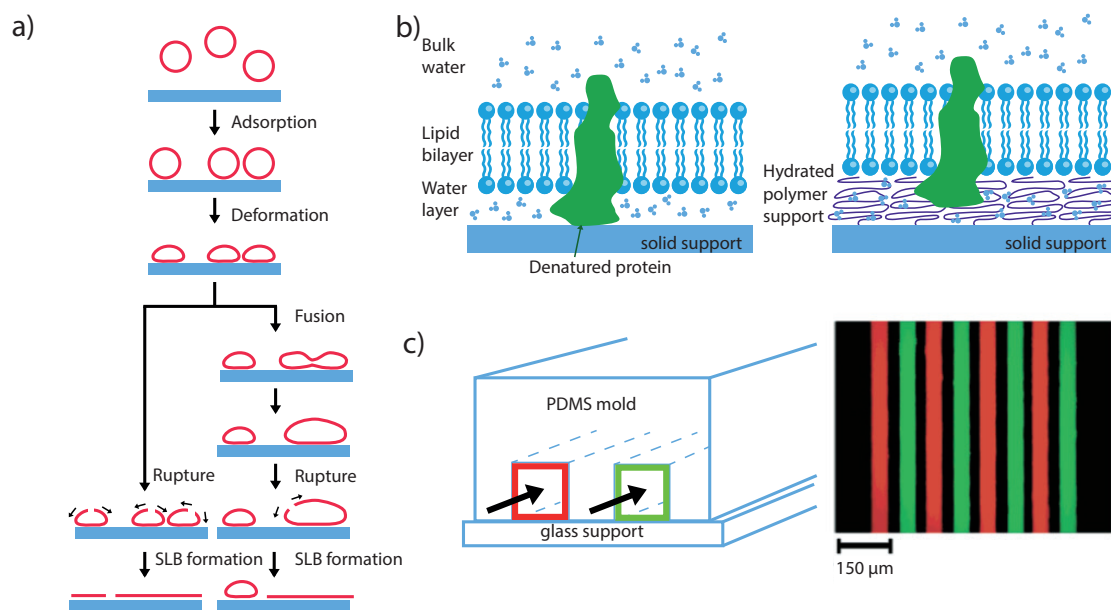


Figure 1.10: Microfluidic platforms for supported lipid bilayers. a) Illustration of the possible formation processes of SLBs on surfaces in microfluidic devices after vesicles were added. Reproduced from [86]. b) Cartoon of SLB with integrated membrane protein without (left) and with (right) polymer support. The polymer support increases the space for the protein. Reproduced from [78]. c) First report of SLB in microfluidic channel. Left: Parallel channels were coated with SLBs. Right: simultaneous detection of the different channels was possible (here illustrated with lipid-dyes). Images from [85].

branes were developed to solve this problem and to increase the gap distance between the support and the bilayer [82].

Groves *et al.* were the first to pattern SLBs in so-called corrals [83]. Corrals were created by fabrication of borders of gold and resist by photolithography. Lipid bilayers were found not to be able to cross these borders and remained restricted in their corral. Later, it was shown that these borders can also be created by microcontact printing of proteins like fibronectin in microfluidic channels [84]. However, microfluidics was first used in combination with SLBs by Yang *et al.* for on-chip immunoassays [85]. Many parallel channels were coated with lipid bilayers which enabled simultaneous detection of binding events of antibodies to the bilayer at several different concentrations (see figure 1.10 c)).

1.4.2 Applications of microfluidic platforms for membrane analysis

Lipid membranes in microfluidic devices have been used for various different applications in the past. In the following, the experiments are divided in four main categories: permeation, channels/transporters, binding and quantification of surface markers, and fusion. Other

studies are also discussed in the end of this section.

1.4.2.1 Permeation

As already discussed in the previous chapter, passive permeation is an important transport mechanism for drugs into the cell and there is an urgent need for high-throughput techniques to test permeation characteristics. Surprisingly, although microfluidics offers a great potential for parallelization and reduction of sample consumption, only few examples have been reported where passive permeation was studied.

Kuyper *et al.* used immobilized LUVs inside a microfluidic channel to study proton permeation across lipid bilayers [87]. A pH-sensitive dye, carboxyfluorescein, was encapsulated in the liposomes and facilitated the observation of the intravesicular pH. By using surface sensitive total-internal reflection microscopy (TIRF) and rapid buffer exchange with microfluidics they were able to detect pH changes in individual vesicles. Proton permeation was found to occur in a two step mechanism, first governed by a transient pore and then by the solubility-diffusion mechanism. Also, by studying single vesicles, heterogeneities between the vesicles could be observed.

The permeation of poly(ethylene glycol) (PEG) of different lengths across membranes was studied by Malmstadt and co-workers [88]. GUVs were immobilized with biotin-streptavidin in microfluidic channels to allow rapid fluid exchange. Permeation was monitored by spinning-disk confocal microscopy and the fluorescent labeling of the PEG. It could be shown that longer PEG molecules permeated slower, which was also in agreement with Overton's rule. In a second publication, the same authors showed that they were able to measure the permeation of unlabeled carboxylic acids into the GUVs by using a pH sensitive dye [89]. Again, they could show that more lipophilic molecules passed the membrane more rapidly than less lipophilic ones.

Recently, Ohlsson *et al.* presented a similar setup to the one from Kuyper where single liposomes could be analyzed by TIRF microscopy [90]. First, they showed that it is possible to measure the permeation of acetic acid into single carboxyfluorescein filled vesicles with fast buffer exchange of less than 10 ms. Then they used calcein at quenched concentrations to monitor water and glycerol transport upon changes in osmolarity.

1.4.2.2 Channels and transporters

Channels in lipid membranes can be formed either by peptides, like gramicidin and melittin, or by channel forming proteins, like α -hemolysin and OmpF (outer membrane protein F). Peptides and α -hemolysin are mostly used in experiments as they partition into the membrane from solution. Other membrane proteins need to be purified from cells over-expressing the desired protein and subsequently added to the desired membrane. This process is very labour-intensive and needs highly trained personnel.

Only few examples have been reported where membrane channels or transporters have been used in conjunction with microfluidics for experiments which result in new insights into the working principle of the membrane protein. Often, only the integrity and functionality of the lipid membrane is tested by incorporation of a membrane pore from solution without

any further investigation of the properties of the pore. These, much more valuable experiments for the scientific community are still mostly performed without microfluidics. In the following, only the reports are discussed which investigate the transport process and not only the functionality of the membrane.

The first natural ion-channel linked receptor was successfully implemented under flow conditions by Favero *et al.* in 2005 [91]. To achieve this, a bilayer was suspended on a microporous polycarbonate support (see figure 1.11 a)). Glutamate receptor (GluR) was purified from rat brains and incorporated directly into the pre-assembled bilayer. The conductance of ions through the membrane channel was linearly dependent on the concentration of glutamate present (figure 1.11 a)). Additionally, it could be shown that the channel conductivity was greatly influenced by a coagonists (glycine) and a blocker (Mg^{2+}).

Zagnoni *et al.* were the first who investigated the addition of membrane proteins to suspended bilayers by proteoliposome fusion in a microfluidic device [69]. The so-called nystadin/ergosterol technique was used to fuse proteoliposomes (with the potassium channel KcsA incorporated) with the bilayer under a salt gradient. Membranes with channels were shown to be intact for 1.5 – 2 h and the membrane was stable enough to exchange the solution on one side of the membrane.

In a similar device, also with a suspended bilayer, Shoa *et al.* investigated ceramide channels [92]. Ceramide is a sphingolipid that can form lipid ion channels and is proposed to play a role in cell death [93]. Due to the microfluidic chip design, the authors were able to perfuse solutions rapidly and determine kinetics of the pore formation process due to inhibition with La^{3+} and its reversal by complexation with EDTA.

Although many groups are working on implementing BLMs inside microfluidic chips for membrane protein studies, much work is also conducted with liposomes. This is simply due to the fact that liposomes are much more stable, allow encapsulation of molecules, and due to the availability of protocols to embed proteins in their membrane. Braenden and others developed a device where liposomes are immobilized with DNA-tags on a gold surface [94]. By employing surface plasmon resonance (SPR) they could show that it is possible to distinguish molecules inside the liposome and in bulk solution which enabled kinetic studies. In their first work, they showed how sucrose permeates through melittin channels in liposomes [94]. After the proof of concept was successful, they investigated aquaglyceroporin (PfAQP), a potential drug target for malaria. Several measurements about the transport of sugar alcohols through the pores could be performed with the same liposomes. However, due to the fact that SPR is a mass-sensitive technique, no discrimination between a compound interacting with the membrane of the liposome or being uptaken into the interior is possible. This is not very important for molecules with low lipophilicity, however some drugs with higher lipophilicity might partition into the membrane leading to incorrect results. The same group recently reported a microfluidic systems that enabled them to measure the transport by aquaporin in single vesicles by optical means [90].

The only study which has been performed up to now with active transporters in microfluidic channels (flow cells are not accounted for) is a brilliant work from Takeuchis group on the P-glycoprotein (PgP) transporter [95]. PgP is one of the most relevant ATP-binding cassette (ABC) transporters. These membrane proteins mediate the export of unwanted molecules from the cell. Since many drugs, and especially cancer treatments, are substrates

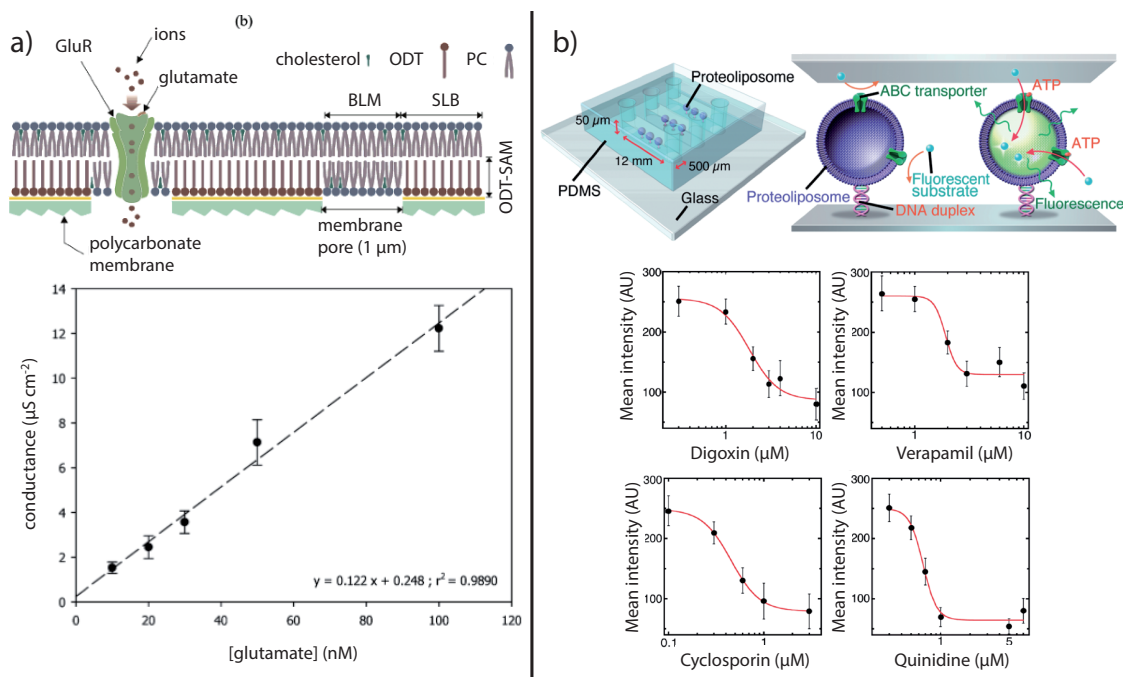


Figure 1.11: Examples for channel and transporter studies in microfluidic devices. a) Top: Schematic illustration of the setup used from Favero *et al.* in their experiments with glutamate receptors. When glutamate binds to the receptor, ions can pass and electrical conductance is increased. Bottom: The response from the conductance is in a linear relationship with the concentration of glutamate present. Figures from [91]. b) Microfluidic device from Sasaki *et al.* for PgP measurements. Liposomes with transporters are immobilized inside the channel and fluoresce upon transport of fluorescent substrate. Bottom graphs: Inhibition curves for four substrates of PgP. Figures from [95].

for PgP transporters it is very important to test drugs for their interaction with the protein. Takeuchi's group used liposomes with inside-out transporters (meaning that they transport into the liposome) that were immobilized via DNA duplexes on the channel bottom of a microfluidic device (see figure 1.11 b)). A fluorescent marker (Rh123), which is a substrate for PgP, was used to monitor the transport process. Whenever other substrates were in the channel, less fluorescent substrate could be transported and this relationship was used to determine inhibition coefficients for four different drugs.

1.4.2.3 Binding and quantification of surface markers

Ligand binding to a receptor that normally resides in the cell membrane can neither be easily simulated in bulk experiments where all molecules can diffuse freely, nor in microarray studies where the receptor is completely immobilized. The reason for this is that the lipid bilayer allows the receptors to move freely in two dimensions within the membrane, allowing a multivalent binding of the ligand to the membrane.

Cremer and co-workers conducted several studies in the last years to investigate multivalent ligand-receptor binding [96]. Microfluidic platforms were used to increase throughput of binding experiments and SLBs with different densities of receptors were created inside the channels [97]. A cooperative binding effect was found for bivalent antibodies binding to haptens (small molecules that can bind antibodies when attached to a larger protein) in the bilayer. In a further study, it could be shown that increased surface density of haptens leads to decreased binding due to clustering [98]. Furthermore, it was shown that presentation of haptens plays a critical role in the binding process [99].

In addition, lipid bilayers can also be simply used to host the receptor, which might denature outside a membrane. Goluch *et al.* presented a microfluidic device that could be used for such binding studies [100]. Lipid nanodiscs were immobilized inside channels and binding of streptavidin to biotin and Annexin to phosphoserine were studied at different concentrations with fluorescence. Nanodiscs are robust and very easy to handle due to their small size. This approach can potentially be used to create large arrays comparable to microarrays used for DNA analysis.

1.4.2.4 Fusion of lipid bilayers

The use of microfluidic technology for lipid bilayer fusion has many advantages, the most important one is the superior control over conditions in the channel. Hence, triggers like pH or fusogenic molecules can be easily delivered to the lipid bilayers and fusion observed immediately.

The group of Mayer designed a microfluidic device which enabled the growth of GUVs inside the channel [101] (see figure 1.12 a)). The subsequent delivery of calcium ions, PEG and a fusogenic peptide triggered fusion between these liposomes [102]. By direct observation of the GUVs inside the device, they were able to quantify the aggregation of liposomes and the probability of fusion.

In a seminal work, Floyd *et al.* used a microfluidic flow cell to initiate fusion of influenza virus particles with a polymer-supported SLB [103] (see figure 1.12 b)). Influenza virus employs one of the best understood fusion mechanisms to enter the cell cytoplasm. Only one protein, hemagglutinin plays an essential role in the fusion of the lipid bilayers. In the study from Floyd *et al.*, single virus particles could be imaged during hemifusion and content mixing after exchange of the buffer inside the channel to an acidic environment. This allowed very interesting mechanistic studies that led to the understanding that many HA proteins need to be activated by proton binding before fusion occurs. Recently, others showed that the fusion can also be initiated by uncaging protons with UV light with the advantage that possible shear stress on the virus particles can be eliminated [104].

A similar device was used to study fusion of vesicles with a SLB by SNARE proteins [36]. Fluorescently labeled vesicles were used in low concentrations so that binding to the SLB could be easily distinguished from vesicles in flow. Hence, the lag-time between docking and fusion, and the rate of fusion could be determined. This information lead to an estimate for the minimum SNAREpins that are required for fusion.

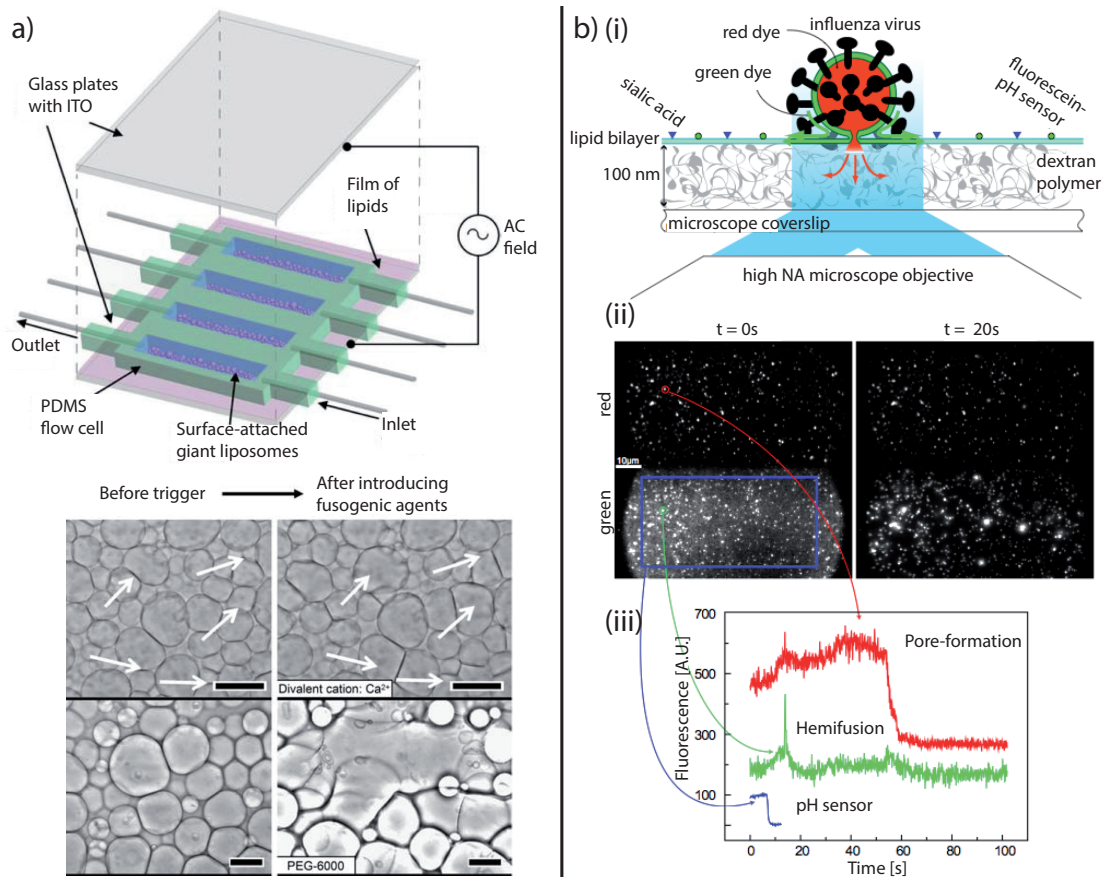


Figure 1.12: Examples for fusion studies in microfluidic devices. a) Fusion of GUVs inside a flow-channel. GUVs were grown inside the channel between two ITO electrodes by applying an AC field. GUV fusion could be visualized after an external trigger was flushed into the chamber. Figure from: [102]. b) Illustration of the system used by Floyd *et al.* for influenza virus fusion. (i) Virus particles are labeled in the membrane and the core, which allows to track both fusion events in parallel with TIRF microscopy. Virus particles bind to sialic acid inside the bilayer and fusion is initiated by changing the pH. (ii) Images from an experiment. Hundreds of virus particles can be imaged at the same time. (iii) Example traces of a fused virus particle. Figures from: [103]

1.4.2.5 Other lipid membrane studies

Of course many other interesting properties of biological or synthetic membranes can be tested in microfluidic devices. For example, Mao *et al.* employed SLBs in parallel channels to study the phase transition temperature of DPPC bilayers [105]. To achieve this, they generated a linear temperature gradient across the parallel channels by flowing a hot and a cold solution next to the area of interest. Thereby, every SLB in each channel was exposed to a different temperature. Fluorescence recovery after photobleaching (FRAP) was used to determine the diffusion of the lipids, which drastically changed at the phase transition temperature.

SLBs were also integrated in microfluidic channel to measure the partitioning kinetics of bio-molecules into different lipid phases (liquid-ordered raft phase with cholesterol or liquid-disordered with unsaturated lipids) [106]. Two regions were patterned by laminar flow inside the microchannel and biomolecules were added. Association and dissociation kinetics could be obtained for different membrane-bound molecules.

Another example where biomolecules were separated in SLBs inside a microchannel was presented by Kam *et al.* [84]. Charged lipids accumulated at micropatterned barriers when an electric field was applied. This facilitated the selective recovery of this lipid species by using a stripping solution that removed the SLB with the accumulated lipids.

1.4.3 Cell-based platforms

Many different microfluidic devices for cell handling and analysis have been developed in the last decades [50, 107] and much effort was also directed in the analysis of membranes of whole cells. Some of the most interesting examples will be discussed in the following.

Since the advent of planar patch-clamp devices in 2002 [108], where a substrate with small orifices is used to trap cells, many groups have succeeded in the development of microfluidic platforms for ion channel recordings. These devices have matured in the last years and are nowadays available from many different companies [109]. More recently, multilayer microfluidic chips have been used to trap single cells at small channel openings for patch-clamp experiments with the advantage to also perform optical measurements at the same time [110].

To test for passive permeation properties of drugs through cell membranes, it was recently shown that the down-scaling of the traditional Caco-2 cell monolayer experiment offers many advantages. In the traditional experiment, cells are grown on a filter support between two compartments. The permeation rate of a drug from one compartment to the other is very similar to the rate expected *in vivo*. Microfluidic devices require less sample and reagents, offer the integration of sensors and the control over shear stress on the cells in the experiment. Kimura *et al.* were the first to report a successful device for miniaturization of the Caco-2 assay [111]. Cells were grown on a membrane inside the device with integrated sensors and the permeation of a fluorescent molecule was monitored. A similar device was used later to study the permeation through a layer of endothelial cells at different shear stresses [112]. The most advanced measurements for drug permeation were reported by Yeon *et al.* in 2009 [113]. Cells were trapped in microholes in their device and permeation was monitored through these trapped cells. This avoided the need to culture of the cells which can take up

to several days. Ten drugs were tested for permeation rates and the results correlated with other published values.

The fusion of cells is very interesting because it allows the combination of the genetic information of two cells. This is especially attractive for the generation of hybridomas for antibody production. Because it is difficult to pair two different cells in bulk solution, the success rate is usually very low for traditional fusion approaches. Microfluidic devices have been used to increase the pairing efficiency of two cells either by electric fields [114, 115] or by attaching the different cells by avidin-biotin linkers [116]. However, the most elegant solution to pair large arrays of cells was shown by Skelley *et al.* in 2009 [117]. The first set of cells was captured in hurdle structures inside a microchannel. By reversing the flow, cells were flushed into another, bigger trap and the second set of cells was added. Pairing efficiencies of 70% could be achieved.

The detection and quantification of surface markers of single cells is another interesting application where microfluidics can be employed. Joensson *et al.* presented a microfluidic device based on two-phase flow, so-called droplet microfluidics, for detection of low-abundance biomarkers on the cell membrane [118]. Single cells were isolated within small, picoliter-sized, droplets and surface markers were detected by ELISA. The group was able to discriminate cells with no surface marker and those with very low concentrations better than with conventional FACS because of the superior sensitivity provided by the enzymatic amplification. In another work, Wang *et al.* showed the possibility to analyze protein translocations from the cytosol to the membrane (and vice versa) at single cell resolution [119]. Cells were imaged by TIRF microscopy, which mostly interrogates the cell membrane, and a kinase and a transcription factor were used as models.

1.5 Scope of this thesis

As discussed in the previous sections of this introduction, research on membranes can largely benefit from miniaturization approaches, such as microfluidics. Much progress has been made to integrate natural or artificial membranes into microfluidic devices and different platforms have been proposed. However, these systems are often only used in proof-of-concept studies where model ion channels are tested, often with not too much scientific merit in the area of membrane research. Additionally, not many platforms described in literature are available for studies of permeation and fusion and those are often limited to a certain application. The work in this thesis thereby concentrates mostly on studies of permeation of molecules and fusion of lipid bilayers. New methods and microfluidic devices are presented that allow complex experiments and high throughput, without being limited to the experiments discussed in this thesis.

Liposomes are simple model systems for cell membranes and are therefore used in most of the experiments in this thesis. As discussed previously, liposomes need to be immobilized in microchips as they would otherwise be washed away under flow conditions. Two methods to immobilize liposomes are discussed in the following chapters, one is a modification of the protocol of Stamou *et al.* [57], where liposomes are tagged with PEG-biotin, and the other a completely new approach where liposomes do not need to be tagged at all. For this, a water-soluble molecule (cholesterol-PEG-biotin) is used as a linker, which can be immobilized to a

glass surface. It is shown that the approach can be used to successfully immobilize artificial liposomes of different sizes, native (cell-derived) vesicles, vaccinia virions, yeast and bacteria cells, simply by flushing the objects through the channel.

In a first application, a versatile method to study the kinetics of tetracycline permeation across liposome membranes on a microchip is presented. Liposomes are immobilized onto the glass surface in a stripe pattern and covered by microchannels to allow continuous delivery of tetracycline and buffer. Total internal reflection fluorescence (TIRF) microscopy was used to image the formation of a fluorescent drug-europium complex inside the liposomes. The permeation rates of various tetracyclines were investigated and the results compared to a conventional method (water-octanol partitioning). Additionally, with the use of different cholesterol concentrations, the influence of membrane composition on the permeation rate can be investigated conveniently.

To study fusion of lipid bilayers in a microfluidic device, the protocol to immobilize liposomes with cholesterol-PEG-biotin is used. The microfluidic system allows to bring a defined number of liposomes in close contact to a cell, and to induce fusion at a predefined time. The device was used to study the kinetics of this fusion process by using self-quenched fluorescent dyes in the membrane and in the lumen of the liposomes. Furthermore, the setup was used to deliver β -galactosidase enzymes into single cells, which also allowed to assay the transfection efficiency.

In the last set of experiments, a microfluidic device with a cell trap array for immobilization of cells is presented, with which the acid-dependent fusion of single virions on individual cells was analyzed. In this case, no artificial membrane could be used as the binding mechanism of vaccinia virus is not yet completely understood. Vaccinia virus particles incorporating EGFP and labelled with self-quenching concentrations of R18 membrane dye were used in combination with TIRF microscopy. The kinetics of R18 dequenching and thus single hemifusion events initiated by a fast low-pH trigger could be measured.

Taken together, this thesis shows examples how microfluidic devices can be used to study transport across lipid bilayers. The focus is on permeation and fusion, but the presented platforms could also be used for other lipid membrane studies, such as transport by membrane proteins.

2 Materials and Methods

This chapter describes the most common methods used in this thesis. These methods are micro-fabrication, microfluidic device production and assembly, liposome formation, microscopy and microfluidic device operation. All other methods will be discussed later in the corresponding results chapters.

2.1 Materials

Product	Supplier
1,2-dioleoyl- <i>sn</i> -glycero-3-phosphoethanolamine (DOPE)	Avanti Polar Lipids
1,2-dioleoyl- <i>sn</i> -glycero-3-phospho-(1'- <i>rac</i> -glycerol) (DOPG)	Avanti Polar Lipids
1,2-Dilauroyl- <i>sn</i> -glycero-3-phospho-choline (DLPC)	Avanti Polar Lipids
Sphingomyelin (brain, porcine) (SM)	Avanti Polar Lipids
1,2-dioleoyl- <i>sn</i> -glycero-3-phospho-choline (DOPC)	Avanti Polar Lipids
1,2-distearoyl- <i>sn</i> -glycero-3-phosphoethanolamine-N-biotinyl(poly-ethylene glycol)-2000 (ammonium salt) (DSPE-PEG-biot)	Avanti Polar Lipids
1-palmitoyl-2-oleoyl- <i>sn</i> -glycero-3-phospho- <i>rac</i> -(1-glycerol) (POPG)	Sigma-Aldrich
Cholesterol	Sigma-Aldrich
TritonX-100	Sigma-Aldrich
Octadecyl rhodamine B (R18)	Invitrogen
1,10-dioctadecyl-3,3,30,30-tetra-methylindocarbocyanine perchlorate (DiI)	Invitrogen
Calcein	Fisher Scientific
8-Hydroxypyrene-1,3,6-trisulfonic acid trisodium salt (HPTS)	Acros Organics
Bovine serum albumin (BSA)	Sigma-Aldrich
Biotinylated BSA (bBSA)	Sigma-Aldrich
StreptAvidin-fluorescein isothiocyanate (FITC)	Sigma-Aldrich
Avidin	AppliChem
Biotin-PEG-cholesterol	Nanocs Inc.
FITC-PEG-cholesterol	Nanocs Inc.
Dulbeccos PBS	Sigma-Aldrich
2-(N-morpholino) ethanesulfonic acid (MES)	Sigma-Aldrich
Tris(hydroxymethyl)-aminomethane (TRIS)	BioRad

Product	Supplier
Tetracycline hydrate	Sigma-Aldrich
Rolitetraacycline	Sigma-Aldrich
Demeclocycline hydrochloride	Sigma-Aldrich
Meclocycline sulfosalicylate	Sigma-Aldrich
5-sulfosalicylic acid dihydrate	Sigma-Aldrich
Minocycline hydrochloride	Sigma-Aldrich
Doxycycline hydrate	Sigma-Aldrich
Oxytetracycline	Acros Organics
Metacycline hydrochloride	Acros Organics
β -galactosidase from <i>Escherichia coli</i> (Grade VIII, \geq 500 units/protein)	Sigma-Aldrich
ImaGene Red TM C ₁₂ RG lacZ Gene Expression Kit (with choloquine)	Invitrogen
Cytochalasin B	Sigma-Aldrich
Serum free medium RPMI	Invitrogen
Agar	AppliChem
BactoYeast and Bactopeptone	Becton Dickinson
Dextrose	Brunschwig
Hexamethyldisilazane (HMDS)	Sigma-Aldrich
SU-8 and developers for the resists	Microchem
AZ1518 and developer	AZ Electronic Materials
1H,1H,2H,2H-Perfluorodecyl-dimethylchloro-silane	ABCR
Poly(dimethyl- siloxane) (PDMS) (Sylgard 184)	Dow Corning
Calcium chloride (CaCl ₂)	Sigma-Aldrich
Europium(III) chloride hexahydrate	Sigma-Aldrich
Disodium dihydrogen ethylenediaminetetraacetate (EDTA)	Sigma-Aldrich
1-octanol	Sigma-Aldrich
Phosphoric acid 85 %	Sigma-Aldrich
Sodium acetate trihydrate	Sigma-Aldrich
Chloroform	Acros Organics
Methanol (99.9 % semiconductor grade)	ABCR
Citric acid monohydrate	Brenntag Schweizerhall AG
Hydrogen chloride	VWR
Sodium hydroxide	VWR
Sodium chloride	VWR

All reagents were used as received unless mentioned otherwise.

2.2 Microfabrication

PDMS microfluidic chips and PDMS stamps for microcontact printing were made by soft lithography [120, 121]. The required master molds were fabricated by photolithography (see Figure 2.1) in the ETH cleanroom facilities (FIRST).

For the microfluidic chips, a 4 inch silicon wafer was dehydrated for at least 5 min at 180 °C. The negative photoresist SU-8 was spun on the silicon wafer to the desired height by using different spin-speeds and SU-8 types. SU-8 is available in different viscosities thus providing the option to fabricate low (around 1 μm) and very high features (up to 500 μm). Hence, the processing parameters for every used SU-8 type were carefully adjusted and checked with a profilometer to meet the requirements. Table 2.2 shows the parameters for the SU-8 heights used within this thesis. Before the third, and height-defining spin-coating step, two other steps were used. First, the wafer was spun at 100 rpm for 20 s while dispensing the SU-8 resist (dynamic dispensing). This step was followed by another step at 500 rpm for 10 s to spread the resist over the whole wafer.

After the spin-coat, the wafer was heated on a hotplate to remove most of the solvent in the resist (softbake). A mask aligner was used to illuminate the resist at 365 nm through a film mask (Circuit Graphics, Essex, U.K.), which was designed in AutoCAD. After a post-exposure bake (PEB) on a hotplate, wafers were developed with SU-8 developer, rinsed with isopropanol and blown dry. Every wafer was visually inspected under a microscope and developed longer if necessary. A hardbake at 200 °C was done for 2 h to remove any residual solvent and thus to fix the SU-8 features.

Table 2.2: SU-8 processing parameters for the different structure heights used within this thesis. Only the third spin-coating step is shown.

Height	SU-8 type	Spincoat [rpm]	Softbake duration		Exposure [mJ/cm ²]	PEB dura- tion		Development
			65 °C	95 °C		65 °C	95 °C	
5 μm	3005	5000	-	120 s	110	-	120 s	2 min
40 μm	2050	3250	180 s	360 s	160	60 s	360 s	5 min
70 μm	2050	1900	300 s	600 s	215	120 s	480 s	7 min
100 μm	2050	1500	300 s	1260 s	245	300 s	600 s	10 min

For some of the designs presented in this thesis, two-layer SU-8 features were used. For these type of structures two different SU-8 resists were processed on the same wafer. The first layer was processed as described above but with a shorter hardbake of only 10 min in the end. Additionally to the structures used for microfluidic chips, the first wafer also had marks that could be used to align the second mask with the first structures. When the resist layer of the first wafer was lower than around 10 μm , it was necessary to cover the alignment marks with adhesive tape during the second spin-coating step. The adhesive tape was removed after the spin-coating, thus leaving the alignment marks uncovered by SU-8. Covering the marks by a thick layer of SU-8 would result in problems of finding the marks under the microscope of the mask aligner. After the removal of the tape, the wafer was

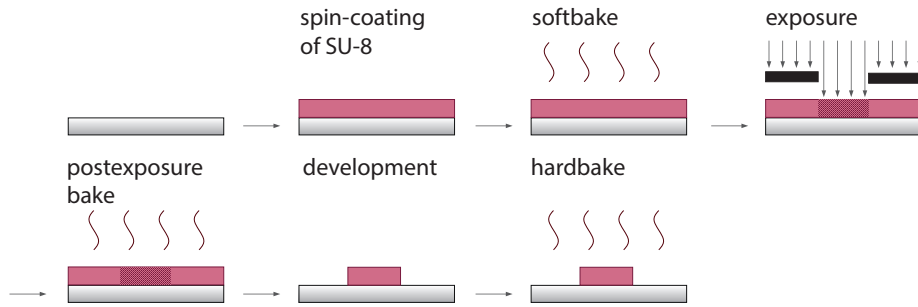


Figure 2.1: Schematic of the processing steps of a negative resist (e.g. SU-8).

softbaked according to its height. Before exposure of the second resist, the marks on the wafer from the first layer and the marks on the mask for the second layer were carefully aligned. This alignment step is as precise as the printing of the film mask (about $5\ \mu\text{m}$). The rest of the processing was done as described above for a single layer wafer.

The master molds for microcontact printing were prepared with AZ1518 positive resist. First, a 2 inch silicon wafer was dehydrated for at least 5 min at $180\ ^\circ\text{C}$ on a hotplate. To enhance the adhesion of the resist on the silicon substrate, the surface was silanized with hexamethyldisilazane (HMDS). HMDS was spun onto the wafer with a spin speed of 7500 rpm for 30 s. After the silanization, AZ1518 was dispensed on the wafer and was spun at 500 rpm for 5 s to spread the resist. This was followed directly by 4000 rpm for 60 s to achieve a height of $2\ \mu\text{m}$. The wafer was baked on a hotplate at $100\ ^\circ\text{C}$ for 50 s and then exposed through a film mask with $21\ \text{mJ}/\text{cm}^2$ at 365 nm. After development in AZ726 developer for 75 s and rinsing with water, the wafer was blown dry with nitrogen. The process was finished with a hardbake at $115\ ^\circ\text{C}$ for 50 s.

Before the wafers with SU-8 and AZ1518 features could be molded with PDMS, they were silanized to render the surface omniphobic. This greatly reduces the sticking of PDMS residues on the features and thus prolongs the lifetime of the wafers. Silanization was done with 1H,1H,2H,2H-perfluorodecyl-dimethylchloro-silane by adding $20\ \mu\text{l}$ and the wafer in a desiccator and leaving both overnight under vacuum. This creates a monolayer of silane which was renewed if the PDMS began to stick to the features again after a few weeks.

2.3 Microfluidic device fabrication

2.3.1 PDMS top part

The fabrication of the top part of a microfluidic device made from PDMS is shown in figure 2.2. First, PDMS oligomer and curing agent were mixed at a ratio of 10:1. The mixture was degassed in a desiccator and poured over the wafer with the SU-8 features taped onto the bottom of a petri dish. The PDMS was degassed again to remove gas bubbles sticking to the resist. The silicone was hardened at $80\ ^\circ\text{C}$ for minimum 3 h, thereby forming the channels of the microfluidic chip. After peeling the microchips from the wafer, single chips were cut with a razor blade. Holes were punched into the chips with a 1 mm or a 1.5 mm (depending

on the application) biopsy punch (Miltex, York, PA) to connect the channels with tubing. Adhesive tape was used when necessary to remove debris from the surface.

If no modification of the surface inside the channel was necessary, the chip could be directly bonded to a clean glass cover slide. The cover slide was washed with acetone, isopropanol, ethanol and water. Dried cover slides and the PDMS chips were placed into a plasma chamber (Harrick Plasma, Ithaca, NY, USA) and plasma activated [45]. Both parts were bonded together by this process and heated on a hotplate at 100 °C for 30 min.

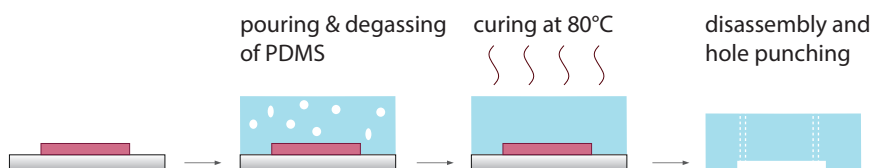


Figure 2.2: Schematic of the fabrication of a microfluidic device from PDMS. A silicon wafer bearing the inverse features of the channels is taped onto the bottom of a petri dish, which is then filled with PDMS mixture. After degassing, the PDMS is cured in an oven. Following the hardening of the silicone, the chips are diced and holes are punched for fluidic connection.

2.3.2 Microcontact printing

The PDMS stamps for microcontact printing (see figure 2.3) were prepared the same way as the microfluidic devices (see 2.3.1). Before use, the stamps were cut into 5 mm * 10 mm pieces.

Stamps were incubated with a 5 mg/ml protein solution in PBS for 1 h. For all the experiments discussed in this thesis, either bovine serum albumin (BSA) or derivatives of this protein (like biotinylated BSA (bBSA) and BSA-fluoresceinisothiocyanat (BSA-FITC)) were printed. After the incubation, which results in a monolayer of the protein on the surface of the stamp, stamps were thoroughly washed with MilliporeTM filtered water and dried with nitrogen. The protein monolayer was then transferred onto a cleaned glass cover slide by leaving the PDMS stamp for approximately 30 s on the glass. In this step the proteins transfer completely to the glass [121].

2.3.3 Device assembly

If the microcontact printed pattern of proteins needed to be enclosed within a microfluidic channel, the process described above was slightly changed. Here, the stamp remained on the slide and was placed together with the PDMS chip into a plasma chamber (Harrick Plasma, Ithaca, NY, USA) and treated with oxygen plasma (see figure 2.4). Because the

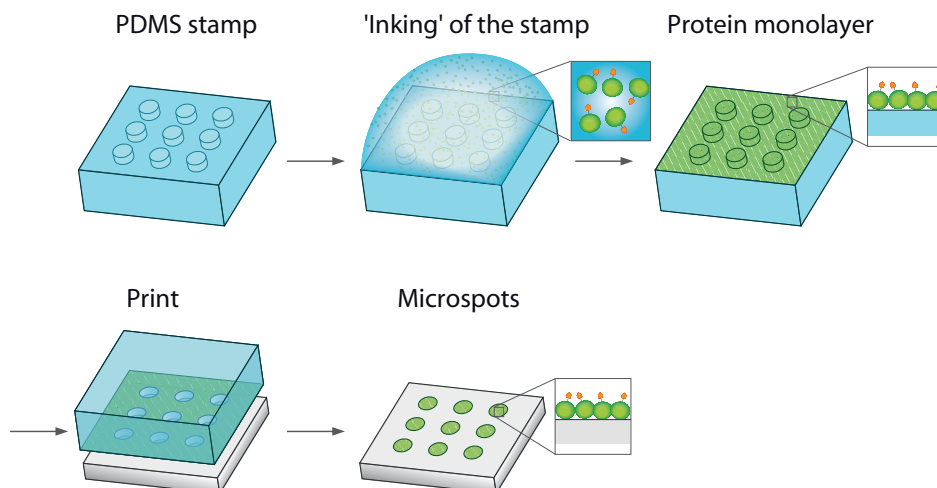


Figure 2.3: Schematic of microcontact printing. A PDMS stamp bearing features is 'inked' with a protein solution. After a period of incubation, the proteins self-assemble on the surface and build a monolayer. The residual solution is then washed away with water and the stamp is blown dry. The monolayer is then transferred to a glass substrate by printing. Removal of the stamp leaves a microarray on the glass.

stamp protects the proteins during this harsh procedure, the proteins remain active [122]. After the stamp was removed, the PDMS microfluidic chip was bonded onto the glass cover slide. To improve the bonding process, the assembled chip was left on a hotplate at 50 °C for 30 min. Afterwards, the chip was immediately filled with 40 mg/mL BSA in PBS to block all surfaces that have not been covered by microcontact printing. After incubation for minimum 1 h at room temperature, residual, unbound BSA was washed out with PBS buffer. For some experiments the BSA was left in the chip till the time of the experiment. The microfluidic device was then stored in a fridge in a box with humid atmosphere (by adding a wet tissue).

2.3.4 Further surface modifications

In a second incubation step, the chips were filled with 0.01 mg/ml avidin in PBS for another 2 h. Finally the chip was thoroughly washed with at least 500 μ l buffer (either TRIS 0.2 M pH 7.4, or PBS). Chips filled with buffer were stored at 4 °C for up to one week before use without any noticeable loss of performance. Microfluidic devices that were fabricated in this manner were ready for loading either biotinylated liposomes or molecules bearing a biotin moiety.

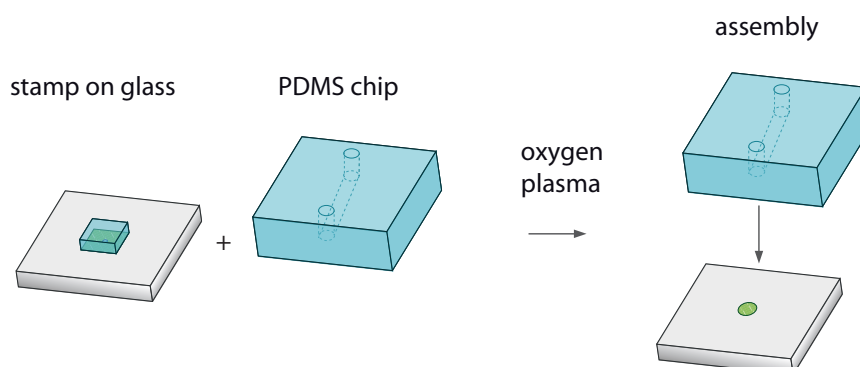


Figure 2.4: Plasma bonding of microcontact printed glass and a microfluidic device. The stamp protects the proteins during the harsh plasma treatment which would usually destroy all proteins.

2.4 Liposome formation

Vesicle preparation followed a procedure described previously [123] and which is shown schematically in figure 2.5.

Lipid mixtures were dissolved in a 5 ml methanol and chloroform mixture. The solvent was evaporated in a glass flask to create a lipid film on the glass wall. This was done in two steps while heating the flask at 40 °C and rotation (medium speed). First, the pressure was reduced to 230 mbar until no solvent was visible anymore in the flask. Second, the pressure was reduced for at least 3 h to the best vacuum possible with the pump (less than 1 mbar) to ensure no solvent is left in the lipid film. The film was then rehydrated in buffer resulting in a multilamellar vesicle suspension. The rehydration was done with two additions of 1 ml to bring most lipids in suspension.

Ten cycles of freezing and thawing were applied to the suspension to create unilamellar liposomes [123]. Afterwards, the suspension was extruded 19 times through a polycarbonate membrane of 200 nm pore size (Micro-Extruder, Avanti Polar Lipids with Whatmann Nucleopore Track-Edge Membrane), if not mentioned otherwise.

The size of the vesicles was determined by dynamic light scattering (DLS) with a Zetasizer 3000 HSA (Malvern Instruments, UK). The mean hydrodynamic diameter of preparations with a 200 nm pore membrane was between 160 and 200 nm (intensity distribution). The polydispersity index of around 0.1 indicated a narrow size distribution. The liposome formation was also checked by cryo-TEM if it yields unilamellar liposomes. Indeed, most of the produced liposomes are unilamellar and of comparable size (see figure 2.6).

The vesicle suspension was stored at 4 °C for maximal one week in the buffer. For some experiments the vesicle suspension was passed through a size-exclusion column to exchange the outside solution.

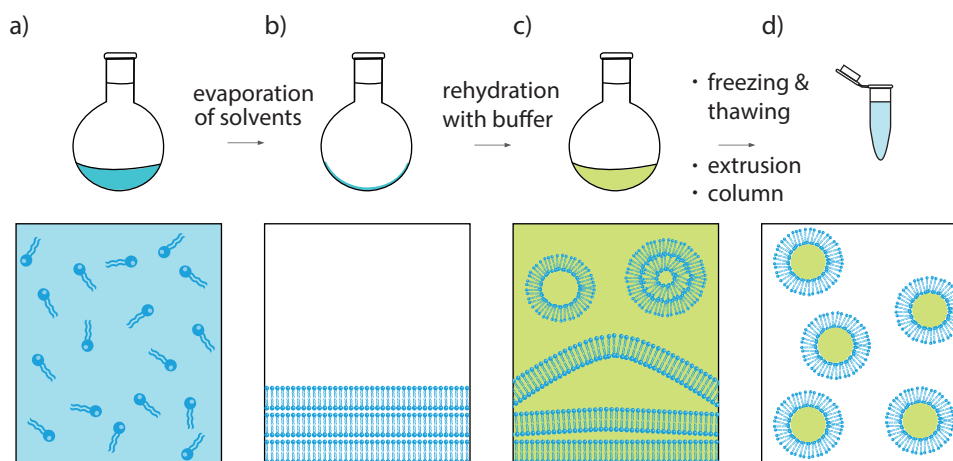


Figure 2.5: Schematic of liposome preparation with thin-film rehydration. a) Different lipids are added in a methanol/chloroform mixture into a round bottom flask. The lipids can diffuse freely in this solvent mixture (see bottom). b) After the evaporation of the solvent with a rotavap, the lipids form thin films on the surface of the glass. c) This lipid film is then rehydrated with a buffer containing molecules like for example calcein. The buffer swells the lipid film and liposomes are created. These liposomes are of different sizes and mostly multilamellar. d) After freezing and thawing followed by extrusion through a porous membrane, the suspension is passed through a size-exclusion column to exchange the outside buffer. After these steps, the liposomes are unilamellar, homogeneous in size and contain a different solution than the surrounding buffer.

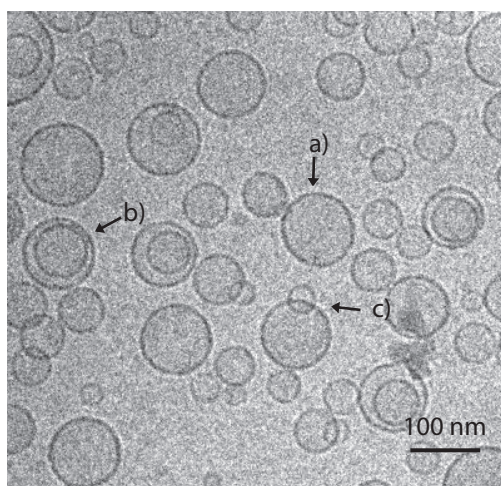


Figure 2.6: Cryo-TEM image of liposomes prepared with thin-film rehydration. (a) unilammellar, (b) multilammellar, (c) unilammellar vesicles on top of each other. Note that for the preparation of the liposomes shown in this image a 100 nm pore membrane was used.

2.5 Microscopy

Wide-field fluorescence images were obtained on an inverted microscope (IX70, Olympus), equipped with a mercury arc lamp. Different objectives ranging from 4x to 60x were chosen for the given application. Images were recorded with an EMCCD camera (iXon 887, Andor).

The filter sets for imaging were:

- filterset 1: Ex: 455/70, Dichro 494 LP, Em: 515 LP
- filterset 2: Ex: 525/50, Dichro 565 LP, Em: 588 LP

For total internal reflection microscopy (TIRF), a 100x oil immersion objective (NA 1.47, HCX Plan Apo) was chosen to focus the laser light (used laser lines: 405, 488, 561 nm) onto the glass slide at the correct angle for total internal reflection therefore producing the evanescent field above the glass surface (imaged area: $80\ \mu\text{m} \times 80\ \mu\text{m}$). The fluorescence emitted was collected by the same objective, passed through a band pass filter (used filters: 525 and 605 nm) and recorded using a front-illuminated EMCCD camera (iXon, Andor). Data was collected using Leica LAS AF software.

2.6 Microfluidic device operation

Microfluidic devices were operated in two modes for the work presented in this thesis (see 2.7). Both modes have distinct advantages and disadvantages which are described in the following.

2.6.1 Pump mode

In pump mode, syringes were filled before the experiments with the solutions needed. During the filling, attention was paid to not enclose any bubbles in the syringe or in the tubing leading to the microfluidic device. By using neMESYS pumps from cetoni, many syringes could be used in parallel. The pumping mode has the clear advantage over the sucking configuration that laminar flows are easily accomplished and controlled. This means that two flows can flow next to each other due to low Reynolds numbers (see section 1.3.1) and their flow rates can be changed to control which fluid is covering which part of the channel bottom. This was especially important for the experiments described in chapter 4 where rapid fluid exchange was needed. Disadvantages are that once a fluid is connected to the chip, it cannot be removed anymore without disturbing the chip. This is often unwanted when solutions need to be changed frequently. Also, the dead volume in the tubings often leads to a significant loss of sample, which can be problematic when working with expensive biochemicals.

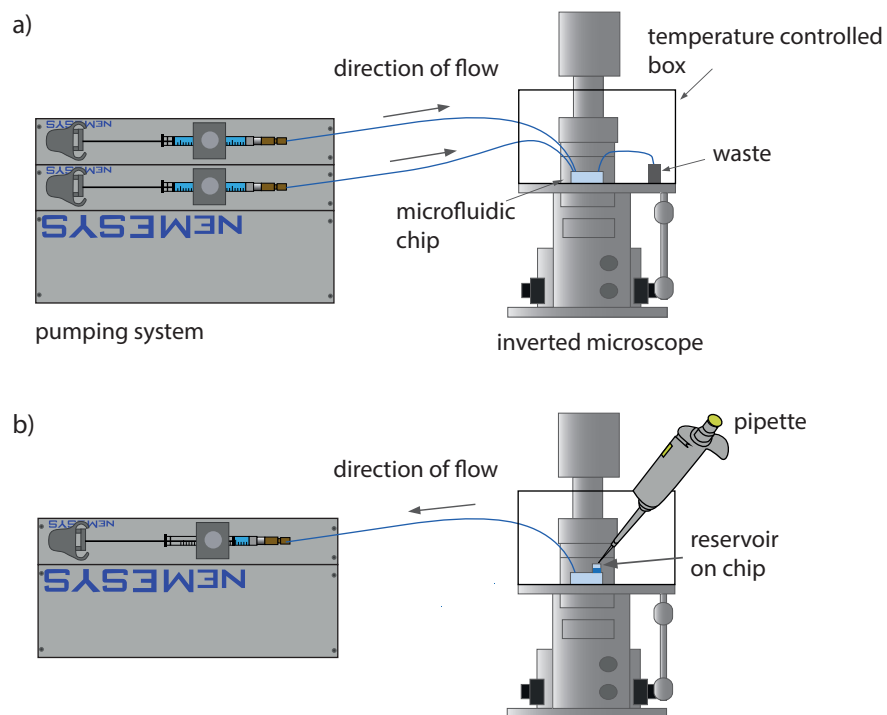


Figure 2.7: Schematic representation of microfluidic chip operation. a) Pump mode. Fluids are pumped into the microfluidic device by actuation of a syringe. The chip is fixed on a inverted microscope and enclosed in a box with controlled temperature (important for experiments with living cells). A waste container is used to collect fluids that passed the chip. b) Withdrawal mode. The syringe is used to withdraw fluids through the chip from a reservoir that is fixed on the device. A pipette can be used to exchange fluids in the reservoir.

2.6.2 Withdrawal mode

A reservoir was attached to the PDMS device and almost empty syringes were used to withdraw the sample from the reservoir through the chip. The reservoir consisted out of a cut pipette tip which was fixed with some uncured PDMS over the hole of the device. One syringe and tubing was filled with water, emptied so that only the tubing was filled and then connected to the outlet of the chip. This ensured that no fluctuations due to air bubbles occurred. The fluid in the reservoir was exchanged during the experiment by washing at least 3 times with the new solution. This ensured that less than 1 % of old solution stayed in the reservoir. This is sufficient if buffers are exchanged to change the pH.

The advantages to use this configuration are that low amounts (in the microliter range) of fluids can be used, that the probability to entrap bubbles in the chip is low and that fluids can be exchanged multiple times without problems. One disadvantage is the slow fluid exchange (approx. 20 s for 5 $\mu\text{l}/\text{min}$). The fact that the solution in the reservoir can never be completely exchanged can be a problem for some experiments.

Once the microchip is fabricated, aligned and connected to external controls, it is used for various applications described in the following chapters.

3 Immobilization of liposomes, virus particles, bacteria and yeast cells in microfluidic devices

Immobilization of liposomes and cells is often a prerequisite for long-term observations. The most common immobilization approaches rely on surface modifications, encapsulation in porous materials or trapping in microfluidic channels by means of hurdle-like structures. While these approaches are useful for larger mammalian cells, the immobilization of smaller organisms like bacteria and yeast or membrane model systems such as liposomes typically requires modification of their outer membrane to ensure that they are stably arrested at a defined position. Here, a protocol is presented to immobilize biological objects, which can interact with hydrophobic cholesterol. A water-soluble molecule (cholesterol-PEG-biotin) is used as a linker, which can bind via avidin to biotinylated BSA (bBSA) previously absorbed on a glass surface. For better visualization, bBSA is arranged in a dot pattern by means of microcontact printing, and a microfluidic channel is used for sample supply. It is shown that the approach can be used to successfully immobilize artificial liposomes of different sizes, native (cell-derived) vesicles, vaccinia virions, *Saccharomyces cerevisiae* and *Escherichia coli*, simply by flushing the objects through the channel. Under these conditions, small liposomes and biological objects are stably arrested at high flow rates, while larger cells and liposomes can be released again by application of high shear stress. This protocol can be applied for long-term studies where fluids must be changed repeatedly, for measuring fast kinetics where rapid fluid exchange is essential, and to study the effects of shear stress.

This chapter was published in:

Kuhn, P., Robinson, T., Eyer, K., Schmidt, F.I., Mercer, J., Dittrich, P. S. (2012) A facile protocol for the immobilization of vesicles, virus particles, bacteria and yeast cells. *Integrative Biology* 4(12), 1550-1555.

3.1 Introduction

Long-term observations of single cells or liposomes require the use of immobilization techniques. The most common immobilization strategies for biological objects include entrapment within a porous substrate or adsorption onto a surface. The latter is often preferred due to its simplicity and has several advantages, including isolation and arraying, the possibility to use surface-sensitive techniques for detection, and the possibility to exchange the surrounding solution [55, 57]. Mammalian cells are typically immobilized by growing them

on an adherent surface, which also be performed in patterns using adhesion promoting (or preventing) surface coatings [124]. Microfluidic-based traps can be used to mechanically confine non-adherent cells (e.g. mammalian cells in suspension, bacteria and yeast cells) for observations over long time periods [125]. However, this requires the fabrication of complex devices with small, embedded features [126, 127]. To immobilize liposomes, several tethering approaches have been developed (see chapter 1.1). The most commonly used method employs biotinylated lipids which can bind to immobilized avidin [57]. Other approaches rely on DNA hybridization [128] or polyhistidine-tags [60]. However, all reported methods involve tagging of the lipid membrane, which can be technically challenging or undesirable as it may influence the membrane properties (for example in fusion, as discussed in chapter 5).

To circumvent these shortcomings, biotinylated polyethylene glycol-cholesterol (biot-PEG-chol) was used that can insert into any lipid membrane allowing the lipid-enveloped objects to be tethered onto a surface. It is known that the cholesterol moiety of biot-PEG-chol preferentially partitions into cholesterol-rich domains within lipid membranes [129]. However, this simple, commercially available linker was never before used to immobilize cells or vesicles to a surface.

The addition of hydrophilic PEG chains to cholesterol increases water solubility, which makes it compatible with physiological experiments in which no or small amounts of organic solvents are allowed. Furthermore, the entire immobilization strategy is not based on harsh or complicated surface chemistry and is therefore easy to implement. Additionally, the biotin moiety of biot-PEG-chol provides the possibility to array liposomes on surfaces by combining the immobilization with existing micropatterning techniques, e.g. microcontact printing.

In this study this facile approach is demonstrated by tethering a wide range of lipid-enveloped objects including, artificial and native vesicles, viruses, bacteria and yeast cells to patterned surfaces. Furthermore, it is shown that this approach can be combined with microfluidics allowing for rapid fluid exchange.

3.2 Materials and methods

3.2.1 Chip fabrication

Microfluidic devices were fabricated as discussed in section 2.3 by bonding a PDMS top part to a functionalized cover glass. The structures, comprising inlet and outlet channels leading to a large chamber [130], in the chip were 100 μm high.

As discussed in more detail in section 2.3.2, BSA was microcontact printed onto the glass and the remaining surface blocked with BSA. The solution was incubated for 2 h and washed out with PBS using a syringe pump. In a second step, 0.01 mg/ml avidin in PBS was incubated for another 2 h. In some experiments StreptAvidin-FITC was added to avidin in the same concentration to visualize the microcontact printed patterns. Another washing step with PBS was followed by incubation of 7 μM cholesterol-PEG-biotin in PBS for a minimum of 1 h. Chips were again washed thoroughly with PBS and could be stored at 4 $^{\circ}\text{C}$ in a humid atmosphere for up to 4 weeks without noticeable loss of capture efficiency.

3.2.2 Cell culturing

HEK-293 human embryonic kidney cells (DSMZ, Germany) were grown in DMEM (4.5 g/L glucose, 2 mM GlutaMAX) containing 10 % fetal bovine serum and penicillin/streptomycin (all Invitrogen) at 37 °C and 7 % CO₂. For vesiculation, cells were grown to 80 % confluence.

BSC-40 African green monkey kidney cells (ATCC, USA) were cultivated in DMEM (4.5 g/L glucose) supplemented with 10 % fetal calf serum, GlutaMAX, non-essential amino acids, sodium pyruvate, and penicillin/streptomycin (all Invitrogen) at 37 °C and 5 % CO₂.

Saccharomyces cerevisiae (strain S288c variant BY4736) colonies were grown on YPD agar plates (1 % BactoYeast, 2 % BactoPeptone, 2 % dextrose, 2 % agar) at 30 °C. Suspension cultures for chip experiments were grown overnight in YPD medium (1 % BactoYeast, 1 % BactoPeptone, 2 % dextrose) at 30 °C with vigorous shaking.

Escherichia coli (BL21-Gold(DE3), Invitrogen) expressing GFP (vector pET-29b(+), Novagen) were cultivated to an OD of 0.4 in LB media supplemented with 30 µg/ml kanamycin sulfate (Sigma). GFP expression was induced by 0.5 mM IPTG (Applichem) and the cells were cultivated for 2 days at 18 °C with gentle shaking.

3.2.3 Vaccinia virus preparation

Octadecyl rhodamine B chloride (R18)-labeled mature virions (MVs) of vaccinia viruses strain western reserve (WR) were produced in BSC-40 cells and purified/labelled using a protocol adapted from Mercer and Helenius [131]. MVs from cytosolic extracts were sedimented through a 36 % sucrose cushion (80 min, 43,000 x g, 4 °C), resuspended in 10 mM TRIS pH 9.0, and incubated with R18 at a final concentration of 22.5 µM for 2 h at room temperature. Labeled MVs were sedimented (40 min, 38,000 x g, 4 °C), purified through a 25 – 40 % sucrose gradient (50 min, 12,000 x g, 4 °C), and virus from aspirated bands sedimented one last time (40 min, 38,000 x g, 4 °C). MVs were resuspended in 1 mM TRIS, pH 9.0, and stored at –80 °C.

3.2.4 Vesicle preparation

Large unilamellar vesicles (LUV) were prepared by hydration of a thin film of dried lipids as described in detail in section 2.4. Briefly, 10 mg lipid mixture of DLPC (77 wt%), POPG (10 wt%), cholesterol (12.9 wt%) and DiI (0.01 wt%) was dissolved in 5 ml methanol. The solvent was evaporated in a glass flask to create a lipid film on the glass wall. The film was rehydrated in 2 ml 0.1 mM HPTS (in 0.2 M TRIS, pH 7.4) resulting in a multilamellar vesicle suspension. Seven cycles of freezing and thawing were applied to the suspension to create unilamellar liposomes.

Native liposomes were prepared according to Pick. *et al.*[132] by blebbing HEK-293 cells. An 80% confluent cell layer was washed twice with PBS and vesiculation was induced by addition of serum free RPMI with 1 µg/ml cytochalasin B (stock: 1 mg/ml in DMSO). After 30 min of incubation, the media was removed and centrifuged at 500 rpm for 5 min to pellet cellular debris. To collect the vesicles, the supernatant was removed and centrifuged for 20 min at 2000 rpm. The medium was aspirated and vesicles were resuspended in PBS for storage at 4 °C until up to 1 week.

To guarantee a uniform size of the vesicles, the liposome suspensions (artificial and native) were extruded nine times through a polycarbonate membrane of 200 nm pore size .

3.2.5 Giant unilamellar vesicle preparation

Giant unilamellar vesicles (GUVs) were prepared using the electroformation method [133] in a custom-built temperature controlled chamber consisting of two transparent indium tin oxide (ITO) coated glass slides ($15 - 25 \Omega/\text{sq}$, Sigma-Aldrich) separated by a 1.5 mm thick silicone spacer. The device was held together by a heated aluminum plate and an AC field was generated using a function generator (HMF2525, HAMEG Instruments, Mainhausen, Germany) attached to the ITO surfaces via copper strips. Lipid mixtures of DLPC and sphingomyelin/DOPC/cholesterol (1:1:0.5 (mol/mol)) at a concentration of 1 mM with 1 μM DiI were dissolved in a mixture of methanol and chloroform (10:1 (v/v)). The solutions were then dried overnight on an ITO surface under vacuum to remove the solvents, rehydrated using MilliporeTM filtered water and sealed in the chamber with the aid of silicone paste. GUVs were formed by applying 0.7 V at a frequency of 10 Hz over 4 h at 60 °C for sphingomyelin/DOPC/cholesterol and 22 °C for DLPC. After turning off the heated plate and the AC field, the GUVs were harvested by gentle pipetting. GUV suspensions were stored at room temperature and used within 48 h.

3.2.6 Immobilization

Generally, all presented biological objects could be immobilized with a very similar procedure. However, due to different concentrations and sizes (e.g. artificial vesicles and *E. Coli*), the incubation times and washing procedures had to be optimized.

Small vesicles (artificial and native) were flushed through the channel containing the immobilized biot-PEG-chol at a flow rate of 5 $\mu\text{l}/\text{min}$ for approximately 15 min. The channels were then washed with PBS at 50 $\mu\text{l}/\text{min}$ for 10 min to remove unbound vesicles. Vaccinia viruses were immobilized with the same procedure as the vesicles but were washed with 1 mM TRIS pH 9 to avoid clustering of virions.

Bacteria, yeasts and GUVs were filled into the channel and immobilized without flow for a few hours at 4 °C. This ensured sufficient time for interaction with the cholesterol on the channel surface. The PBS solution inside the microfluidic chip was exchanged with de-ionized water before adding the GUVs to prevent osmotic pressure. Unbound bacteria were washed away with PBS at a flow rate of 50 $\mu\text{l}/\text{min}$. Unbound yeast cells and GUVs were removed from the channel by low flow rates ($\sim 1 \mu\text{l}/\text{min}$) of PBS or water, respectively, which was accomplished by adding more fluid to the inlet than to the outlet reservoirs.

3.2.7 Imaging

Immobilized vesicles and virus particles were imaged with TIRF microscopy, bacteria and yeast with wide-field fluorescence microscopy and GUVs with confocal microscopy.

For TIRF microscopy (see section 2.5 for details) DiI and R18 were excited with a 561 nm laser and emission collected with a bandpass filter (600/32). Calcein was excited with 488 nm and emission was collected with a 525/35 bandpass filter.

Wide-field fluorescence images were obtained with filterset 1 as described before (see section 2.5 for details).

GUVs were imaged using a confocal microscope (LSM 510-NLO, Zeiss) to show their unilamellarity. FITC conjugated to streptavidin on the glass surface and DiI incorporated into the GUV membrane were excited using 488 and 543 nm lasers, respectively. A 40x oil immersion objective lens (NA 1.3, Plan-Neofluar, Zeiss) was used to focus the light into the microchannel. The emitted fluorescence was collected using the same lens and filtered from the scattered excitation light using a dichroic mirror (HFT UV/488/543/633). The signal from the two fluorophores was separated using a second dichroic mirror (HFT 545), a band pass filter for FITC (BP 500-530) and a long pass filter for DiI (560 LP). The 3-D image was created by acquiring 43 confocal images at 0.43 μm intervals and rendered using Imaris (Bitplane AG, Zurich, Switzerland).

3.3 Results and discussion

3.3.1 Description of the immobilization assay

The immobilization assay requires the tethering of cholesterol molecules onto a surface. Upon contact with a lipid bilayer, the cholesterol inserts into its hydrophobic interior and captures the lipid-enveloped object (Figure 3.1 a and b). Cholesterol bound to a biotinylated PEG linker was used, which is water-soluble and can in turn be bound to the surface of a glass slide via avidin and biotinylated bovine serum albumin (bBSA). For this, bBSA was adsorbed to the surface, followed by a supply of avidin and the biotinylated PEG-cholesterol. In order to achieve an inhomogeneous pattern, micrometer-sized spots of bBSA were generated by micro-contact printing while the remaining surface was blocked with BSA [57]. Therefore, specific binding due to cholesterol insertion into the membrane could be directly distinguished from non-specific binding to BSA. Furthermore, the surface was enclosed inside a microfluidic channel (100 μm high) to allow the surface to be easily washed, and solution exchange without disturbing the immobilized objects. The use of a microfluidic device also enables precise control over flow rates, which can be important for reproducibility of the immobilization and washing steps, especially if low concentrations of samples are used.

3.3.2 Immobilization of artificial lipid vesicles

First, the immobilization of lipid vesicles of different sizes was tested, which were either prepared from artificial membranes (phosphatidylcholines) or derived from mammalian cells. Lipid vesicles are often used to study lipid membrane properties, e.g. lipid rafts [134], and membrane proteins in their natural scaffold [135, 136]. They can also serve as functional nanocontainers for biochemical reactions [1], enzyme and gene expression assays [137–139].

LUVs were prepared via thin-film hydration and extrusion through a polycarbonate membrane with 200 nm pores. The lipid membrane of the LUVs was stained with DiI, a hydrophobic dye, while the lumen of the vesicles contained HPTS. The hydrophilic HPTS molecule contains sulfonic acid groups that are negatively charged at physiological pH. This property greatly hinders the passage through the lipid bilayer thus the molecule can be used to assay

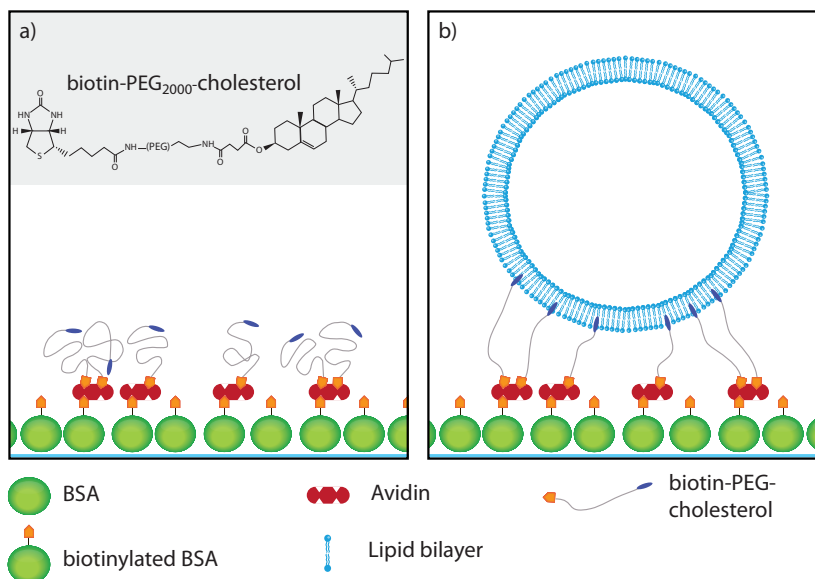


Figure 3.1: Schematic of the immobilization method. a) The surface of a glass slide is covered with bBSA (either completely or patterned by microcontact printing). Avidin binds to the bBSA on the one side, and to biotin-PEG-cholesterol on the other. b) Cholesterol inserts into the hydrophobic portion of the lipid membrane with sufficient strength to immobilize the liposome. Images are not drawn to scale.

the integrity of the liposomes. After a short incubation of the micropatterned surface with the liposome suspension and a washing step with buffer, the immobilized liposomes were clearly visible on microcontact printed spots inside the microchannel. The DiI and HPTS signals co-localized suggesting that intact liposomes were tethered to the surface (Figure 3.2 a) and b). To investigate the influence of membrane cholesterol content on tethering efficiency, LUVs with and without cholesterol were used. No differences in tethering to the cholesterol-rich spots could be observed (data not shown).

Furthermore, GUVs with diameters up to 30 μm were immobilized onto the functionalized microspots. Two different lipid compositions were tested for immobilization. GUVs containing cholesterol (sphingomyelin/DOPC/Cholesterol) were strongly attached to the spots and could not be washed away at velocities of up to 60 $\mu\text{m/s}$ (corresponding to a flow rate of approximately 1 $\mu\text{l/min}$), while GUVs with a DLPC membrane lacking cholesterol could not be immobilized inside the chip (data not shown). The presence of cholesterol in the membrane is therefore necessary for tethering of these large vesicles. The strong binding to the cholesterol containing membrane allows multiple confocal images to be acquired for 3-D rendering of GUVs (Figure 3.2 c)). Unlike cells of a similar size (see below), the bound GUVs could not be easily washed away with flow rates up to 1 $\mu\text{l/min}$ as they were able to adapt to the fluid flow due to their flexibility.

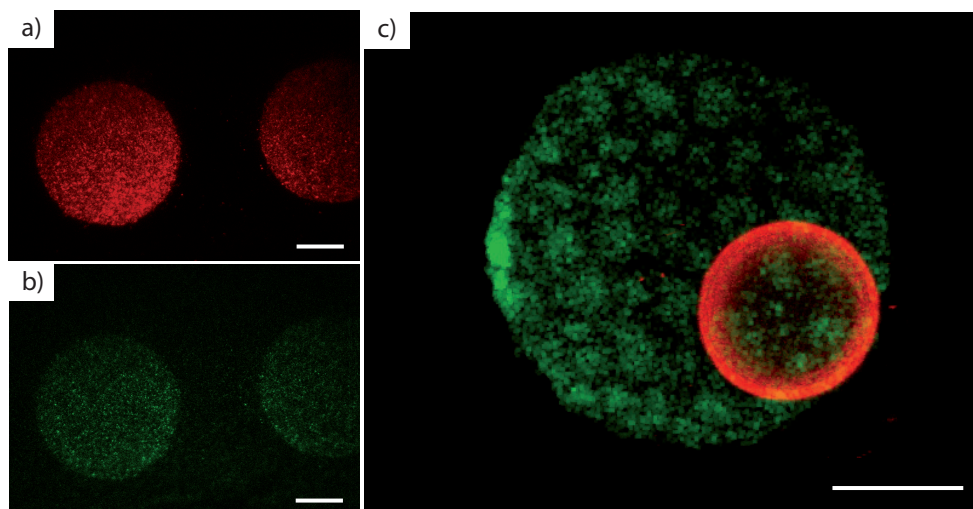


Figure 3.2: Immobilization of artificial liposomes in a microfluidic channel. Signal from DiI in the membrane of LUVs (a) and fluorescence from the water-soluble dye HPTS enclosed in liposome lumen (b). c) 3-D rendering of an immobilized GUV stained with DiI on a microspot (shown in red), that is partly visualized with FITC-labelled streptavidin (shown in green). Scale bars $10\ \mu\text{m}$

3.3.3 Immobilization of native vesicles

To test if native vesicles can be immobilized, cell-derived vesicles were prepared by inducing so called 'blebbing' in HEK293 cells [132]. Previously, native vesicles have been immobilized on surfaces by electrostatic attraction [132], also in combination with patterning by blocking parts of the surface with supported bilayers [140]. However, it was not shown how stable this immobilization procedure is under shear stress.

The blebbed vesicles were extruded through a 200 nm pore membrane for a more uniform size distribution and DiI was added to the solution to stain the vesicles. After the immobilization procedure, bright red-fluorescent spots on the microcontact printed areas were observed, indicating successful immobilization (Figure 3.3 c)). We further proved the integrity of the cell-derived vesicles by means of a fluorescence assay based on Calcein AM, which is normally utilized for visualization of live cells. Calcein AM is a non-fluorescent membrane permeable ester of calcein, which is converted to calcein by cytosolic esterases (see figure 3.3 b)). Calcein, like HPTS, is membrane impermeable and highly fluorescent. Indeed, after 15 min incubation with Calcein AM solution and a subsequent washing step, the immobilized native vesicles became green fluorescent (Figure 3.3 d)). Hence, intact native liposomes could be successfully immobilized without the need for prior modification of the membrane. Furthermore, these native vesicles contain cytosolic enzymes, which are still functional after the immobilization.

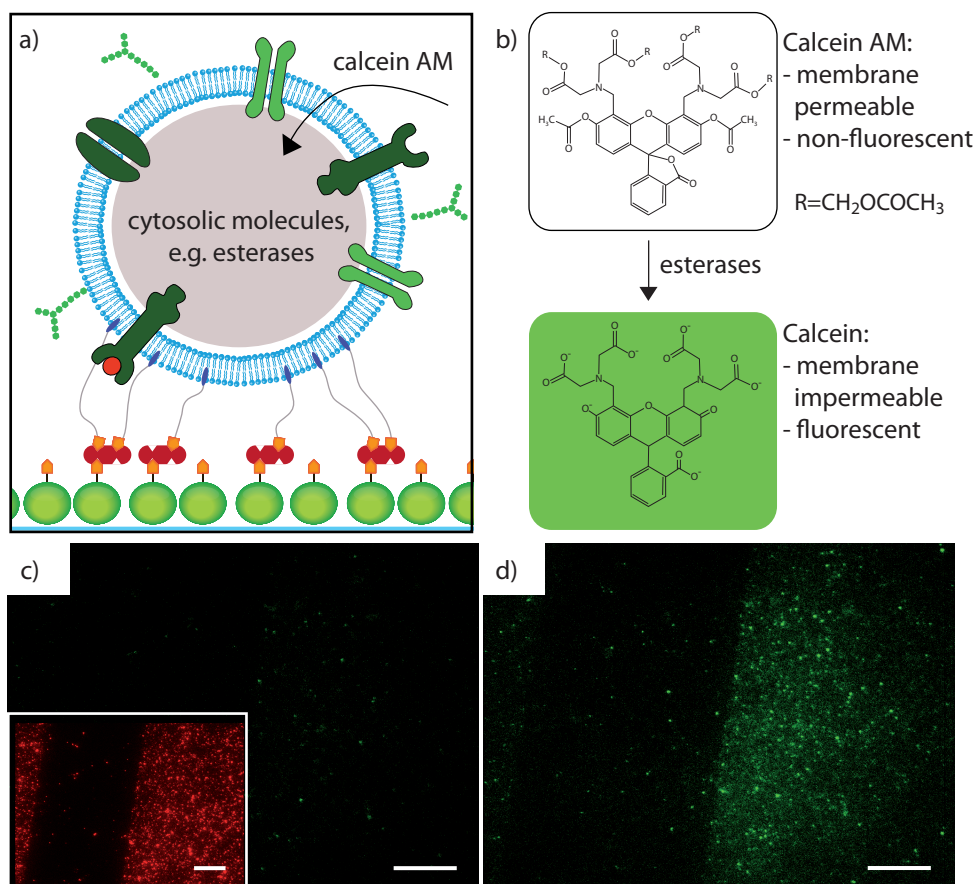


Figure 3.3: Immobilization of native vesicles derived from cell membranes. a) Schematic of the immobilization. The native liposome retains the membrane proteins and cytosolic molecules. b) Chemical drawing of the assay inside the liposomes. Non-fluorescent calcein AM permeates over the lipid bilayer into the liposome where it is hydrolysed by esterases, yielding fluorescent calcein. c) TIRF microscopy images from the immobilized liposomes before addition of calcein AM and d) after 15 min incubation with Calcein AM. The inset in c) shows the fluorescence from the membrane-dye DiI before addition of calcein AM for comparison. Scale bars $30 \mu\text{m}$.

3.3.4 Immobilization of biological objects

Next, several different biological objects were tested to determine if they can be tethered by the cholesterol linker. Lipid-enveloped mature virions (MVs) of vaccinia virus [131, 141] were added into the chip in a 1 mM TRIS buffer at pH 9 to avoid aggregation of the virus particles. After a short incubation and a washing step with TRIS buffer, the majority of the MVs were bound to the microspots (Figure 3.4a). When compared with liposomes and cell vesicles, more nonspecific binding to non-functionalized surfaces was detected. This is likely due to unspecific protein-protein interactions between the viruses and BSA. Nevertheless, the functionalized spots could be easily identified.

Next, *E. Coli* were successfully immobilized on the patterned surface (Figure 3.4 c) and d)). This finding is particularly interesting since the outer membrane of gram-negative bacteria contains lipopolysaccharide (LPS), which reduces the diffusion of hydrophilic molecules and small hydrophobic molecules through the membrane [142]. However, this does not exclude an insertion of a small hydrophobic molecule, like cholesterol, into the LPS layer. We therefore hypothesize that the cholesterol interacts with the hydrophobic LPS layer. Bacterial cells were immobilized almost as well as the liposomes and viruses and could not be washed away with higher flow rates (200 $\mu\text{l}/\text{min}$ in a 2 mm wide, 100 μm high channel. However, increased shear forces released *E. Coli* from the surface (200 $\mu\text{l}/\text{min}$ in a 300 μm wide, 70 μm high channel).

Patterned cholesterol can also be used to immobilize yeast cells (Figure 3.4 b). The yeast cell envelope consists of a plasma membrane, a periplasmic space and a cell wall (from inside to outside). Polysaccharides, mostly glucans and mannans, are the main constituents of the cell wall. It was recently shown that the cell wall is involved in the uptake of ergosterol (a typical sterol found in fungi which is structurally similar to cholesterol) by binding the sterol [143]. Due to the structural similarities of cholesterol and ergosterol, we expected a similar interaction with the cell wall of yeast cells. In experiments with *S. cerevisiae*, alignment of the cells on the patterns was observed, most probably due to an insertion of the cholesterol into the cell wall. In an additional experiment, we added cholesterol-PEG-FITC to yeast cells in suspension to test if the cell wall of the yeast cells interacts with the molecule. Indeed, the yeast cells were highly fluorescent after 90 min incubation at room temperature with cholesterol-PEG-FITC, but remained non-fluorescent with the same concentration of fluorescein (see figure 3.5). The immobilized yeast cells could withstand low flow rates of approximately 0.5 $\mu\text{l}/\text{min}$ but were easily released at higher flow rates.

The size of the cells is certainly an important factor that determines the shear stress that the immobilized cells can withstand without being washed away. Hence, the larger size of mammalian cells is probably the reason that we were not able to reliably immobilize U937 suspension cells under flow.

3.3.5 Summary and outlook

In summary, a simple protocol for immobilization of various liposomes and living organisms was demonstrated. The method is useful for long-term studies where automated imaging requires fixed positioning, and where repeated additions of chemical agents and washing steps are needed. Of particular interest is that the surrounding fluid can be rapidly exchanged

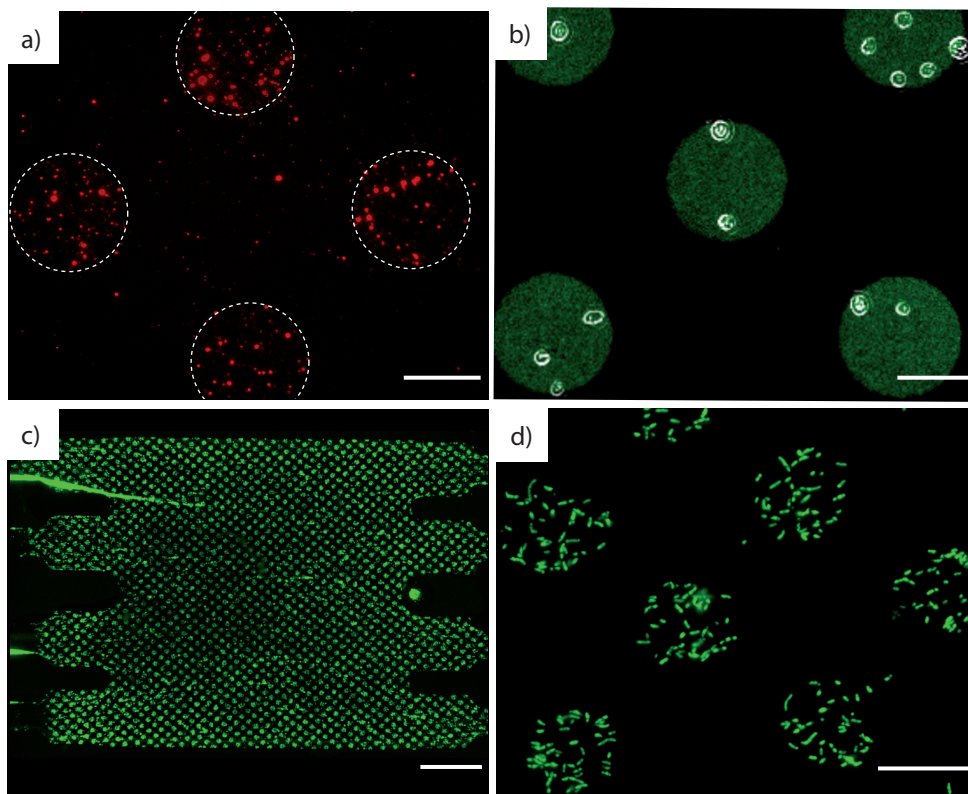


Figure 3.4: Immobilization of different organisms. a) Immobilized vaccinia viruses. Viruses were labelled with R18 dye for visualization and the patterned spots are outlined with dashed lines. Scale bar: $20\ \mu\text{m}$. b) Yeast cells on cholesterol-modified spots. The image is an overlay of a background subtracted bright field image (yeast cells in white) and a fluorescent image (FITC-labelled streptavidin to visualize patterns in green). Scale bar: $30\ \mu\text{m}$. c) Low-magnification image of the microfluidic chamber with *E. Coli* immobilized mainly on the printed spots. Scale bar: $400\ \mu\text{m}$. d) With a higher magnification, single GFP expressing *E. Coli* cells can be identified on the immobilization spots. Scale bar: $30\ \mu\text{m}$.

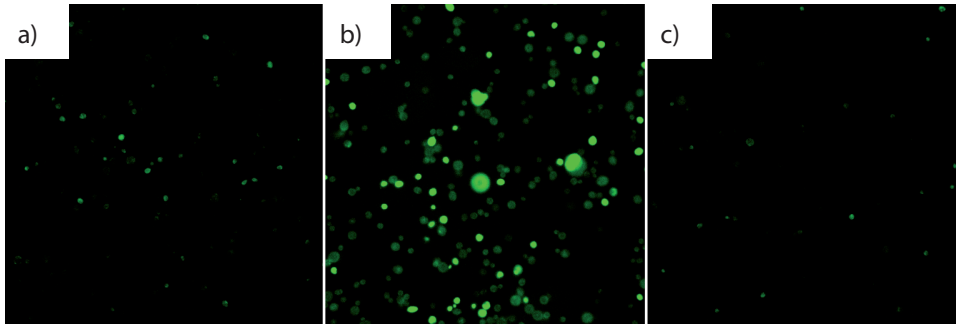


Figure 3.5: Staining of yeast cell membranes. Yeast cells were incubated for 90 min at room temperature with a) PBS, b) 5 μM cholesterol-PEG-FITC in PBS and c) 5 μM fluorescein in PBS. Images show cells after 3 washing steps with PBS. Only the yeast cells incubated with the tagged cholesterol exhibit a higher fluorescence than the autofluorescence of yeast cells.

(within seconds). Hence, kinetic studies can be performed with a high time resolution. A further interesting application is the investigation of the influence of flow and shear stress on artificial and cell membranes. Most importantly, the immobilization protocol was a pre-requirement for the liposome-cell fusion studies described later in this thesis.

4 Permeation of tetracyclines across lipid bilayers

For many drugs including antibiotics such as tetracyclines it is crucial that the molecule has the ability to quickly and passively permeate lipid membranes. Hence, the understanding of the permeability in relation to the molecular structure is an important aspect to rationally design novel pharmaceutically active compounds with high bioavailability. Here, a versatile method to study the kinetics of tetracycline permeation across liposome membranes on a microchip is presented. Liposomes are immobilized onto the glass surface in a stripe pattern via an avidin-biotin bond and covered by microchannels to allow continuous delivery of tetracycline and buffer. The fluid flow provides a constant concentration profile and thereby resembles the drug transport via blood in the human body. Total internal reflection fluorescence (TIRF) microscopy was used to image the formation of a fluorescent drug-europium complex inside the liposomes. The permeation rates of various tetracyclines were investigated and the results compared to a conventional method (water-octanol partitioning). The findings largely confirm the correlation between membrane permeability and lipophilicity of the permeating molecules (Overton's rule). However, slight deviations reveal that lipophilicity is an important but not the exclusive parameter for the prediction of permeation. The method is fast enough to study the permeation of unstable tetracyclines such as rolitetracycline. Additionally, with the use of different cholesterol concentrations, the influence of membrane composition on the permeation rate can be investigated conveniently. The microfluidic approach can be easily applied to investigate the kinetics of other processes such as ligand-membrane receptor association and dissociation, provided that the process can be visualized by means of fluorescence spectroscopy.

This chapter was published in:

Kuhn, P., Eyer, K., Allner, S., Lombardi, D., Dittrich, P. S. (2011). A Microfluidic Vesicle Screening Platform: Monitoring the Lipid Membrane Permeability of Tetracyclines. *Analytical Chemistry*, 83(23), 8877-8885.

4.1 Introduction

In the search for a novel drug candidate, it is essential to find compounds with superior pharmacodynamic properties. However, to evaluate the applicability of a drug, further properties have to be considered. For example, the absorption of an orally administered drug corresponds to its ability to cross biological membranes via membrane protein-mediated (active) and/or diffusion-based (passive) mechanisms [10]. Indeed, many drugs diffuse passively

through lipid bilayers [144] and their protonation behavior along the pH gradient of the cell is sufficient to explain accumulation in living organisms [145–147].

Passive permeation can be predicted by a widely accepted simple rule, introduced by Overton about 110 years ago, which states that the permeation rate corresponds to the lipophilicity of the compound. Hence, the permeation coefficient can be estimated by measuring the partition coefficient of the compound from the aqueous into the organic phase (typically, 1-octanol). While this method seems to provide a good approximation for some (uncharged) compounds, deviations from Overton's rule have been reported recently [16, 148].

In the last few decades, alternative methods have been established such as the parallel artificial membrane permeability assay (PAMPA) or diffusion assays across cell monolayers (typically Caco-2 cell line or MDCK). While cell-based assays are more comparable to the real situation in the body, they allow only limited throughput, are labor-intensive and are therefore more expensive. Additionally, the drug may be metabolized during passage and they cannot discriminate between passive and active transport. PAMPA, on the other hand, is a cost-efficient and commonly applied method in which a solution containing the drug is separated from an initially drug-free buffer by an artificial membrane [18]. Residual solvent in the membrane, however, may influence the permeation kinetics and the relevance of this method for drug transport into cells is still under discussion [149, 150]. The cell-based assay and PAMPA methods also face another limitation, the presence of an unstirred water layer (UWL) which may be absent *in vivo* [151]. Concentration gradients caused by reduced mass transport close to the membrane may affect the measured permeation kinetics. Furthermore, systematic investigations to understand the influence of membrane composition on the permeation rate are not feasible using the current techniques.

Recently, novel methods have been proposed to reveal insights into the mechanism and kinetics of passive permeation [57, 152]. In particular, the use of artificial lipid membranes (most often, unilamellar vesicles) has proven to be very helpful as they provide a very realistic cell membrane model, where natural transporter systems and metabolizing enzymes are absent, or can be selectively reconstituted. As discussed in section 1.4.2.1, Malmstadt and co-workers presented a method to study passive transport of molecules into giant unilamellar vesicles (GUVs) [88]. Fluorescently tagged molecules (polyethylene glycols) entering the vesicles could be monitored in real-time using confocal fluorescence microscopy. However, the bound fluorophore certainly influences the diffusion across membranes and limits the applicability and relevance of the method. In a similar approach, Grime et al. visualized the permeation of carboxylic acids across a lipid membrane by means of a pH-sensitive dye [16]. This technique was also used by Kuyper et al. to detect the permeation of protons into single vesicles [87]. Alternatively, stopped-flow measurements can be used [17], but this method requires fairly large amounts of reagents and is difficult to parallelize.

Here a novel method is presented to determine the permeation rates of small molecules into vesicles [17]. By using a microfluidic device with vesicles immobilized onto the glass bottom and delivering the drug by laminar flow (4.2), a situation close to that in the human body is simulated [151], and experimental uncertainties of the standard methods associated with the UWL are eliminated. The performance of the device is shown for tetracycline antibiotics (see figure 4.1), which are frequently used for the treatment of infections such as syphilis, acne and lyme disease. Tetracycline was originally extracted from soil-dwelling

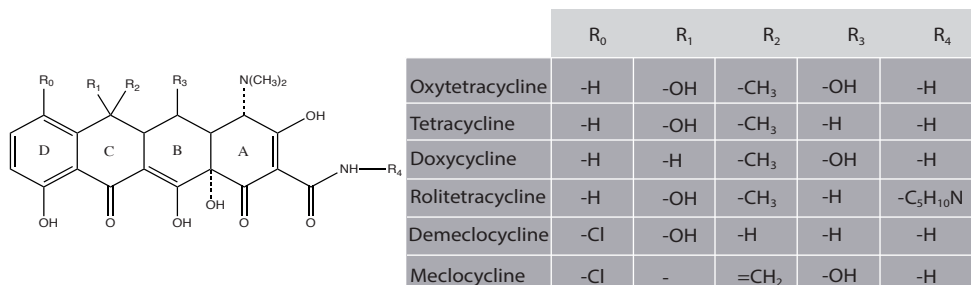


Figure 4.1: Structure of tetracyclines

bacteria (*Streptomyces*), but nowadays second and third generation tetracyclines are obtained using semi-synthetic approaches [153, 154] and more recently by total synthesis [155]. All compounds are structurally similar to the first generation of tetracyclines, but chemical modifications of the side groups have improved the drug efficacy and cell uptake.

Imaging of the tetracycline permeation was achieved when the drug binds to europium that was enclosed inside the vesicles. The resulting red fluorescent complex was monitored by TIRF microscopy. Both the emergence of fluorescence only after complexation with the membrane-permeating molecule and the use of TIRF microscopy ensured the highly sensitive monitoring of permeation. The low background signal was detected at the same time at positions where no vesicles are immobilized (negative control). Finally, alterations in the flow rates of buffer and tetracycline in combination with time-resolved TIRF microscopy enable the determination of the permeation kinetics. While it has been demonstrated before that immobilized vesicles can serve as biosensors, either to enhance the signal of a binding reaction [5, 156] or as reaction vessels within microplatforms and microarrays [55, 57], the here presented system was optimized to derive kinetic constants for the permeation of europium-binding substances. Furthermore, a versatile method to create a microfluidic channel with patterned vesicles on the channel surface is described.

4.2 Materials and methods

4.2.1 Microfluidic chips with immobilized liposomes

Microfluidic chips were prepared as discussed in the materials and methods chapter in this thesis (2.3). After this preparation, stripes of bBSA were on the surface of the chip. The rest of the chip was blocked with BSA and avidin was bound to the bBSA.

Liposome preparation followed the procedure described in section 2.4 with a composition of the lipid mixture close to the one described by Stamou et al. [57]. A lipid mixture of DLPC (88 wt%), POPG (10 wt%), DSPE-PEG₂₀₀₀-biot (2 wt%), DiI (0.01 wt%), and cholesterol (0, 10, 20, or 30 mol%) was used. The lipid film was rehydrated in 300 μ M europium solution

(in 0.2 M TRIS, pH 7.4).

The content of total phosphorus (corresponding to the phospholipid concentration) in the final formulation was quantified according to a procedure published by Bartlett [157]. Read-out was done by absorption at 820 nm with a Tecan infinite m200 plate reader. Additionally, the final cholesterol concentration was measured by HPLC with UV detection. These measurements confirmed that the concentrations of lipids and cholesterol in the final liposome suspension did not significantly change (less than 10%) during the preparation process.

4.2.2 Permeation kinetics experiments

Before each experiment, the vesicles were immobilized on the chip by injecting 80 μl of the vesicle suspension (approximately 5 mg/ml) into the chip at a flow rate of 5 $\mu\text{l}/\text{min}$ for 16 min. Unbound vesicles and free, extraventricular europium were washed away with TRIS buffer at 45 $\mu\text{l}/\text{min}$ for 15 min. As shown schematically in 4.2, the chip was placed on a chip holder of an inverted microscope (DMI6000B, Leica Microsystems) for TIRF microscopy. Tetracycline and its derivatives were dissolved in TRIS buffer at a concentration of 20 μM , and EDTA at 300 μM was added to the solution to bind free europium (although free europium could not be detected outside the immobilized vesicles, see section 4.3.1). All tetracycline solutions were freshly prepared on the day of experiments, usually 1 – 4 h before (except otherwise stated). TRIS buffer and drug solutions were supplied to the two inlets via TeflonTM tubing with a syringe pump (neMESYS, cetoni, Korbussen, Germany). Fluorescence from DiI was used in order to identify patterns on the chip and to adjust the focus. At the start of the experiment, the drug was flushed at 5 $\mu\text{l}/\text{min}$ while the buffer was flushed at 45 $\mu\text{l}/\text{min}$. A total flow rate of 50 $\mu\text{l}/\text{min}$ was kept constant while the drug flow was increased by 10 $\mu\text{l}/\text{min}$ for each permeation experiment (Fig. 4.3). Thus, four subsequent permeation experiments could be performed on one chip. All data reported in this work represents an average from at least three kinetic experiments, measured on at least two different microfluidic chips.

4.2.3 Data acquisition

The TIRF microscope described in the chapter materials and methods in section 2.5 was used for all experiments. A 405 nm laser was used to excite the europium-tetracycline complex and the fluorescence emitted from the vesicles was collected by the same objective, passed through a 600 nm band pass filter and recorded with an exposure time of 500 ms and a gain of 500. Images were recorded every 5 s for 4 min. Each image series was analyzed with ImageJ by choosing a window of approximately 15 $\mu\text{m} \times 3 \mu\text{m}$ and recording the mean greyvalue over time. Figure 4.4 shows typical raw data before any processing was performed.

4.2.4 Data processing

Data obtained with ImageJ was exported and normalized. Background signal originating from the weak tetracycline fluorescence was eliminated by subtracting the fluorescence signal emitted from the stripes with immobilized vesicles from the signal emitted from the vesicle-free region. Additionally, bleaching of the europium-tetracycline complex has to be

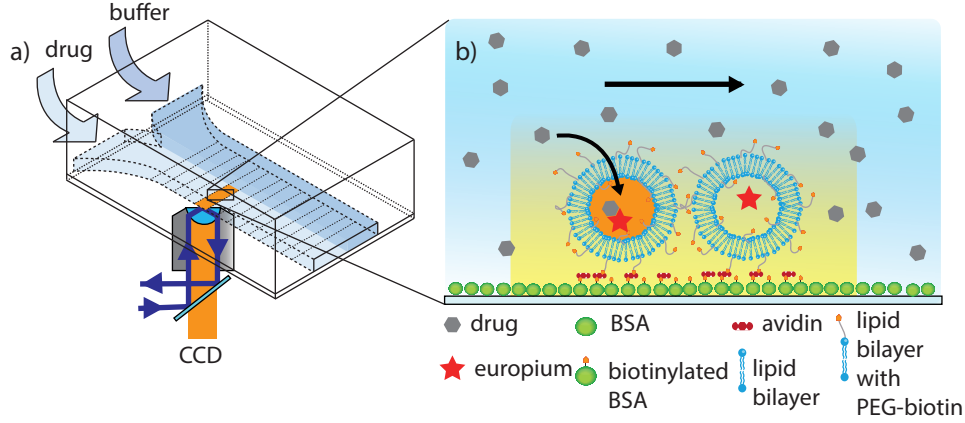


Figure 4.2: Scheme of the experimental setup and detection assay. a) A microfluidic chip, mounted on a TIRF microscope, is used to supply buffer and tetracyclines through a microchannel to vesicles immobilized on the bottom glass slide. b) Vesicles enclosing Eu^{3+} are immobilized via avidin to biotinylated BSA, which was patterned onto the surface by microcontact printing. Upon permeation of tetracycline across the lipid membrane, a fluorescent europium-tetracycline complex is formed.

considered. For this, the bleaching kinetics was obtained from immobilized vesicles containing Eu^{3+} -tetracycline complexes (in equilibrium) and the raw data was corrected accordingly.

The resulting kinetic curves $I(t)$ were fitted with a mono-exponential function to obtain the rate constants k_p :

$$I(t) = I(0) + (1 - I_{max}) \cdot e^{-k_p \cdot t} \quad (4.1)$$

The mono-exponential fit is sufficiently accurate for our measurements allowing discrimination of the global permeation rate for different tetracyclines and membrane compositions. However, it does not allow elucidating the by far more complex mechanism of permeation, i.e., it does not consider individual steps of the molecule passing the membrane [11] or for the fast complexation of the tetracyclines to europium (in the ms range, data not shown) and their diffusion to each other inside the vesicle (ms range).

For the measurements on fast-decaying drug molecules, we used a bi-exponential fitting function:

$$I(t) = I(0) + (1 - I_{max1}) \cdot e^{-k_{p1} \cdot t} + (1 - I_{max2}) \cdot e^{-k_{p2} \cdot t} \quad (4.2)$$

In order to generate size-independent kinetic parameters, apparent permeation coefficients $Perm$ were calculated from the rate constants k_p and the liposomal radius r as follows [158]:

$$Perm = k_p \cdot r/3 \quad (4.3)$$

where $r/3$ is used as an approximation for the ratio between the total inner aqueous volume of the liposomes and the total membrane area. The radius r (i.e. an average of 90 nm) was

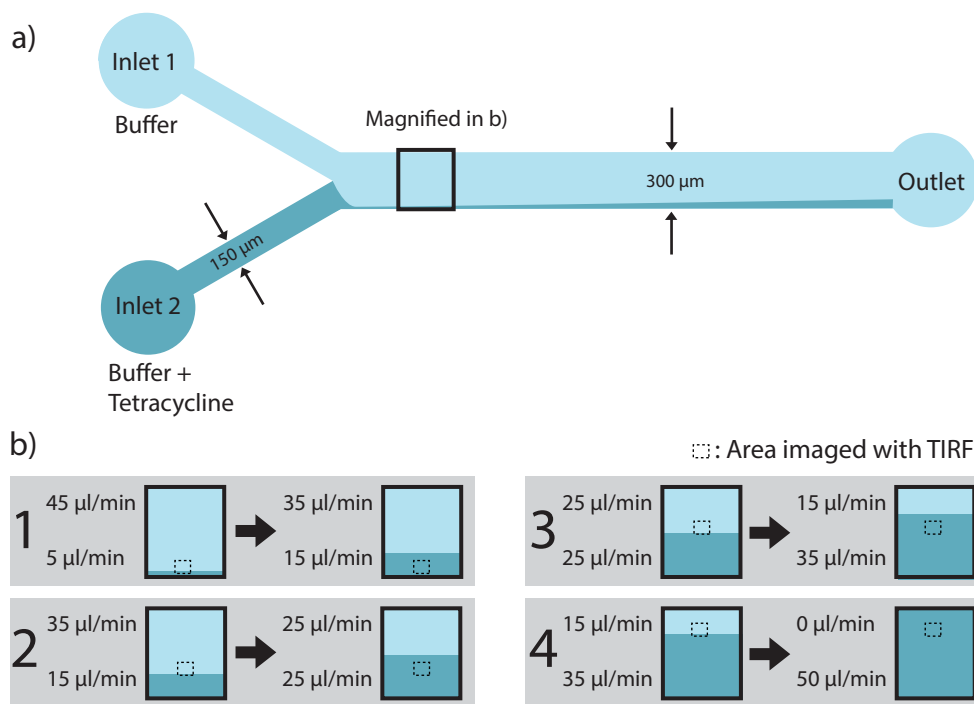


Figure 4.3: Illustration of the experiment for drug permeation kinetics. a) A microfluidic chip with two inlet channels and one main channel is used. Inlet 1 is used to deliver buffer into the main channel and inlet 2 for buffer with tetracycline. Due to low Reynolds numbers, laminar flow can be observed in the main channel. Note that the interface between the two co-flowing streams is slightly broadening downstream due to diffusion. The TIRF images for kinetic studies were taken just after co-flowing the solutions. Height of the channels: 70 μm . b) Movement of the interface by changing the flow rates of buffer and buffer + tetracycline streams. The situations before and after flow rate changes are shown. Four experiments were performed subsequently on the same chip. The rectangle indicates the area that is imaged by TIRF microscopy during the flow rate changes.

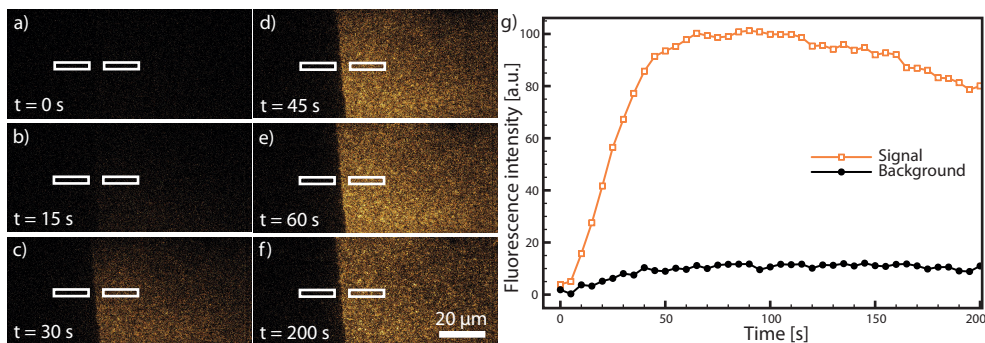


Figure 4.4: Raw data from a permeation experiment with oxytetracycline (20 mol% cholesterol in vesicles). Images from different points in time are shown on the left. a) without tetracycline no fluorescence can be observed. b) After the flow rates of oxytetracycline and buffer were changed, tetracycline can permeate into the vesicles. c)-e): the signal increases noticeably over time. f) photobleaching occurs and needs to be accounted for in data analysis. g) the graph shows the time traces of the fluorescence from the stripes with vesicles (signal) and between the stripes (background) recorded in the white-framed rectangles indicated in the images on the left. Contrast and brightness of images were increased slightly for illustrative purposes (graphical data is from non-corrected images).

estimated from the mean hydrodynamic diameter of the liposomes. The different diameters of liposomes were taken into account for the permeation rate $Perm$ (see equation 4.3) if different liposome preparations were used.

4.2.5 Stopped-flow measurements

For the stopped-flow investigations the free europium was removed by size exclusion chromatography on a Sephadex G-25 PD-10 desalting column (Amersham Biosciences, Freiburg, Germany) with 0.2 M TRIS pH 7.4 immediately before the measurements. The liposomes were diluted to a concentration of approximately 1 mg/ml. Oxytetracycline concentration was 20 μM , and 5 mM EDTA was added to the buffer to prevent the remaining extraliposomal europium from interfering with the measurements. The kinetics of oxytetracycline permeation into europium-containing liposomes were determined according to Thomae *et al.*[17] on a Perkin Elmer LS50B spectrofluorimeter equipped with a Hi-tech Scientific SFA-20 Stopped Flow device. Equal volumes were mixed at room temperature and the fluorescence was monitored at excitation wavelength (λ_{ex}) 395 nm and emission wavelength (λ_{em}) 612 nm.

4.2.6 Octanol-water partitioning

The 1-octanol-water distribution coefficient at pH 7.4 ($\log D_{7.4}$) was determined with the shake flask method with a shaking time of 1 h. Tetracycline stock solutions (1 mM) were

prepared in DMSO and the final concentration in the experiments was 10 μM . Since pH has to be constant during the measurements, Teorell and Stenhagen universal buffer (SUBS) [159] was chosen as the water phase (boric acid 11.45 mM, citric acid 6.66 mM, phosphoric acid 3.59 mM, sodium hydroxide 68.6 mM, hydrogen chloride 30.6 mM, sodium chloride 120.5 mM, pH 7.4).

The amounts of tetracycline or its derivatives in the corresponding phases were determined via reversed phase HPLC (Merck Hitachi D7000, fluorescence detector L7485, Pump L7100) equipped with a LiChrospher 100 RP-8 column (5 m, 125x4 mm, Merck). The probes were diluted with pure methanol 1:10. The mobile phase flow rate was set at 1.0 ml/min. The mobile phase consisted of an aqueous phase (75 mM sodium acetate, 35 mM calcium chloride, 25 mM Na_2EDTA , pH 6.5) and an organic phase (HPLC grade methanol:water 95:5)[160]. Both were degassed for 15 min in an ultrasonic bath. The amount of organic phase was increased linearly from 30 to 50

The tetracycline peaks eluted early in the chromatogram, which was convenient because remaining amounts of 1-octanol would disturb the analysis of retained peaks and would make the comparison of the water and octanol phase peaks difficult. The signal was linear in the concentration range observed as tested with tetracycline. Each tetracycline compound was measured three times to obtain averages.

4.3 Results

4.3.1 Vesicle immobilization and device operation

The principle of the screening platform is depicted in figure 4.2. The microfluidic device consisted of a microchannel with two inlets, imprinted in a PDMS substrate and covered by a glass slide. Inside the microchannel, vesicles with a diameter of about 180 nm were immobilized in a stripe pattern onto the bottom glass slide. To achieve this, stripes of bBSA were created on the glass surface before assembling the microchip. After plasma treatment, the PDMS substrate was bonded onto the glass slide, and inter-stripe areas were covered by BSA. Vesicles were immobilized via an avidin- and PEG-biotin-bond exclusively on the bBSA stripes (Fig. 4.2 b). The stripe pattern comprised clear edges as confirmed using vesicles that are additionally stained with DiI (Fig. 4.2 c). For the permeation experiments it was crucial that the vesicles remain intact and immobilized on the surface. To confirm that they were not washed away due to shear stress under high flow rates we investigated which flow rates were suitable for our experiments. We observed constant fluorescent signals over the entire surface from the DiI-stained vesicles over several minutes with flow rates less than 150 $\mu\text{l}/\text{min}$, while for higher flow rates a significant reduction of signal was found. Therefore, a maximum flow rate of 50 $\mu\text{l}/\text{min}$ was used.

The detection of tetracycline permeation was facilitated by the enclosure of europium salt in the vesicles. Like many other lanthanides, europium forms luminescent complexes with organic ligands [161]. The light is absorbed by the organic ligand (λ_{ex} 370 – 400 nm for tetracycline and its derivatives), and due to a resonance energy transfer to the coordinating lanthanide ion, the fluorescence of the lanthanide is increased (by a factor of ten at λ_{em} 610 – 670 nm) [162]. While molecules from the tetracycline family are able to permeate the

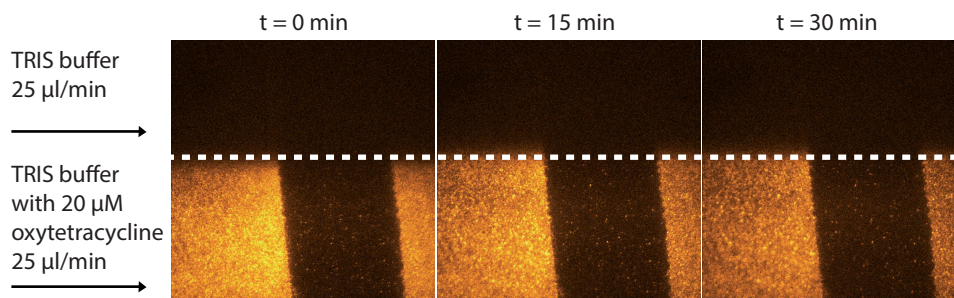


Figure 4.5: Diffusion interface of buffer and tetracycline in buffer solution. Images were taken for 30 min with 1 min interval (other acquisition parameters are equal to those described in the main text). The diffusion of drug into the buffer flow, and thus the liposomes underneath the buffer, is negligible over time. Decreases in fluorescence of the liposomes are due to photobleaching.

lipid membrane, neither the europium ions nor the europium complex can cross it and remain enclosed in the vesicle (for stability tests, see below). Furthermore, the dissociation of the europium-tetracyclines complex was considered negligible [163].

To verify that there is no absorption or unspecific binding of europium to the bBSA, we loaded the BSA/bBSA patterned chip with free europium solution. After incubation, washing and finally supplying tetracycline, no fluorescence could be detected. In a further control fluorescence from immobilized vesicles, pre-filled with the complex, was constant over time, but vanished after supply of a 1 %v/v TritonX-100 solution, which is known to destroy vesicles.

The microfluidic channel comprised two input channels, one of which was used to supply the tetracyclines and the other channel to supply the buffer solution (Fig. 4.3). The co-flowing streams created a distinct interface (Fig. 4.5) due to the laminar flow regime (the Reynolds number under our experimental conditions was 0.45) that remains stable at the same position for long time (at least up to 30 minutes).

By reducing the buffer flow rate and increasing the tetracycline flow rate, the interface could be moved to study the uptake of tetracycline. The switching time of the fluids was far below a second and considered negligible for the kinetic experiments described herein. On a single chip the flow rates were changed four times, and each time the kinetics of tetracycline permeation of the previously drug-unexposed region could be measured. Usually experiments on one microfluidic chip were done directly after each other. However, for longer time delays between the measurements (see Fig. 4.6), no changes were observed even when buffer is flushed constantly through the channel. This proves the stability of the liposomes in the chip and their tightness to europium, since the lack of stability might lead to changes in the permeation rates. The variation between measurements on different chips was also tested and found to be very low (see Fig. 4.7).

After the tetracycline solution was flushed through the channel, fluorescence arose from vesicles immobilized below the stream, while the regions without vesicles remained dark (Fig. 4.4). For data analysis, photobleaching of the complex and the weak fluorescence of

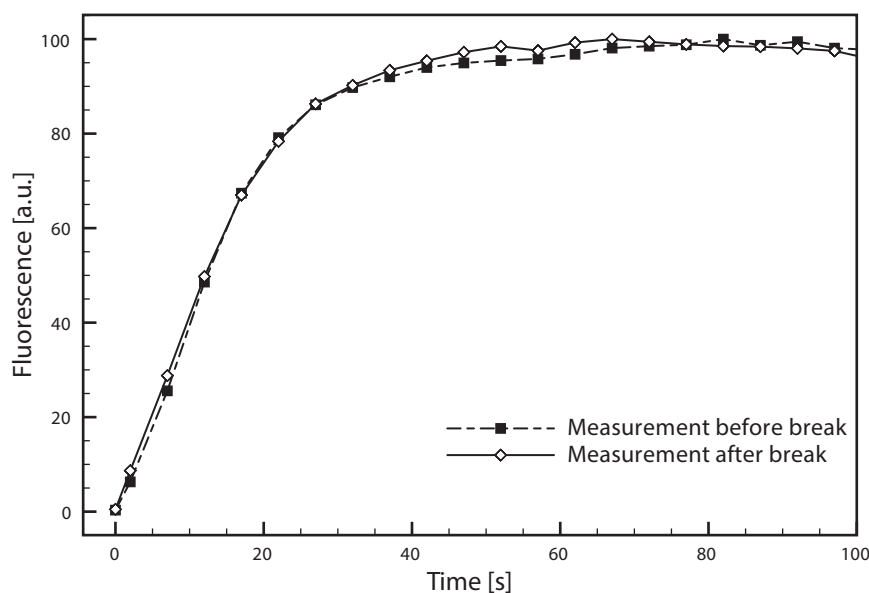


Figure 4.6: Stability of liposomes over time. The graph shows the comparison of two kinetic measurements on the same chip with a 30 min time delay. During this time, buffer and oxytetracycline are constantly flushed through the channel (total flow rate $50 \mu\text{l}/\text{min}$). No change can be observed.

the free tetracycline molecules had to be considered. The latter was reduced significantly by using TIRF microscopy since excitation only occurs within the evanescent field (about 250 nm) above the glass surface where mainly the immobilized vesicles are present [87]. To minimize photobleaching we reduced the light exposure time and measured periodically. Light exposure and image acquisition every 5 seconds was found to be a good compromise between time resolution and photobleaching. The remaining photobleaching was determined by measuring the decrease in fluorescence signals of vesicles with enclosed europium tetracycline complex. Note that the photobleaching measurement was taken for every type of tetracycline-europium complex individually.

4.3.2 Quantitative structure-permeation analysis of tetracycline derivatives

After establishing the device operation protocol, kinetic data for several commercially available tetracycline derivatives were determined for vesicles composed of DLPC/POPG and 20 mol% cholesterol. The increase in fluorescence was specific for a given complex and sufficiently large to be clearly distinguished from the weak fluorescence of the free drug for most tetracycline-europium complexes except for metacycline and minocycline. Minocycline appeared unable to form a complex with europium, and the metacycline-europium signal was too low. Figure 4.8 shows representative kinetic curves including fitting functions (equation 4.1) for tetracycline and four different derivatives. The fastest rate was found for

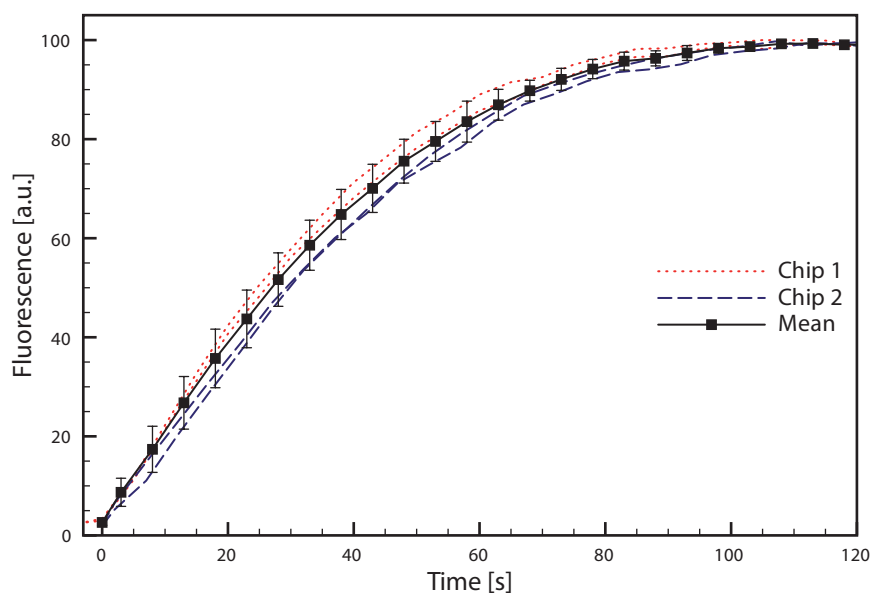


Figure 4.7: Comparison between kinetics measured on different microfluidic chips. The dotted line represents two kinetics measured on chip 1, while two kinetics curves measured on another chip are shown with a dashed line. Both curves are within the error of the mean kinetic curve (rolitetracycline 20 min after preparation; same liposomes used on both chips; different rolitetracycline preparations).

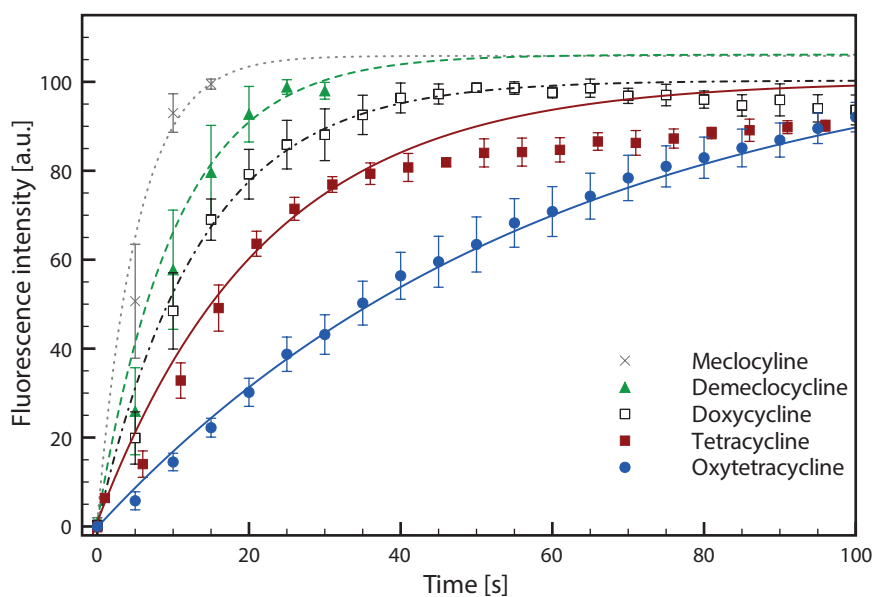


Figure 4.8: Fluorescent intensity measurements (after background and photobleaching correction) for several tetracyclines. The cholesterol composition was held constant at 20 mol% for the experiments. The fluorescence intensities of mecloicyline and demecloicyline decreased very rapidly after reaching a plateau and thus data points are not shown for ease of illustration.

mecloicyline and the slowest for oxytetracycline. It should be noted that mecloicyline is commercially only available with the counterion sulfosalicylate, which has been reported to complex europium as well [164]. However, the lack of signal in control experiments with pure sulfosalicylate revealed that sulfosalicylate was not able to cross lipid membranes and thus we fully attributed the signal the mecloicyline-europium complex.

Figure 4.9 summarizes the results for five tetracyclines and correlates the permeation with the distribution coefficients obtained from conventional water-octanol partitioning experiments. In agreement with Overton's rule, the lipophilicity correlates very well to the measured permeability, i.e. a highly lipophilic drug crosses the lipid bilayer faster than a less lipophilic compound. Furthermore, we compared the results with predictions for lipophilicity obtained from various different calculation methods available at VCClab.com [165] (4.1). Although the calculated lipophilicities mainly follow the experimental trend (except for rolitetracycline), standard deviations are very large.

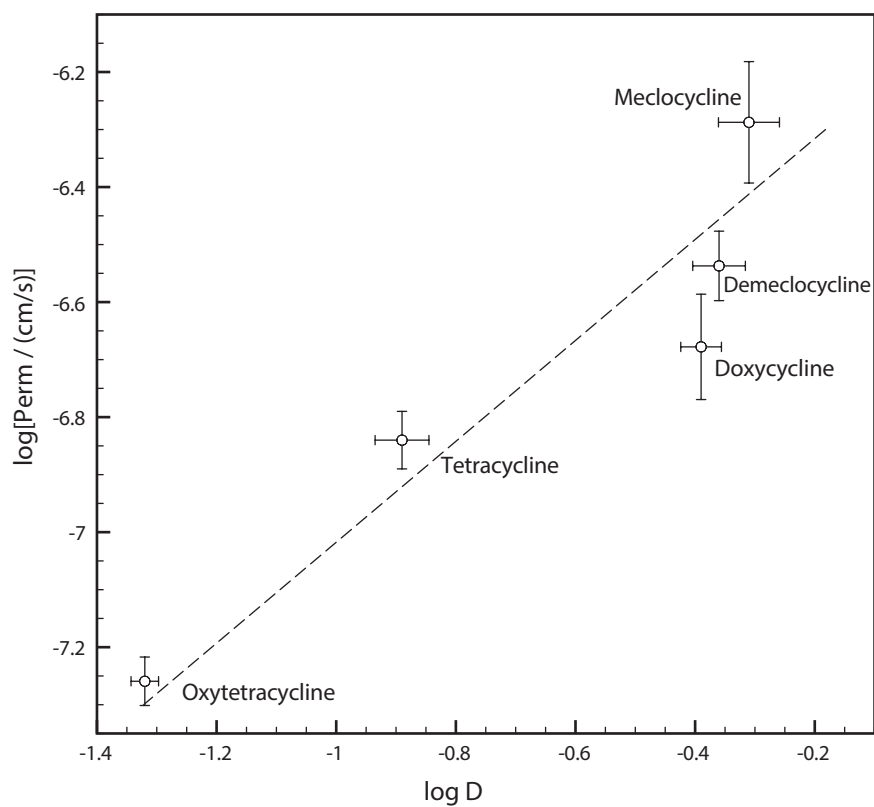


Figure 4.9: Comparison of the results from the chip method for several tetracycline derivatives and correlation of the data with lipophilicity values obtained by the octanol-buffer partition system. Following Overton's rule, the permeability correlates with the lipophilicity.

Table 4.1: Mean apparent permeabilities and standard deviations for all measured tetracycline derivatives and their corresponding lipophilicity.

	Apparent permeability (20 mol% cholesterol in liposomes)		Lipophilicity Measured by octanol-water partitioning		Lipophilicity Calculated from VCClab.com, Average logP
	$-\log$ [$Perm(\text{cm/s})$]	σ	logD	σ	logD
Oxytetracycline	-7.26	0.042	-1.32	0.023	-1.68 ± 0.66
Rolitetra-cycline	-7.20	-	-	-	-0.03 ± 0.41
Tetracycline	-6.84	0.05	-0.89	0.045	-0.82 ± 0.34
Doxycycline	-6.68	0.092	-0.39	0.034	-0.65 ± 0.59
Demeclocycline	-6.54	0.06	-0.36	0.044	-0.50 ± -0.46
Meclocycline	-6.29	0.106	-0.31	0.051	-0.14 ± 0.72

Because the microfluidic method proved to be reliable, we further demonstrated its potential using two experiments where routine methods are not applicable.

4.3.3 Permeation rates for unstable compounds

Some tetracyclines, such as rolitetra-cycline and lymecycline, hydrolyze once they are dissolved in buffer [166]. When determining the permeation rates of unstable molecules, the method has to be fast concerning sample preparation and most importantly, data acquisition to ensure that the ratio of intact to degraded molecules is approximately constant during the measurement. These requirements are satisfied using our method, where the sample preparation takes a few minutes and the data acquisition only takes 4 min for one kinetic measurement. Figure 4.10 shows kinetic curves for rolitetra-cycline at three different times after sample preparation.

The data revealed that the permeation rate of rolitetra-cycline is slow just after dissolving it, and increases with time. This indicates that the molecule decomposes into tetracycline and a smaller molecule, which presumably does not form a fluorescent complex with europium. The curves were fitted to a bi-exponential function to extract the permeation rate for tetracycline and the intact rolitetra-cycline.

The permeation rate of rolitetra-cycline was extrapolated to $\log [Perm(\text{cm/s})] = -7.20$. The pre-exponential factors represent the concentration of both species, from which the decay curve (Fig. 4.10 inset) and the half-life of rolitetra-cycline (89 min at $pH = 7.4$, room temperature) are derived. This was also confirmed by UV absorption measurements (data not shown) for rolitetra-cycline at room temperature and compares well with literature (43 min at 35 °C) [167]. Rolitetra-cycline has been considered as a pro-drug of tetracycline having a better water solubility,[166] but the originally assumed improved membrane permeability of such N-Mannich bases could not be confirmed for rolitetra-cycline by our measurements.

Additionally, it should be noted that in the case of tetracycline the permeation kinetics deviated from the expected mono-exponential behavior. It can be seen in Fig. 4.8 and

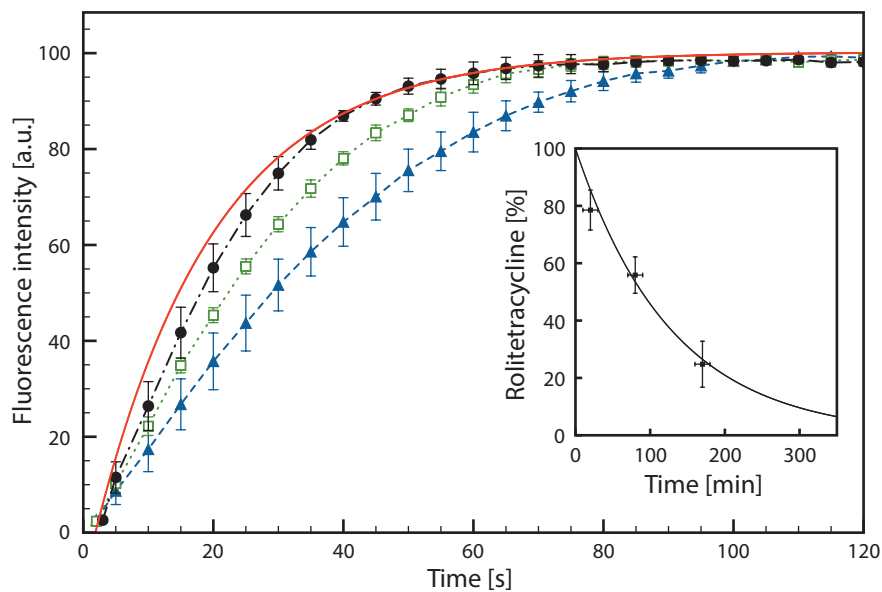


Figure 4.10: Kinetic curves for rolitetracyclines are shown measured at different times after sample preparation. Fresh rolitetracycline (20 min after preparation of solution), shown in blue triangles, permeates slower than rolitetracycline after 80 min (green squares) and 170 min (black circles). For comparison, the solid red line shows the fit for tetracycline with the same liposome composition (20 mol% cholesterol). Inset shows decreasing percentage of rolitetracycline in the solution (calculated from bi-exponential fits) together with a mono-exponential decay fit, yielding a half-life of 89 min at room temperature.

Fig. 4.11, that fast and slow permeation rates occur, with increasing percentage of the slow kinetic with time. These findings suggest a reaction or rearrangement into another derivative. However, so far it was not possible to obtain structural information by NMR spectroscopy or another method to confirm this assumption.

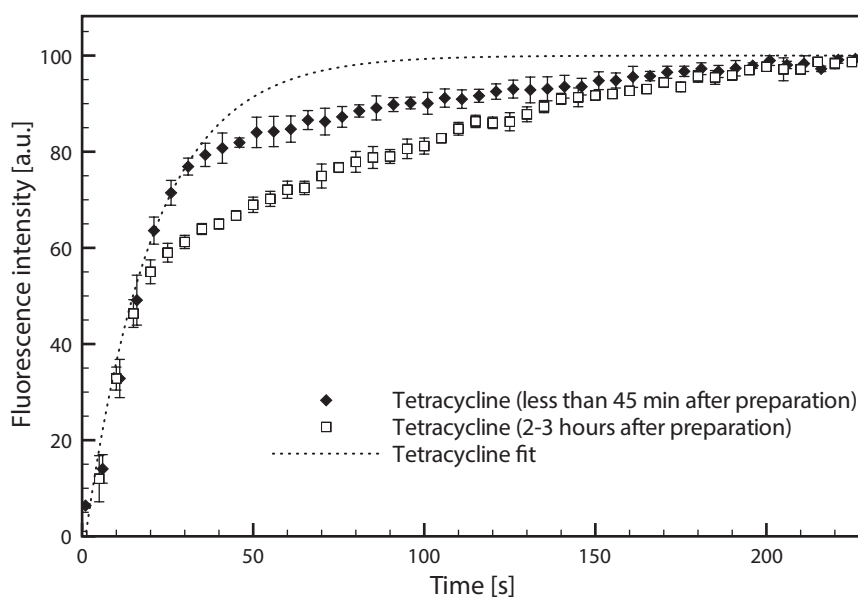


Figure 4.11: Tetracycline seems to degrade quickly (in less than 30 min) and is therefore difficult to use in permeation experiments.

4.3.4 Influence of Cholesterol on Permeation Kinetics

The method enables systematic studies of the permeation rates for varying membrane compositions. This ability is shown by investigating the influence of cholesterol content in the membrane on the permeation rate of oxytetracycline. Figure 4.12 a) shows the kinetic curves of oxytetracycline for four different membrane compositions containing between 0 and 30% cholesterol. The experiments revealed that vesicles without cholesterol had the fastest permeation rate and there was a linear decrease of the permeation rate with increasing cholesterol concentration. These findings are in agreement with previous studies, in which the presence of cholesterol reduced the permeability of the membrane [168, 169].

The results were compared to stopped-flow measurements in a commercial instrument, and similar permeation coefficients were determined (see Figure 4.12b)). Additionally, the standard deviations are comparably low for both methods. There are a number of other

advantages offered by the microfluidic method. When compared to stopped-flow measurements, the sample consumption is significantly reduced (from milliliters to microliters) and has the potential to parallelize the measurements of various vesicle compositions. In general, the approach can be used to study very slow kinetics as well as the diffusion of compounds out of vesicles.

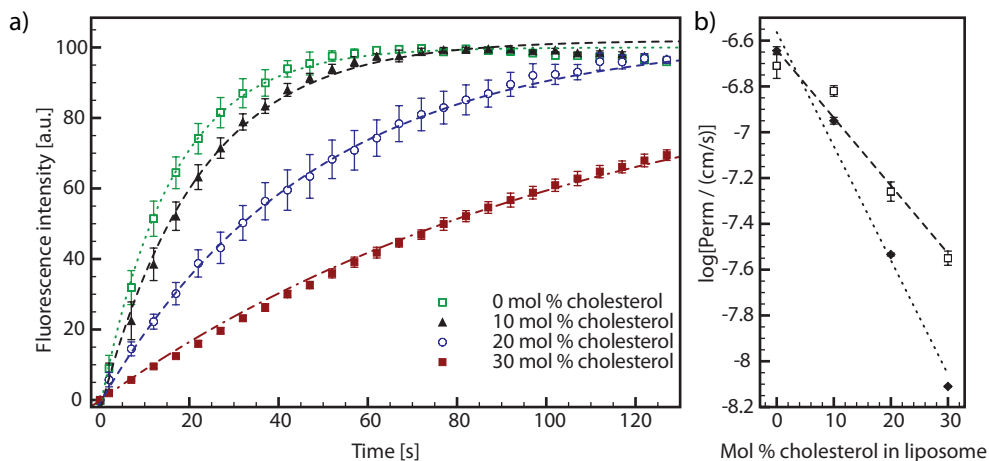


Figure 4.12: Influence of cholesterol on membrane permeability of oxytetracycline. a) Fluorescence intensity measurements (after background and photobleaching correction) for different liposome compositions, i.e., with different cholesterol amounts and respective monoexponential fits. Membranes with higher cholesterol proportions, show slower kinetics than the one that is without cholesterol. b) The apparent permeation shows a linear relationship with the amount of cholesterol added. Stopped flow measurements (black diamonds) are comparable to the permeabilities measured on-chip (open squares).

4.4 Conclusion and outlook

In conclusion, a new method was presented for measuring permeation coefficients of tetracyclines into vesicles. This advanced method has several benefits compared to the established methods. It allows the measurements of slow and fast kinetics with a good temporal resolution, requires only short measuring times, consumes very small volumes of drug solution and vesicle suspension, and allows sensitive detection at low concentrations using TIRF microscopy. The method can be easily parallelized to measure different conditions such as drug concentration or different pH levels simultaneously. This is important because a linear dependency for concentration and permeability is only true for neutral molecules or charged ones at low concentrations [10]. Compared to a similar technique based on surface plasmon resonance (SPR) [170], the method presented here is able to differentiate between molecules that are either binding to or diffusing into the membrane and those that permeate across the membrane. Additionally, it can be used to measure the release of compounds out of vesicles.

The major strength of this approach is the ability to reliably resemble the *in vivo* situation since the drug concentration is kept constant and no UWL is present.

Furthermore, artificial cell-like vesicles could be prepared with various lipid compositions and embedded membrane proteins, so that their individual influences on permeation behavior could be investigated systematically. This will also allow a better understanding of the permeation mechanism. Besides permeation studies, the device can be easily applied to investigate the kinetics of other processes such as membrane receptor-ligand association and dissociation or activities of membrane enzymes, provided that the process can be visualized by means of fluorescence spectroscopy.

5 Delivery of enzymes into single cells by liposome fusion

Liposomes, and especially negatively charged pH -sensitive liposomes, have been used successfully to deliver molecules into the cytoplasm of cells. These liposomes are designed to release their cargo into the cytoplasm after fusion with the endosomal membrane. Much work has been dedicated to identify fusogenic lipid mixtures, but mechanistic and systematic studies to understand the underlying fusion process are challenging.

In this chapter, a microfluidic device is presented that facilitates the fusion of a small set of liposomes with single cells. This is accomplished by the co-immobilization of both fusion partners on top of each other. This approach circumvents the need to attach liposomes to the cell membrane prior to changing the environment to a fusion buffer and allows the fast supply of a fusion trigger. Liposome-cell fusion is verified with two assays, a dequenching assay with fluorescent membrane and content dyes and an enzymatic assay where β -galactosidase is delivered into the cytosol.

These studies could help to reducibly test for lipofection efficiency, which could ultimately lead to novel, cell-targeting therapeutic strategies. Furthermore, the setup could also be used to deliver minute amounts of enzymes into single cells, possible in a microarray format.

5.1 Introduction

Liposomes have been studied extensively in the last decade as carriers for therapeutic agents, e.g. for cancer therapy [3, 9]. While hydrophobic and amphiphilic drugs can permeate lipid bilayers and can be released over time from the liposome, water-soluble drugs, DNA and peptides are retained in the interior because of their inability to cross the membrane. Hence, the cargo of the liposome needs to be released at the target tissue, preferentially inside the cytosol of the cell. One class of liposomes that is used in this context is the pH-sensitive liposome, where a low pH triggers membrane destabilization and/or fusion [171]. pH-sensitive liposomes were initially designed to release their therapeutic molecules in cancerous tissues, triggered by the mildly acidic pH in these environments [30]. Yet, it proved difficult to design liposomes that release the cargo due to a rather small change in pH, which are otherwise stable in vivo. However, since targeted liposomes are usually uptaken by endocytosis, pH-sensitive liposomes can be triggered to release their cargo by the low pH inside the endosome [172]. During endocytosis, ATPases transport protons into the endosomal compartment, which lowers the pH in late endosomes to pH 5. The fusion also circumvents the degradation of liposomes by lysosomes that fuse with late endosomes in the cell.

Especially negatively charged liposomes have been used successfully to deliver molecules into the cytoplasm of cells [173]. These liposomes are designed to release their cargo into the cytoplasm after fusion with the endosomal membrane, which is very similar to the pathway that several lipid enveloped viruses use [37]. In the case of anionic liposomes, the pH-sensitivity originates from the combination of unsaturated phosphatidylethanolamines (PE), such as dioleoyl phosphatidylethanolamine (DOPE), with acidic amphiphiles to stabilize the bilayer at neutral pH [33, 34]. The protonation of the amphiphile inside the endosome leads to a destabilization of the membrane leading to fusion.

Much work has been dedicated to identify these fusogenic lipid mixtures, but mechanistic studies to understand the underlying fusion process are challenging. Imaging of rapid kinetic processes inside the endosome is very complicated, even with sensitive imaging, like confocal microscopy and total internal reflection fluorescence microscopy (TIRF-M), because the acidification cannot be synchronized. For this reason, many viral fusion experiments start with the binding of virus particles to the membrane and are followed by an initiation of the fusion by a pH buffer [103], see also chapter 6. However, this is not feasible when liposomes bear the same negative charge as the plasma membrane. Therefore, a technique to bring a defined number of liposomes in close contact to a cell, and to induce the fusion at a predefined time is highly desirable.

Microfluidic technology offers many advantages for lipid bilayer fusion studies; the most important one is the high control over the chemical conditions in the channel. Triggers, like pH or fusogenic molecules, can be easily delivered to the lipid bilayers and fusion observed immediately by optical means [103]. Additionally, microfluidic devices also have recently been shown to be superior in cell handling over conventional techniques [50]. Especially the defined trapping of single cells at predefined locations has extended the tool-box for single cell experiments [125, 174] and allowed the rapid exchange of buffers surrounding the cells without inducing movement of the cells.

In this study, a microfluidic device is presented, which enables the fusion of a small set of liposomes with single cells. This is accomplished by the co-immobilization of both fusion partners on top of each other. This approach circumvents the need to attach liposomes to the cell membrane prior to changing the environment to a fusion buffer and allows the fast supply of a fusion trigger. Furthermore, the alignment allows the use of TIRF microscopy, which is highly sensitive and also greatly reduces background fluorescence. Liposome-cell fusion is verified with two assays. First, membrane fusion is monitored using a dequenching assay with fluorescent membrane and content dyes. Second, the setup is used to deliver β -galactosidase into the cytosol, which is verified with a gene transfection kit. This enzyme itself is available in large quantities and high purities, rendering controls possible and affordable. β -galactosidase has also been used as a model enzyme where the delivery of enzymes by gold nanoparticles was assayed [175].

5.2 Methods

5.2.1 Cell lines

Chinese hamster ovary (CHO) cells were grown in Ham's F12 nutrient mix supplemented with 10 % fetal bovine serum and 1 % penicillin/streptomycin (all Invitrogen) at 37 °C and 7 % CO₂ atmosphere. For experiments, cells were washed twice with PBS and afterwards suspended in enzyme free cell dissociation buffer (Invitrogen).

U937 histocytic lymphoma cells (DSMZ, Germany) were grown in RPMI 1640 media containing 10 % fetal bovine serum and 1 % penicillin/streptomycin (all Invitrogen) at 37 °C and 7 % CO₂ atmosphere. For experiments, cells were collected and pelleted (5 min, 700 g). Cell culture media was aspirated and cells were gently resuspended in PBS containing freshly prepared ImaGene Red C₁₂RG substrate reagent (33 μM) and 300 μM chloroquine. The cells were then incubated in this mixture for 30 minutes at 37 °C to assure sufficient incorporation of the dye into the cellular membrane. After incubation, free substrate was removed by centrifugation and the cells were resuspended in PBS containing 300 μM chloroquine.

5.2.2 Microfabrication

Microfluidic chips were prepared as discussed in chapter (2.3) in this thesis. After this preparation, chips with dot or square patterns of bBSA were on the surface of the chip. The rest of the chip was blocked with BSA. The surfaces inside the microfluidic devices were functionalized as previously described in chapter 3, resulting in cholesterol tethered to the surface.

5.2.3 Liposome preparation

Large unilamellar vesicles (LUV) were prepared by lipid film hydration (see Table 5.1), as described in chapter 2.4.

Table 5.1: Liposome formulations used in this study

	Lipid mixture	Content	Pore size of extrusion membrane
I	DOPE/DOPG (83/17 mol %), + approx. 5 mol % R18	100 mM calcein in wa- ter/PBS (1/1 vol %)	200 nm
II	DOPE/DOPG (83/17 mol %)	100 μM calcein and 400 μg/ml β-galactosidase	400 nm
II	DOPC	100 μM calcein and 400 μg/ml β-galactosidase	400 nm

5.2.4 Immobilization of liposomes and cells

Approximately 100 μl of liposome suspension was flushed through the microchip at a flow rate of 5 $\mu\text{l}/\text{min}$. Liposomes that were not captured by the tethered cholesterol were washed away by flushing PBS (10 min, 20 $\mu\text{l}/\text{min}$). 100 μl cell suspension (1mio cells/ml) was introduced into the reservoir and cells were withdrawn into the chip at 5 $\mu\text{l}/\text{min}$ for 2 min. The reservoir was then washed with PBS three times and the flow rate decreased to 2 $\mu\text{l}/\text{min}$.

5.2.5 Fusion of liposomes and cells

After the immobilization of liposomes and cells, fluorescent and brightfield images were taken. At this step, PBS (pH 7.4) was flushed through the channel and the images were used to prove that this buffer did not initiate fusion. Subsequently, the solution in the reservoir of the microchip was exchanged to the actual fusion buffer (PBS/MES pH 5 with 20 mM CaCl_2), which was then flushed through the channels (2 $\mu\text{l}/\text{min}$). In the dye dequenching experiments, imaging was started immediately after buffer exchange to observe the fast dequenching of the dyes upon fusion. In the enzyme experiments, where the ImaGene RedTM assay was used, a 5 min fusion buffer incubation period under flow conditions was set. Afterwards, the buffer was exchanged to PBS (pH 7.4) and imaging was started. Single images were also taken from cells before and after pH 5 to avoid bleaching (during kinetic studies).

5.2.6 Image acquisition

Cells and liposomes were imaged on an inverted microscope (DMI6000B, Leica Microsystems) in an incubation chamber at 37 °C, as described in chapter 2.5. TIRF was used for the dequenching experiments and epi-fluorescence for the enzyme delivery experiments. R18 was excited with a 561 nm laser and emitted light collected with a bandpass filter (600/32 nm), whereas calcein was excited at 488 nm and fluorescence was collected with a 525/35 nm bandpass filter. For both fluorophores an exposure time of 500 ms was chosen. In epi-fluorescence mode, a 40x objective was utilized to image the fluorescence from the ImaGene RedTM substrate and from the calcein, which is used as a quality control for the binding and integrity of the liposomes. Cy3 and a GFP filter sets from Leica were used together with a conventional fluorescence lamp. Images with the Cy3 filter were taken with an exposure time of 100 ms.

5.3 Results and discussion

5.3.1 Cell and liposome immobilization

The principle of the on-chip immobilization of cells and liposomes is shown schematically in figure 5.1. A two-layer microfluidic device, modified from the one described by Di Carlo *et al.* [125] was used for cell trapping. The posts for cell trapping are not in contact with the glass and hence not interfering with surface modifications and TIRF microscopy. The surface was functionalized by microcontact printing of bBSA prior to chip bonding to create binding

spots on the glass surface. The remaining surface was subsequently blocked with BSA. Avidin was bound to the biotin of the bBSA, being itself then the anchor for PEGylated cholesterol with a biotin linker. In chapter 3 it was shown that the use of immobilized cholesterol is an effective way to tether liposomes to a surface inside microfluidic channels. Cholesterol is a hydrophobic molecule that inserts spontaneously into the lipid membrane of the liposomes, therefore immobilizing them onto the surface. The PEG moiety establishes a certain distance to the surface as well as water solubility, which allows easy microfluidic implementation of the linker. Other tethering approaches, e.g. where liposomes are immobilized using biotinylated lipids [57], were not used because this could possibly interfere with the ability of the liposome to fuse. Especially when PEG is used as a linker between the lipid and the biotin, a negative influence on fusogenic behavior is expected by steric hindrance [176]. With the approach used in this study, liposomes are only attached to PEG-cholesterol at the bottom (see figure 5.1 d)), leaving the top of the liposome uncovered for fusion with cell membranes.

Figure 5.2 shows two examples where liposomes and cells are immobilized together on-chip above each other. Depending on the application, two different cell lines as well as patterns were used. Figure 5.2 a) shows the immobilized cells and the immobilized liposomes underneath the cells. In this case, liposomes were labeled with self-quenching concentrations of R18 and exhibited a heterogeneous fluorescence. Theoretically, patterns on the surfaces are not needed for the experiments and alignment of cells with liposomes is more complicated with patterns. However, the detection of the patterns allowed to determine the quality of the immobilization procedure (which would not be possible using a homogeneously treated surface) and also to check the integrity of the liposomes (e.g. by encapsulating calcein inside the liposomes as shown in Figure 5.2 d). Dot patterns were used in the dequenching experiments to create areas where cells are immobilized on edges. At these edges, fluorescence spreading can be observed inside the cells to areas where no liposomes are immobilized. For experiments with enzymes, patterns were used with a higher surface area to deliver as many enzymes as possible as well as to increase the probability of cell-liposomal alignment.

5.3.2 Fusion observed by dequenching

Many different assays have been developed over the years to study fusion [177]. Much focus has been on the dequenching of self-quenched membrane or content dyes in this context due to the relatively easy interpretation of results. Dequenching leads to a signal increase, which is easier to interpret than a loss of signal. Here, two dyes were used, calcein and octadecyl rhodamine B (R18), in self-quenched concentrations (Figure 5.3 a)). R18 is commonly employed to investigate the fusion of membranes as it can be easily incorporated at self-quenching concentrations into lipid membranes, e.g. into viral membranes [38]. Upon hemifusion and full fusion of two bilayers, R18 diffuses into the unlabeled bilayer. Dilution of the dye leads to a dequenching in the liposomal membrane, resulting in an increase of fluorescence. When only small amounts of liposomes are used, this increase is rapidly followed again by a decrease of fluorescence as the dye is further diluted and diffuses out of focus (Figure 5.3 c). However, the dequenching kinetics of R18 does not provide a complete understanding of the fusion process. As dyes can also diffuse from one bilayer into the other after hemifusion, where contents are still separated, content markers are crucial

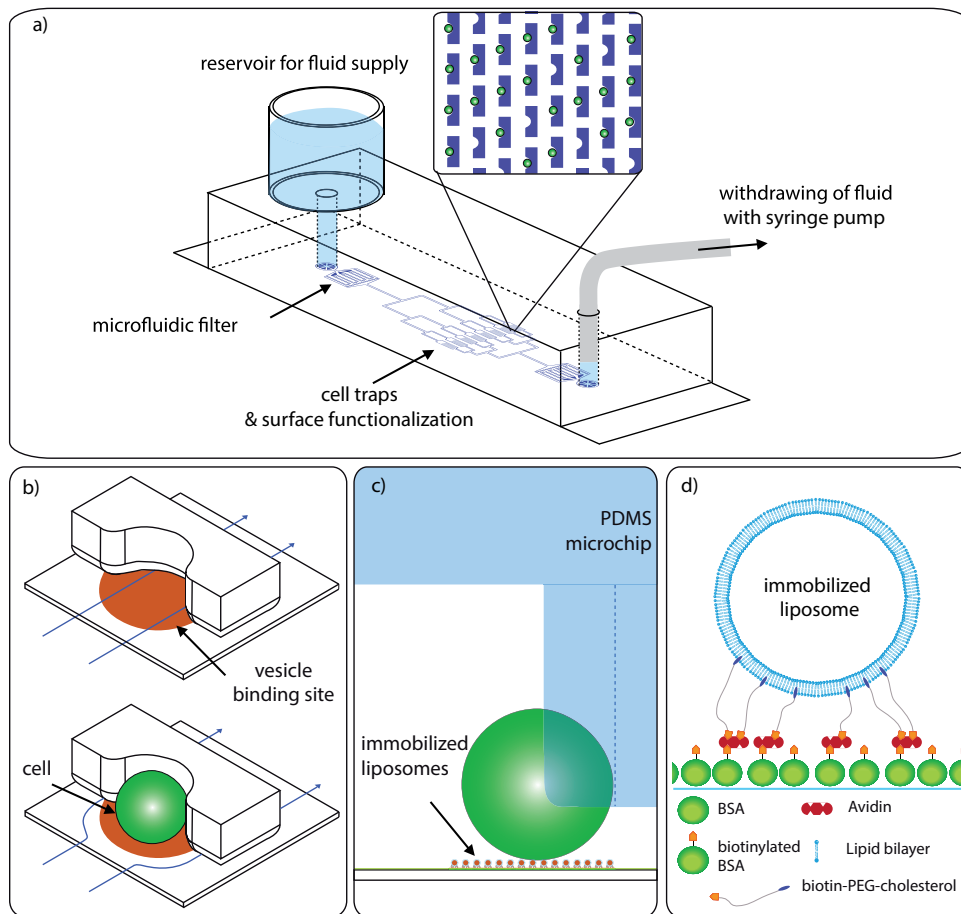


Figure 5.1: Schematics of cell-liposome trapping. a) Microfluidic device used in the experiments. All solutions are withdrawn from a reservoir through the microchannels. Embedded filters hinder agglomerates and debris from entering the cell trapping chambers. b) Liposomes are immobilized under the cell traps. The flow is diverted when cells are trapped, leading to single occupancies in traps. c) Side-view from the microchannel. Cells are trapped above the immobilized liposomes. d) Schematic of the liposome immobilization with chol-PEG-biot. The tethered cholesterol inserts into the lipid membrane, which immobilizes the vesicle from the bottom.

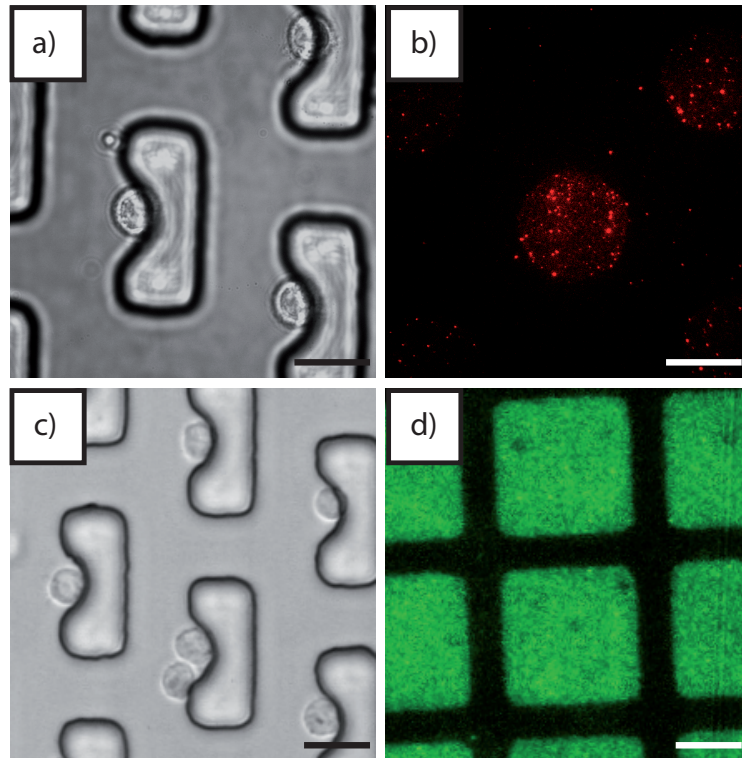


Figure 5.2: Co-immobilization of cells and liposomes. a,b) Brightfield and TIRF image of single CHO cells immobilized in cell traps directly above spots of immobilized liposomes. Liposomes are labeled with R18 in self-quenched concentrations. c,d) Immobilization of U937 cells on squares of liposomes stained with calcein (liposomes imaged with epi-fluorescence). All scale bars: 20 μm

to distinguish hemifusion from pore formation and actual content mixing [26, 178]. Hence, calcein was encapsulated in a self-quenched concentration into the liposomes. Calcein is a hydrophilic molecule that cannot cross lipid membranes, with different spectral properties as R18 and is thereby suited as a content marker. At calcein concentrations above 5 mM [179], the fluorescence is self-quenched. Here, 100 mM calcein were encapsulated inside the liposomes to account for the massive volume difference of liposomes and cells, where a high dilution is expected after fusion.

To create fusogenic liposomes, a lipid mixture of DOPG and DOPE was utilized. This mixture has been reported to undergo fusion with endosomal membranes at low pH [180]. Phosphatidylethanolamine (PE) promotes hemifusion states due to the cone shape and low degree of hydration, which allows bilayers to come into close proximity. Negatively charged DOPG is used to stabilize the lamellar phase of the lipid bilayer at physiological pH. Following a change in pH, and thus the protonation of DOPG, a phase transition from the stable lamellar phase to an unstable hexagonal phase occurs and leads to fusion [180]. The pH sensitivity can be increased by addition of divalent ions, like Ca^{2+} , which are likely to be present in the endosome [34]. Therefore, a buffer at pH 5 that contained calcium ions was used for all fusion experiments.

Figure 5.3 shows the results of liposome cell fusion observed with the dequenching assay using DOPE/DOPG liposomes (I, Table 5.1). After the pH is lowered to pH 5 by changing the buffer in the microchannel, a quick dequenching of R18 indicates the mixing of lipids and thus hemifusion or complete fusion. This is followed by a slower diffusion of calcein into the cell cytosol, probably through a fusion pore. Because cells can be situated at the edge of a liposome-immobilization spot, this is easily distinguishable from possible background effects.

5.3.3 Delivery of enzymes into cells by acid induced fusion

After establishing the fusion protocol and ensuring that fusion occurs between liposomes and cells, the DOPE/DOPG liposomes (II, Table 5.1) were used together with the fusion buffer to deliver β -galactosidase from *E. Coli* into single cells (Figure 5.4 a)). β -galactosidases are enzymes that cleave the galactose sugar moieties from polysaccharides. These enzymes are often used in molecular biology as reporters in transfection experiments. Since β -galactosidases are not naturally occurring in significant concentrations in healthy mammalian cells (only during senescence, [181]), genes expressing these enzymes are often incorporated into the expression construct because their activity can be relatively easily monitored by fluorescent techniques. Furthermore, small amounts of mammalian galactosidase can be inhibited by the addition of chloroquine. Chloroquine results in the alkalization of lysosomes [182], and due to the pH dependent activity of mammalian β -galactosidase, to its inhibition. However, the addition is not interfering with the bacterial enzyme, which is delivered to the cytoplasm. To determine the presence of β -galactosidase in cells after fusion, the ImaGene RedTM C₁₂RG lacZ Gene Expression Kit from Invitrogen, which contains a substrate for β -galactosidase, was utilized. The assay was used as described in the manufacturers description but the cells were incubated with the C₁₂RG substrate off-chip. This has several advantages. Firstly, it allows the removal of unbound substrate before coming into contact with PDMS, which is

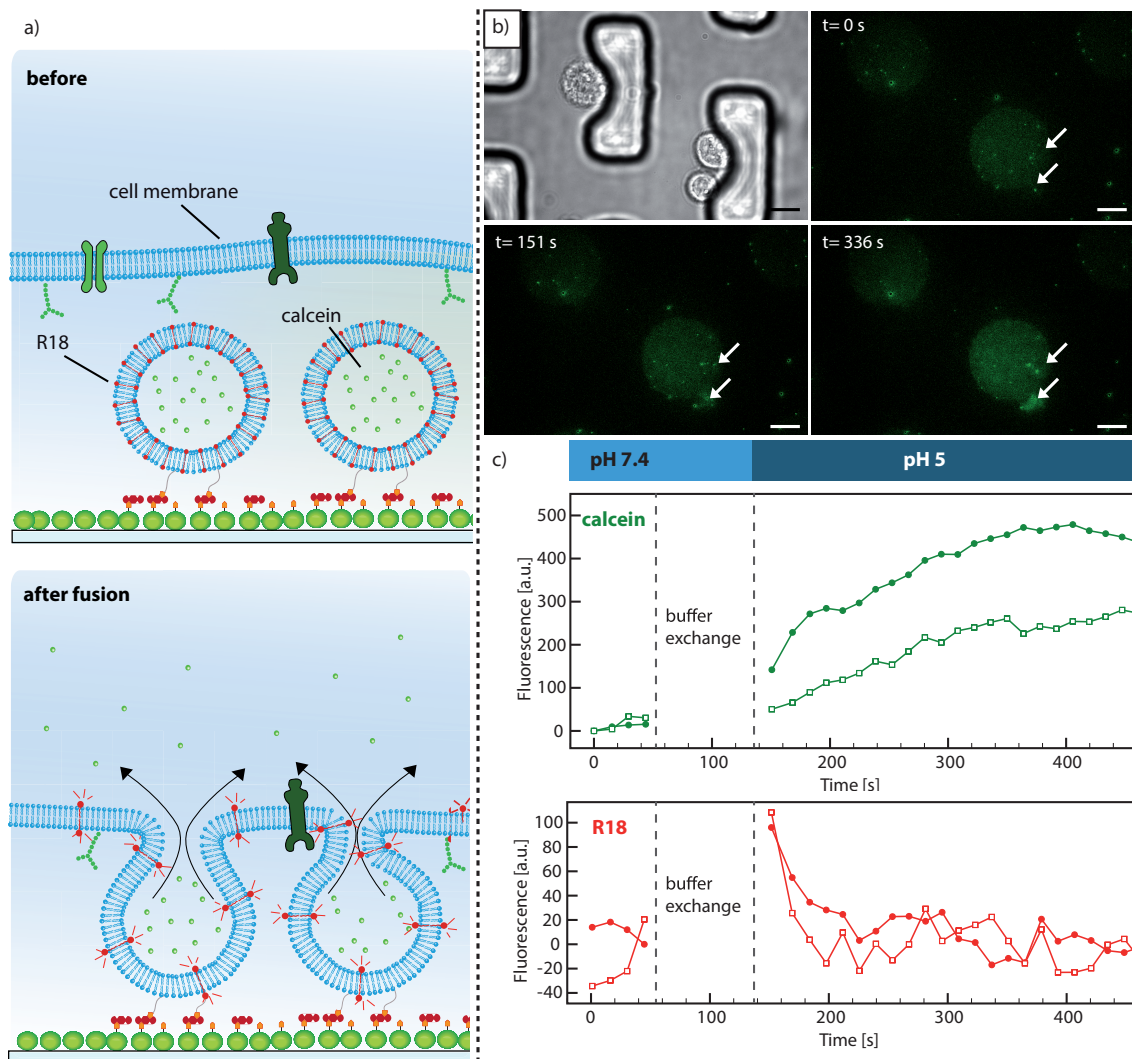


Figure 5.3: Kinetics of acid-induced fusion observed with dequenching assay. a) Schematic of the dequenching assay. Top: Situation at the liposome-cell interface before fusion with both dyes self-quenched. Bottom: Interface after fusion. Calcein diffuses through a fusion pore into the cell cytoplasm while R18 diffuses into the membrane of the cell. Both dyes de-quench. b) Brightfield and TIRF images (calcein channel) from CHO cells fusing with immobilized liposomes (with self-quenched calcein and R18) after pH decrease. The increase of fluorescence due to calcein diffusion is especially striking in the lower cell. All scale bars: $10\ \mu\text{m}$. b) Fluorescence intensity graphs for both indicated cells from b).

important as substrate might diffuse into or attach to the PDMS. The off-chip removal is easily accomplished by centrifugation and re-suspension of the cells. Secondly, immobilized liposomes will not get into contact with free substrate, which could lead to enzymatic substrate conversion already inside the liposomes. Thirdly, it also prevents the accumulation of substrate in the cellular membrane due to constant supply in the flow channel.

After incubation of the cells with the substrate, they exhibit only a weak fluorescence that does not change over time (Figure 5.4 b)). To ensure that only the conversion of substrate from β -galactosidase originating from liposomes was observed, chloroquine was added to the PBS buffer as an inhibitor for endogenous lysosomal β -galactosidase activity. After incubation of the cells for 5 min in fusion buffer, an increase in fluorescence of all cells could be observed, indicating successful enzyme transfer from the liposomes to the cells (Figure 5.4 b) and c)). This increase cannot solely arise from enzymes diffusing out of leaky liposomes, as free enzymes would be washed away quickly under constant flow.

It can be roughly estimated how many enzymes can be delivered in the discussed experiments into a single cell. With the diameter we measured by DLS and the enzyme concentration that was used to form liposomes, it can be calculated that one liposome encapsulates approximately 3-4 enzymes when assuming an encapsulation efficiency of 1 to 1. Considering the enzyme activity given by the manufacturer, this concentration corresponds to 10 pU in one liposome. For a typical U937 cell with a diameter of 12 μm , the fusion of one liposome and the delivery of the liposomal content would yield a conversion rate of 1 $\mu\text{M}/\text{min}$ inside a cell (neglecting time for diffusion of enzymes, etc.). This means that the conversion of 33 μM of substrate in the cells would be in the range of minutes to half an hour. Since the conversion of substrate seems to plateau after 6 min (see Figure 5.4 c)), it can be assumed that probably more than one liposome fused with one cell. The number of delivered enzymes into a single cell is therefore probably in the range of 1-50 enzymes.

After the feasibility of liposomal delivery of enzymes into single cells was shown, the fusogenic behavior of different lipid mixtures was tested. Three different experiments were performed where cells were exposed to 5 min of fusion buffer and fluorescence of substrate was imaged before and 30 min later (Figure 5.5). First, no liposomes were immobilized and therefore the microchip was enzyme-free. In this experiment, no significant increase of fluorescence could be observed. Some fluorescent increase can be due to spontaneous hydrolysis of the substrate over time. In the second experiment, liposomes made from the lipid DOPC (III, Table 5.1) were employed. Phosphatidylcholines (PC) are known to be non-fusogenic [171]. Hence, no enzyme transfer would be expected from liposomes made from DOPC. Consequently, cells in an experiment with DOPC liposomes show only a minor increase in fluorescence, which can be due to some free enzyme (which was not washed away from the buffer) and spontaneous hydrolysis.

In a third experiment, liposomes made with the fusogenic lipid mixture DOPE/DOPG (II, Table 5.1) yielded a significant increase of fluorescence. The relatively large deviation of the data is possibly due to the pattern we used for liposome immobilization and thereby different numbers of fusing liposomes for each cell.

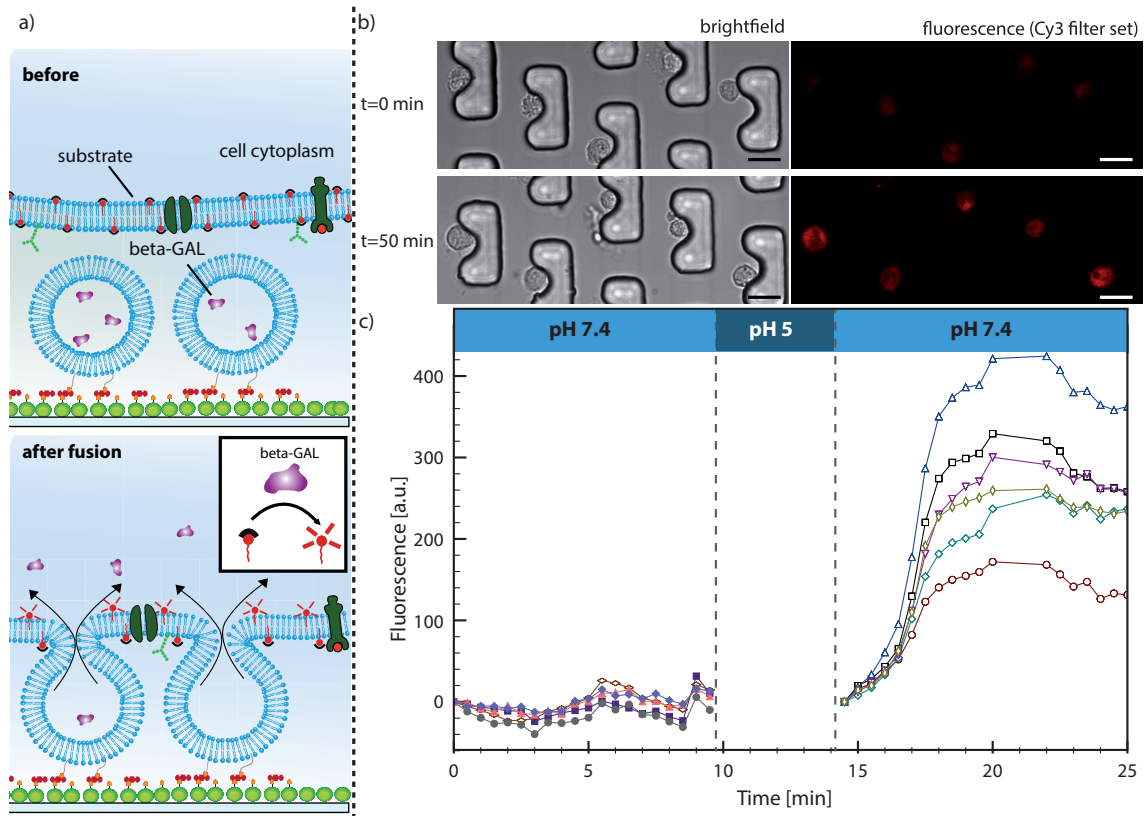


Figure 5.4: Delivery of β -galactosidase into single U937 cells. a) Schematics of fusion assays. Top: Situation at the liposome-cell interface before fusion with β -galactosidase inside the liposomes and the substrate in the cellular membrane. Bottom: Interface after fusion. The enzyme enters the cell cytoplasm and cleaves the sugar groups from substrate, rendering it fluorescent. b) Brightfield and fluorescence images of cells before and after the pH drop. All scale bars: 20 μm . b) Kinetics of enzymatic conversion for 6 single cells. Without pH change no increase in fluorescence can be observed.

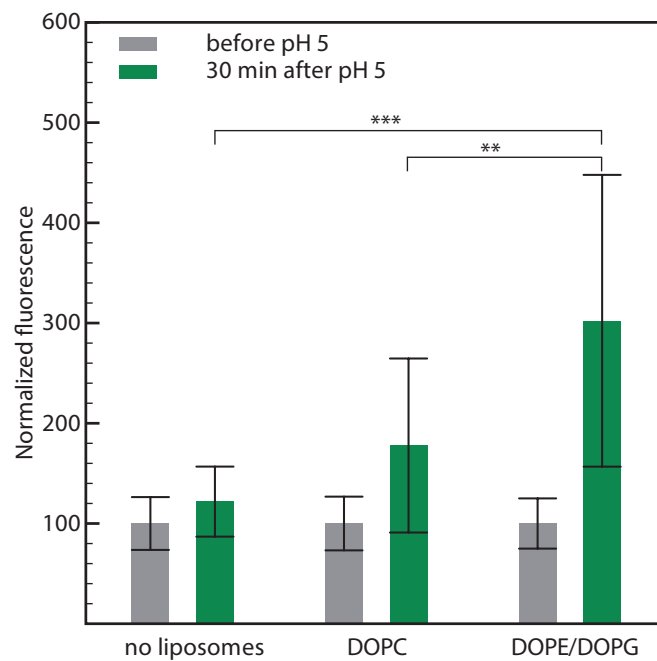


Figure 5.5: Influence of lipid composition on fusion efficiency. Data was normalized to the value before pH change to pH 5. Fluorescence increases markedly when fusogenic liposomes (DOPE/DOPG) are used. Error bars originate from more than 30 single cells measured at different locations on the same microchip. P values of 0.005 (*) and 0.0001 (***) with 0.05 considered statistically significant.

5.4 Conclusion and Outlook

Due to the highly significant statistical relevance of the data it can be concluded that this system can be used to test liposome formulations for their ability to fuse with cellular membranes at pH 5 in the presence of divalent ions. This can lead to a better engineering of liposomes as pharmaceutical carriers *in vivo*, e.g. for cancer therapy. These studies could help to reducibly test for lipofection efficiency, which could ultimately lead to novel, cell-targeting therapeutic strategies.

Further studies with this platform should be directed towards mechanistic studies. As it is now clear that fusion occurs, the process could not be fully elucidated. The use of FRET-pairs could definitely help to gain further insight into the fusion process. By adding lipids with bound fluorophores, that can do FRET, into the membrane of the liposomes kinetic studies are feasible.

Furthermore, the setup could also be used to deliver minute amounts of enzymes into single cells, possible in a microarray format. The technique broadens the portfolio of transfection techniques, such as microinjection and electroporation. Additionally, the platform is also suited to study fusion between two liposomes (e.g. LUVs and GUVs), since the traps can also be used to immobilize giant vesicles (T. Robinson *et al.* 2013). This could also be used in artificial cell studies to deliver molecules into GUVs to improve cell mimics.

6 Acid-induced fusion of single vaccinia virus particles with immobilized cells

Recent studies have revealed new insights into the endocytosis of vaccinia virus (VACV) into host cells. However, the mechanism of fusion between viral and cellular membranes remains unknown. A microfluidic device with a cell trap array for immobilization of cells was developed, with which the acid-dependent fusion of single virions on individual cells was analyzed. VACV particles incorporating enhanced GFP (EGFP) and labelled with self-quenching concentrations of R18 membrane dye were used in combination with TIRF microscopy. The kinetics of R18 dequenching and thus single hemifusion events initiated by a fast low-pH trigger could be measured. These studies revealed unexpectedly long lag phases between pH change and hemifusion. Surprisingly, it was found that EGFP fluorescence in the virus was quenched upon acidification, indicating that protons could access the viral core, possibly through a proton channel. In a fraction of virus particles, EGFP fluorescence was recovered, presumably after fusion pore formation and exposure of the core to the physiological pH of the host cell cytosol. While further studies are needed to identify the mechanisms involved in VACV fusion and transfer of protons through the viral membrane, the described microfluidic device may be highly beneficial to similar studies requiring fast kinetic measurements.

The work presented in this chapter was done in collaboration with Florian I. Schmidt and Jason Mercer from the Institute of Biochemistry at ETH Zurich.

6.1 Introduction

The ultimate goal of a viral particle is to deliver the viral genome into new host cells thus allowing for production of progeny viruses. One of the most challenging barriers in this process is the plasma membrane, which surrounds the host cell cytosol. In the case of enveloped virus particles, this barrier is crossed by fusion of the viral membrane with a cellular membrane. This process can take place at the plasma membrane itself, or at the limiting membrane of an intracellular compartment after endocytosis of virus particles. Triggers that induce the necessary protein rearrangements may involve receptor interactions and changes in the milieu, e.g. pH [183].

Fusion mediated by simple viral fusion proteins, e.g. the influenza A virus hemagglutinin, the dengue virus E protein, and the vesicular stomatitis virus (VSV) G protein, is well-understood, in part even in atomic detail [37]. The more complex fusion machinery of

herpes- and poxviruses, in contrast, is less well understood and requires further investigation [141, 184, 185].

Understanding virus fusion is critical for a complete understanding of virus entry and may help to develop antiviral agents that interfere with viral fusion, such as the HIV fusion inhibitor enfuvirtide [186]. Moreover, virus fusion serves as a model for the multitude of membrane fusion events that take place throughout the cell, both in the secretory pathway or within the endocytic system [25, 187].

Bulk fusion kinetics have traditionally been obtained by using viral particles (or liposomes) labelled with self-quenching quantities of the lipophilic dye octadecyl rhodamine B chloride (R18) [177]. For this, viral particles are bound to cells in suspension and total R18 fluorescence in a cuvette is measured in a fluorometer. Fusion is detected as the increase of R18 fluorescence a direct consequence of dilution of R18 into cellular membranes due to hemifusion and thus dequenching. Measuring fusion in bulk, however, cannot resolve single fusion events and may therefore obscure heterogeneities in virus populations or fusion kinetics. Furthermore, fusion at the plasma membrane cannot be directly distinguished from fusion with limiting membranes of endocytic vesicles.

Supported lipid bilayers (SLBs) are compatible with planar microfluidic devices and have therefore been used to visualize and quantify single fusion events of viruses and other vesicles [36, 103]. However, this approach requires artificial membranes, which are restricted in lipid compositions, such that e.g. only low concentrations of cholesterol are possible [81]. Thus SLBs do not accurately reflect the situation of a complex biological membrane. SLB experiments are, in addition, limited to conditions in which all necessary factors for binding and fusion - mostly proteins and lipids - are known and compatible with the generation of SLBs.

It was aimed to pursue single virus fusion experiments with vaccinia virus (VACV), a complex DNA virus that serves as the model poxvirus and is closely related to variola virus, the causative agent of smallpox [188]. The more abundant mature virions (MVs) was chosen for the studies as their single membrane can fuse with different cellular membranes and is amenable to labelling. MVs normally fuse with the limiting membranes of intracellular, endocytic organelles after uptake by endocytosis [131, 141, 189]. In the case of VACV strain Western Reserve (WR), fusion is triggered by acidification of endosomes [189]. Importantly, fusion at the plasma membrane can also be artificially triggered by briefly treating MVs bound to the plasma membrane with a low pH buffer at 37 °C [190]. While it is clear that the 11 subunits of the VACV entry fusion complex (EFC) are required for fusion [185], the requirements for the acceptor membrane are poorly understood. In fact, preliminary experiments suggested that VACV MVs do not bind efficiently to a variety of artificial membranes, demanding an experimental system with native biological membranes (data not shown).

Total internal reflection (TIRF) microscopy allows the visualization of plasma membrane events, such as clathrin-mediated endocytosis of VSV [191], and could in principle be used to visualize fusion at the plasma membrane. Since endocytosed virus particles leave the evanescent field of the TIRF microscope, no extra-measurements, such as inhibition of endosomal acidification, have to be undertaken to distinguish fusion at the plasma membrane from fusion with endocytic vesicle. However, due to their size, VACV MVs do not diffuse under

adherent cells and therefore cannot be analyzed using the conventional TIRF microscopy approaches used for other virus entry studies.

Microfluidic devices are widely used for single cell studies due to the similar size of the channels and thus the possibility to passively immobilize single cells [125, 174]. To date, single cell experiments based on microfluidic technology have yielded important insights which would be obscured by measurements of the whole population [192–194].

To study single fusion events of VACV MVs, a microfluidic device was established that trapped suspension cells with bound R18-labelled virus particles in hurdle structures (see Figure 6.1). Since the buffer flow pressed the cells gently against the underlying cover slip, bound virions at the plasma membrane were brought into the evanescent field of a TIRF microscope. Fluorescence of R18 in the viral membrane as well as a fluorescent protein in the viral core could be detected microscopically during low pH-induced fusion. The pH was monitored using BSA-FITC immobilized to the cover slip. This allowed to measure the kinetics of single hemifusion events and to determine lag phases and R18 dequenching rates for individual virus particles. These studies furthermore revealed that acidification of the extracellular milieu is transmitted through the viral membrane into the viral core, perhaps by a viral proton channel, whereby the fluorescence of a EGFP fusion protein was quenched. That EGFP fluorescence was recovered suggests that fusion pore formation and thus contact with the host cell cytosol brought the EGFP fusion protein back to physiological pH.

6.2 Methods

6.2.1 Cell lines

Hybridoma cells to produce the mouse anti-L1 (MAb 7D11) [195] were kindly provided by Bernard Moss (NIH, Bethesda, MD, USA) with permission of Alan Schmaljohn (University of Maryland, Baltimore, MA, USA). MAbs were purified from hybridoma supernatants by BioGenes (Berlin, Germany).

BSC-40 (African green monkey) were cultivated in DMEM (Life Technologies) supplemented with 10 % heat-inactivated FCS, GlutaMAX, non-essential amino acids, sodium pyruvate, and penicillin-streptomycin. HeLa S3 suspension cells were grown in RPMI 1640 GlutaMAX medium (Life Technologies) with 10 % heat-inactivated FCS, non-essential amino acids, and penicillin-streptomycin in a spinner bottle.

6.2.2 Viruses

Octadecyl rhodamine B chloride (R18)-labeled MVs of VACV strain WR EGFP-A5 [196] were produced in BSC-40 cells and purified/labeled as described before in chapter 3. Self-quenching of R18 in the viral membrane was verified by comparing emission spectra of virus suspensions in PBS or 1 % Triton X-100/PBS using a Cary Eclipse fluorescence spectrophotometer (Varian Inc.); excitation wavelength = 560 ± 5 nm, emission wavelengths from 566 to $750 \text{ nm} \pm 5$ nm. As negative controls for fusion, labelled MVs were neutralized by incubation with 100 $\mu\text{g/ml}$ 7D11, a mouse monoclonal anti-L1 antibody, for 1 h at 37 °C.

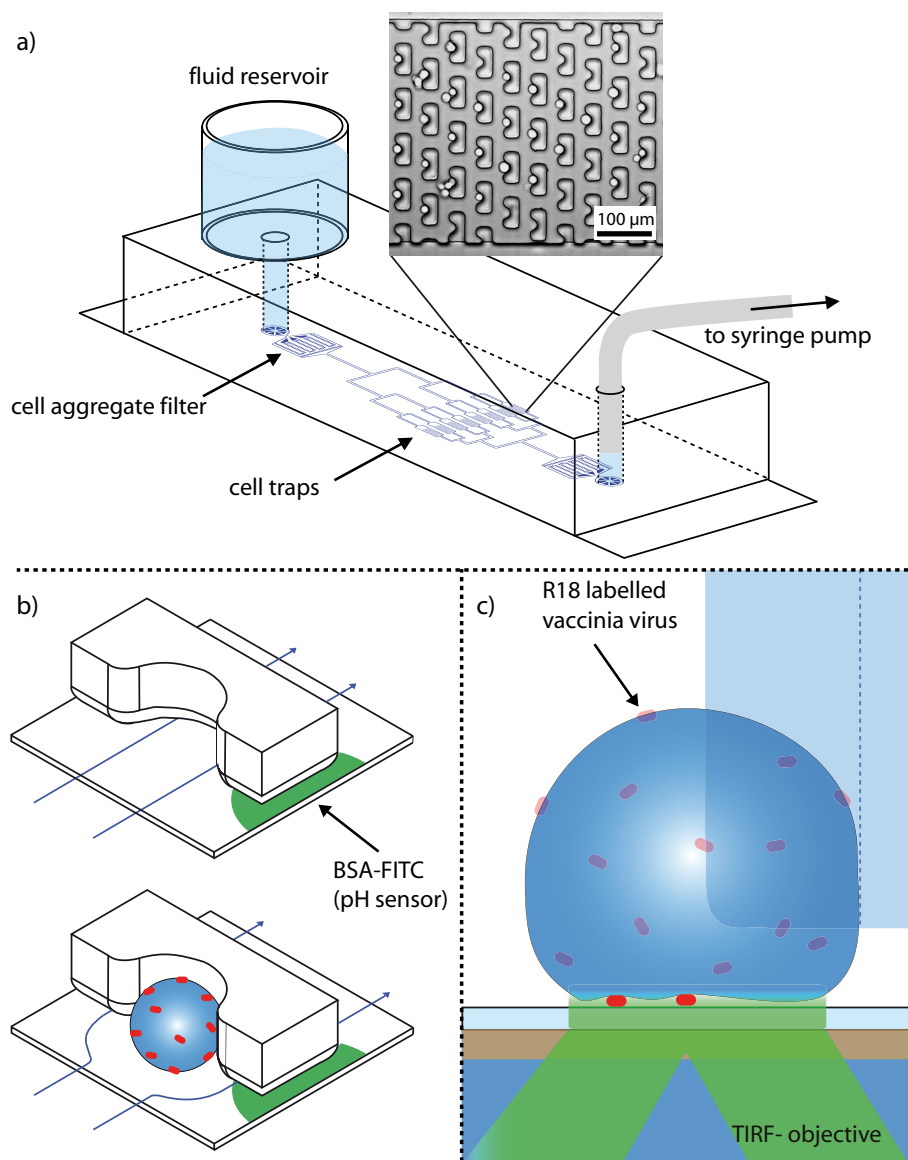


Figure 6.1: Illustration of the microfluidic device used for cell-virus fusion. a) Fluids are withdrawn through the channel network from a reservoir with a syringe pump. Posts inside the channel act as filters to retain large agglomerates of cells and debris, while single cells are captured in cell traps (see brightfield image). b) Working principle of cell traps. Without a trapped cell, the fluid can pass under the traps. After a cell has been trapped, the flow is diverted (around the cell), making it unlikely to trap more than one cell. Microcontact printed BSA-FITC is used to monitor the pH inside the channel directly next to the cell. c) Side-view of the set-up. The cell is slightly pressed onto the glass by the buffer flow. Single virus particles are imaged by two-color TIRF microscopy with an evanescent field of 250 nm.

6.2.3 Microfluidic chips with pH sensors

Microfluidic chips were prepared as discussed in chapter (2.3) in this thesis. After this preparation, chips with dot patterns of BSA-FITC were on the surface of the chip. To achieve this, 0.4 mg/ml mixture of BSA-FITC/ BSA (1:9) in PBS was microcontact printed. The rest of the chip was blocked with BSA.

6.2.4 Bulk fusion experiments

To monitor fusion in bulk, R18-dequenching during low pH-induced fusion was measured using a Cary Eclipse fluorescence spectrophotometer (Varian Inc.) with an excitation wavelength of 560 ± 5 nm, and an emission wavelength of 590 ± 5 nm. To measure R18 and EGFP fluorescence in the same experiments (using the same PMT settings), EGFP fluorescence was excited with 488 ± 5 nm and measured at 509 ± 10 nm, while R18 was excited with 560 ± 5 nm and measured at 640 ± 5 nm. R18 fluorescence was measured at wavelengths longer than the emission maximum to adjust the signal intensities to the EGFP fluorescence. R18-labelled WR EGFP-A5 MVs were bound to $7 \cdot 10^5$ HeLa S3 cells in the cold (MOI 30). After 1 h, cells were sedimented and resuspended in 100 μ l PBS. The cell suspension with bound virions was added to 900 μ l pre-warmed PBS in a 1.5 ml fluorescence cell (119.004-QS, Hellma, Müllheim, Germany). After 1 min, the pH in the cuvette was lowered by addition of 100 μ l MES solution (0.063 to 1 M), resulting in a pH of 6.5 to 5.0. R18 fluorescence was measured for 10 min, when all R18 was dequenched by the addition of 110 μ l 10 % Triton X-100.

6.2.5 Single virus particle fusion experiment

R18-labelled MVs were bound to $5 \cdot 10^5$ HeLa S3 suspension cells (MOI 5) at 4 °C. After 1 h, cells were sedimented and resuspended in 500 μ l PBS. The microfluidic device and all solutions were warmed to 37 °C in an incubation chamber of the TIRF microscope. This avoided bubbles in the device and ensured the correct temperature for the fusion experiment. Fluids were withdrawn through the channels with a neMESYS pump (cetoni, Germany) operating a 2.5 ml Hamilton glass syringe that was connected with Teflon tubing to the chip. 50 μ l cell suspension was loaded into the chip at a flow rate of 5 μ l/min. Cells that were not trapped in the hurdles were washed away with PBS at the same flow rate.

A field of view containing several cells with single virus particles was identified by TIRF microscopy and fusion of bound MVs with the plasma membrane was induced by changing the buffer from PBS (pH 7.4) to 90 mM MES in PBS (pH 5.0). While changing the solution in the reservoir, the flow rate was reduced to the minimal flow sufficient to keep the cells in place (0.1 μ l/min). This made sure that the pH drop in the field of view occurred rapidly and with some delay after buffer exchange. Immediately after the beginning of acquisition, the flow rate was increased to 5 μ l/min again. The decrease in pH at the cell traps occurred approximately 15 s later.

6.2.6 pH-dependent fluorescence of virus particles

50 μl vaccinia virus MVs in 1 mM TRIS pH 9.0 (10^8 pfu/ml) were filled into a chip which had not been blocked with BSA. MVs were allowed to bind to the glass for 1 h at room temperature. Binding was performed at pH 9.0 to prevent aggregation of virus particles. All non-bound particles were washed out with 1 mM TRIS pH 9, which was then replaced with PBS at pH 7.4. A flow of 20 $\mu\text{l}/\text{min}$ or no flow (when the buffer in the reservoir was exchanged) was used in these experiments.

6.2.7 Image acquisition

Virus particles were imaged with an inverted TIRF microscope (see also section 2.5). R18 was excited with a 561 nm laser and emitted light collected with a bandpass filter (600/32). EGFP and FITC were excited at 488 nm and fluorescence was collected with a 525/35 bandpass filter. Leica LAS AF software was used to collect images. An exposure time of 300 ms was used for the observation of the R18 and the GFP channel.

6.2.8 Data analysis

Fluorescence from microcontact printed spots was analyzed with ImageJ (NIH, Bethesda, MD, USA). Imaris (Bitplane AG, Zurich, Switzerland) was used to track individual virus particles and their fluorescence intensities over time. Only virus particles with detectable R18 and EGFP fluorescence were considered and viruses were tracked in the EGFP channel. In the few cases in which viruses could not be successfully tracked due to the complete loss of the EGFP signal, MVs were tracked using the R18 channel. Mean R18 fluorescence in the detected spots was plotted over time to extract the fluorescence intensity at the start (i.e. before pH drop) F_{start} , the maximal fluorescence F_{max} , and the lag-time t_{lag} , i.e. the time until fluorescence increase, by eye. From these values, the relative increase of R18 fluorescence was calculated as follows:

$$Increase = \frac{F_{max} - F_{start}}{F_{start}} \cdot 100\% \quad (6.1)$$

If the increase of fluorescence was higher than 100 %, the dequenching rate of R18 was calculated:

$$Rate = \frac{0.5}{t_{1/2} - t_{lag}} \quad (6.2)$$

where $t_{1/2}$ is the time when the fluorescent intensity reached 50 % of its maximal increase. Mean EGFP fluorescence in the detected spots over time was analyzed similarly and used to calculate the recovery of the fluorescent signal after the pH drop with:

$$Recovery = \frac{F_{t=300s} - F_{min}}{F_{max} - F_{min}} \cdot 100\% \quad (6.3)$$

where $F_{t=300s}$ is the fluorescent intensity 300 s after the pH drop; F_{max} and F_{min} are the maximum and minimum fluorescence intensities before and after the pH drop, respectively.

6.3 Results

6.3.1 Bulk fusion experiments

In order to measure bulk and single particle fusion of VACV MVs with cellular membranes, viral membranes of MVs were labeled with self-quenching quantities of R18. VACV strain WR EGFP-A5 was used, which incorporates the fluorescent fusion protein EGFP-A5 into viral cores and allows the visualization of virus particles based on the EGFP fluorescence. To test whether R18 in viral membranes was indeed self-quenched, the fluorescence spectra of virions in the absence and presence of 1 % Triton X-100 were measured (see Figure 6.2 a). At the emission maximum, R18 fluorescence in the presence of detergent was about 20-fold higher than in the absence, confirming that R18 in the MV membrane was quenched.

Bulk fusion of R18-labelled VACV MVs has to date mostly been measured in cells kept at physiological pH, where fusion presumably occurred after endocytic uptake [197, 198]. Acid-induced fusion has been investigated indirectly by quantifying polykaryon formation, i.e. cell-cell fusion [190, 199]. During polykaryon formation, acid-induced fusion of viral particles with the plasma membrane is thought to deposit viral fusion proteins in the plasma membrane, which can subsequently mediate fusion of the infected cell with neighbouring cells. In some cases, R18 dequenching or infection at physiological pH was measured after a short low pH treatment of MVs bound to the plasma membrane [189, 198]. To measure acid-induced bulk fusion directly and to determine the optimal pH for VACV MV fusion, we first measured acid-induced bulk fusion of R18-labelled MVs to HeLa S3 suspension cells in a fluorescence spectrophotometer (Figure 6.2 b). Of the tested physiological pH values, pH 5.0 resulted in optimal, i.e. fastest and most complete fusion and was thus chosen for further fusion experiments. More than 30 % of all virions fused within 10 min after acidification. In the measured time, no or only minor amounts of fusion was detected at pH 7.4.

To test whether R18 dequenching was indeed the consequence of a genuine fusion event, fusion of MVs pretreated with the neutralizing anti-L1 antibody 7D11, which has been described to inhibit viral fusion [196], was analyzed. Indeed, R18 fluorescence of 7D11-pretreated MVs did not increase over time when treated at pH 5.0 (Figure 6.2 c), indicating that R18 dequenching was not caused by the applied low pH or non-fusogenic dye transfer.

6.3.2 Microfluidic devices to detect single particle fusion

To visualize and record single virus fusion events, a microfluidic device was employed in which single HeLa S3 cells with bound R18-labelled MVs were trapped. Fluorescent virions could thus be followed on the microscope over time, and - more importantly - during fusion with the plasma membrane induced by rapid exchange to a pH 5.0 buffer. Acid-sensitive BSA-FITC immobilized in the device was used to monitor pH changes in the field of view.

The microfluidic device was made from poly(dimethylsiloxane) (PDMS) that was bonded to a functionalized cover glass (Figure 6.1). A mixture of BSA-FITC/ BSA was carefully adjusted to match the fluorescence intensity of EGFP-containing virions under the TIRF microscope. This mixture was microcontact printed on the cover glass before the bonding and served as a pH sensor. Immobilized BSA-FITC was confirmed to be rapidly quenched by a pH 5.0 buffer (see Figure 6.3).

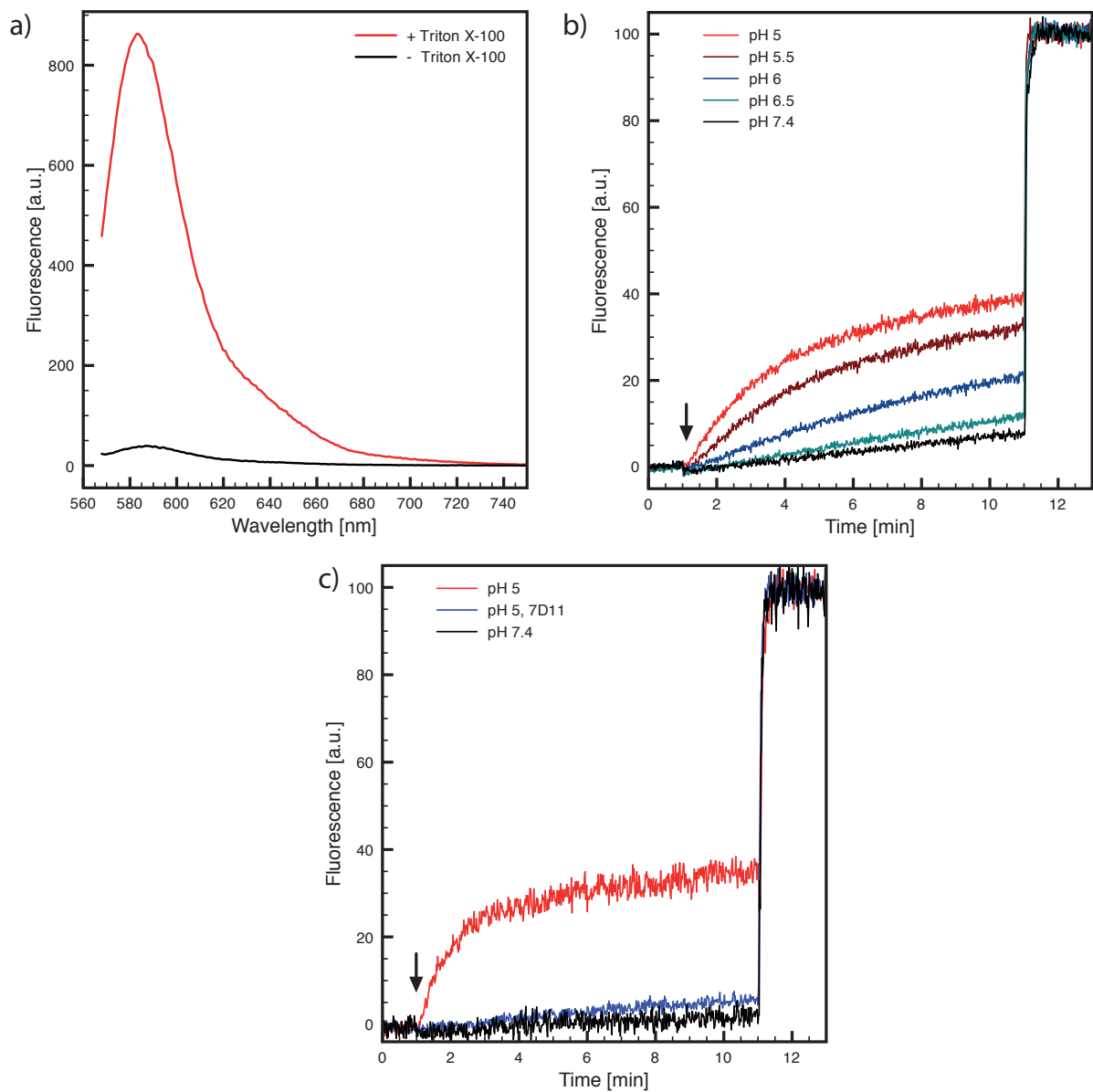


Figure 6.2: Bulk fusion experiments. a) Emission spectrum of R18 labeled VACV WR EGFP-A5 in PBS in the absence or presence of 1 % Triton X-100. b) pH dependence of fusion. R18-labelled WR EGFP-A5 MVs were bound to HeLa S3 cells in the cold and added to warm PBS at $t = 0$ min. The pH was lowered to the indicated pH by addition of different concentrations of MES buffer at $t = 1$ min and R18 fluorescence followed over time. Viral membranes were solubilized and R18 completely dequenched by the addition of Triton X-100 (1 % final) at $t = 11$ min. c) Fusion of MVs neutralized with antibody 7D11. Experimental setup as in b), except that R18-labelled WR EGFP A5 MVs were incubated for 1 h at 37 °C in the absence or presence of 100 $\mu\text{g}/\text{ml}$ 7D11 prior to binding.

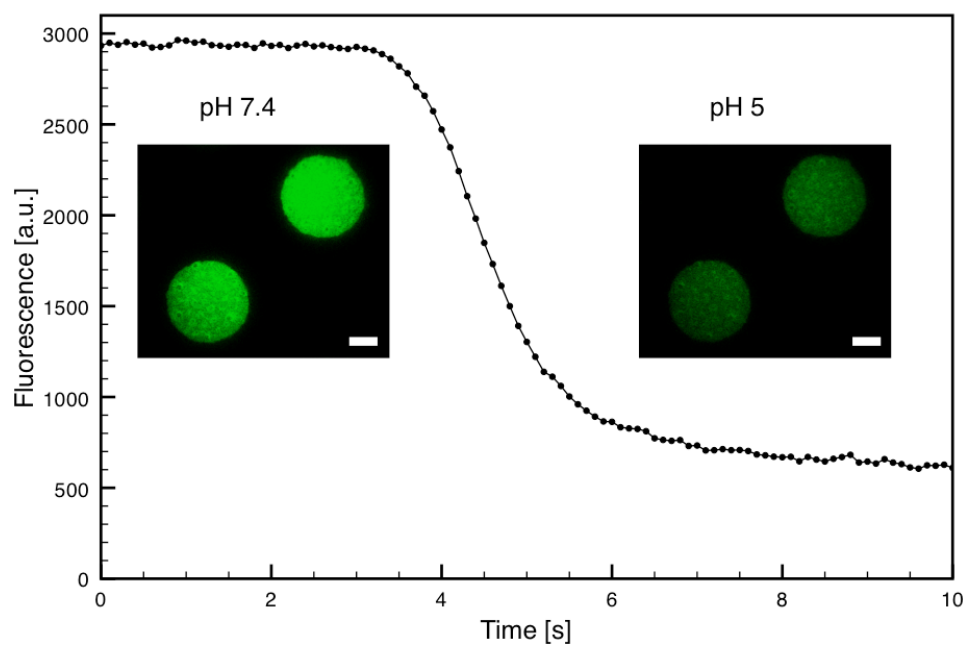


Figure 6.3: Microcontact printed BSA-FITC spots are used as a pH sensor. The graph shows the decrease of fluorescence intensity on the spots due to a change of pH from 7.4 to 5. The data was corrected for background and photobleaching. Fluorescence trace and inset images are acquired by TIRF microscopy. Scale bars: 10 μm

BSA-FITC could be distinguished from EGFP-A5-containing virus particles due to the characteristic pattern of the BSA-FITC spots. This allowed the detection of both fluorophores with similar spectral properties in the same channel. The decrease in fluorescence intensity of fluorescein at acidic pH allowed real-time pH sensing, which is crucial to define the exact time of buffer exchange near the cell immobilization site.

The device incorporated 576 hurdles for single cell trapping. The design is based on a previously described microfluidic device [125], but the gap between the PDMS and the glass was increased to 5 μm in the here described setup. This prevented PDMS bonding to the glass and hence non-functional cell traps.

HeLa S3 suspension cells with bound VACV MVs were loaded into the microfluidic device. The trapped cells were imaged by TIRF microscopy with an evanescent field of approximately 250 nm. Hence, only virions directly in contact with the cell membrane and in close proximity to the glass were excited. In a typical experiment, 3-4 cells were recorded with approximately 1-5 detectable virions (see Figure 6.4). Virions were only considered if fluorescence could be clearly detected in both channels (R18 and EGFP) before the pH decrease. Single virus particles and their fluorescence were tracked throughout the experiment using the fluorescence of the viral core protein EGFP-A5, since R18 was redistributed into the plasma membrane during acid-induced fusion.

Acquisition was started immediately after changing the buffer in the fluid reservoir of the microfluidic device from pH 7.4 to pH 5.0 and continued for about 5 min. The pH 5.0 buffer arrived in the field of view approximately 15 s after buffer exchange. After the decrease in pH, the fluorescence intensity of the BSA-FITC microspots and the EGFP-A5 in the cores dropped immediately. At the used time resolution (3 s), no lag time could be observed between the changes of fluorescence intensity of the directly accessible FITC-BSA and the membrane-surrounded EGFP-A5 within the viral core. This observation will be discussed in more detail later. After a lag phase, the loss of fluorescence intensity in the green channel was followed by a gradual increase in R18 fluorescence in virus particles. The increase in R18 fluorescence was caused by dequenching of R18 during hemifusion and thus dilution of the dye into the plasma membrane. No R18 dequenching was observed when the trapped cells with bound virions were kept at pH 7.4 (see Figure 6.5).

6.3.3 Hemifusion and dequenching rate for individual virus particles

To analyze single fusion events, the R18 fluorescence was plotted of individual tracked virions over time (see Figure 6.6 a). The fluorescent increase was calculated for each single particle and only considered those particles that at least doubled in fluorescence ($\text{Increase} \geq 100\%$). Next, the lag phases between the pH shift and the onset of R18 dequenching was extracted, indicating hemifusion (see Figure 6.6 b). This revealed an unexpected heterogeneity in the lag phases that was not detected in the bulk fusion experiments, in which no clear lag phase was observed. While hemifusion started in most virions between 8 and 24 s after the pH drop, lag phases ranged from a few seconds up to 77 seconds post pH shift in others.

Lag phases between acidification and R18 dequenching have been repeatedly observed in bulk fusion experiments using different viruses undergoing acid-mediated fusion, such as

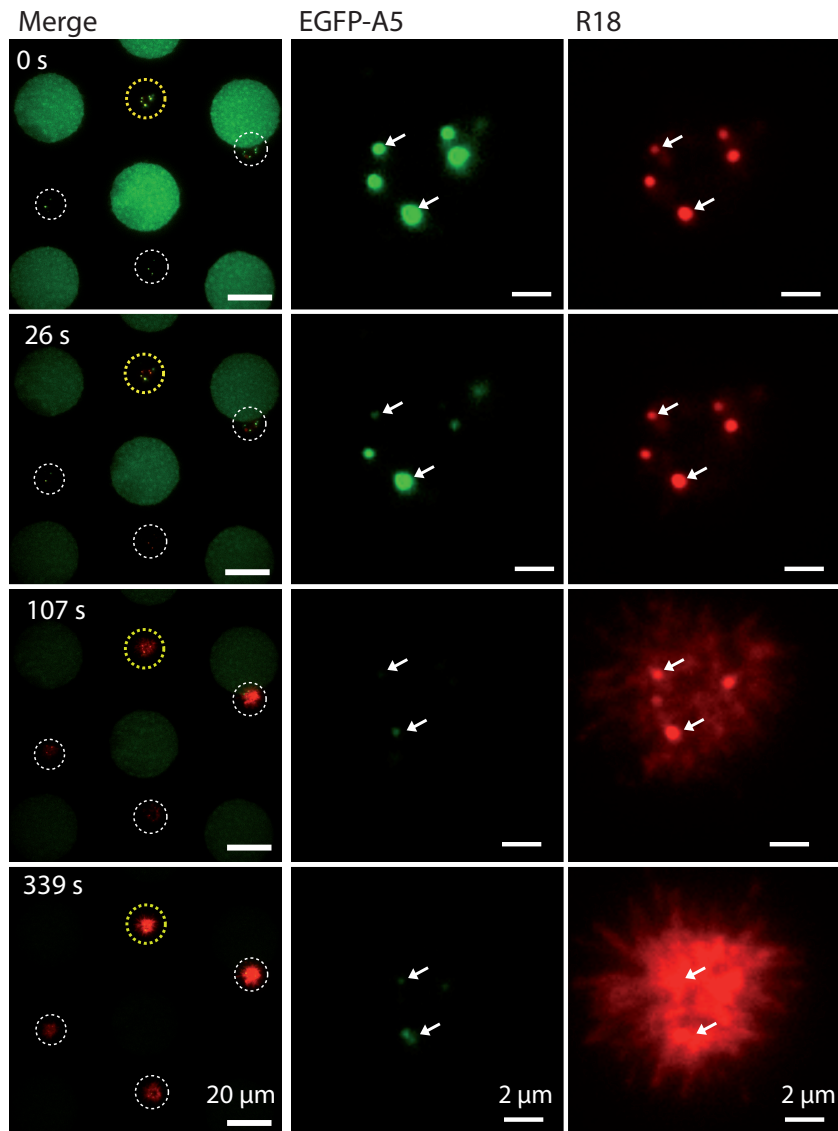


Figure 6.4: Images from a typical microfluidic experiment. R18-labelled WR EGFP-A5 MVs were bound to HeLa S3 cells in the cold. Cells were subsequently trapped in a microfluidic chamber and detected with TIRF microscopy. At $t = 26$ s, PBS was replaced with MES/PBS (pH 5.0). The left column shows a complete field of view (both channels merged). At time zero, single virions could be easily identified due to the co-localization of the R18 and EGFP signals; cells are marked with dashed circles. The other columns represent magnifications of the cell highlighted with a yellow circle. The middle column shows the fluorescence of EGFP-A5, the right column shows the corresponding R18 signal. Arrows mark two typical virus particles undergoing fusion. When the pH was decreased, an immediate decrease of the EGFP fluorescence in the cores and of the pH sensor signal was observed. After a few seconds ($t = 107$ s) the signal at the membrane increased significantly due to hemifusion and dye dequenching. At the end of the experiment ($t = 339$ s), the fluorescence in the core is partly recovered in some of the virions, while R18 was distributed throughout the plasma membrane.

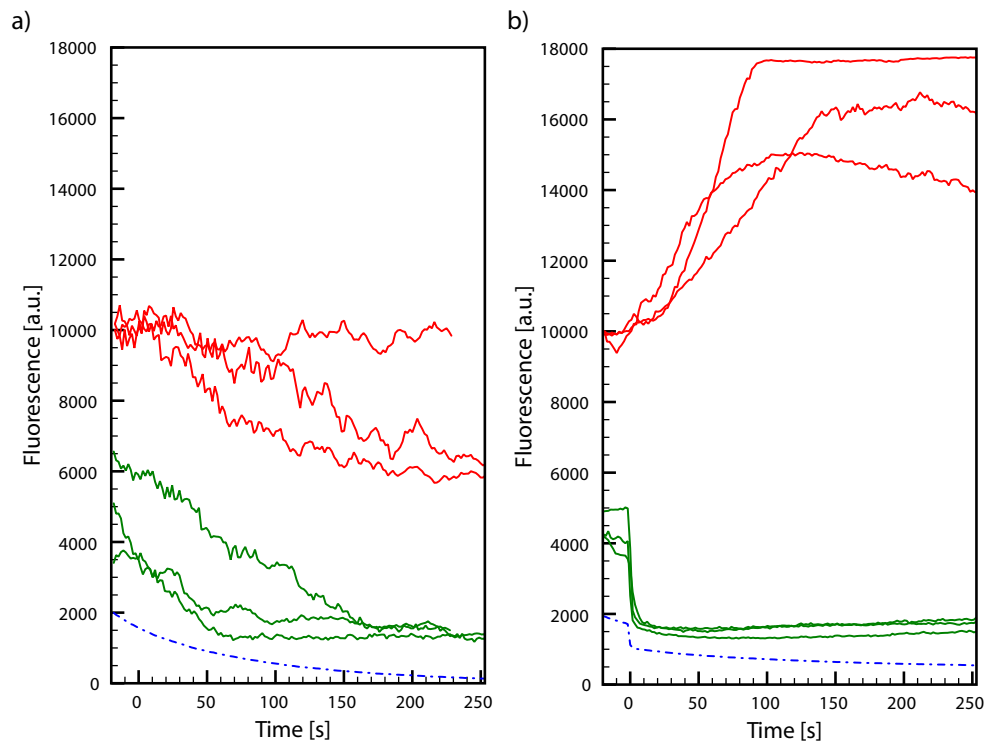


Figure 6.5: Fluorescence of cell-bound virions at a) physiological pH and b) after a pH drop to 5.0. R18-labelled WR EGFP-A5 MVs were bound to HeLa S3 cells in the cold. Cells were subsequently trapped in a microfluidic chamber and were either kept in PBS (a), or treated with MES/PBS (pH 5.0) at 37 °C. Single virus particles were detected by TIRF microscopy and tracked based on their green fluorescence. Traces of representative virions are displayed (red: R18, green: EGFP, dashed: FITC-BSA); importantly no R18 dequenching and only photobleaching were observed at pH 7.4.

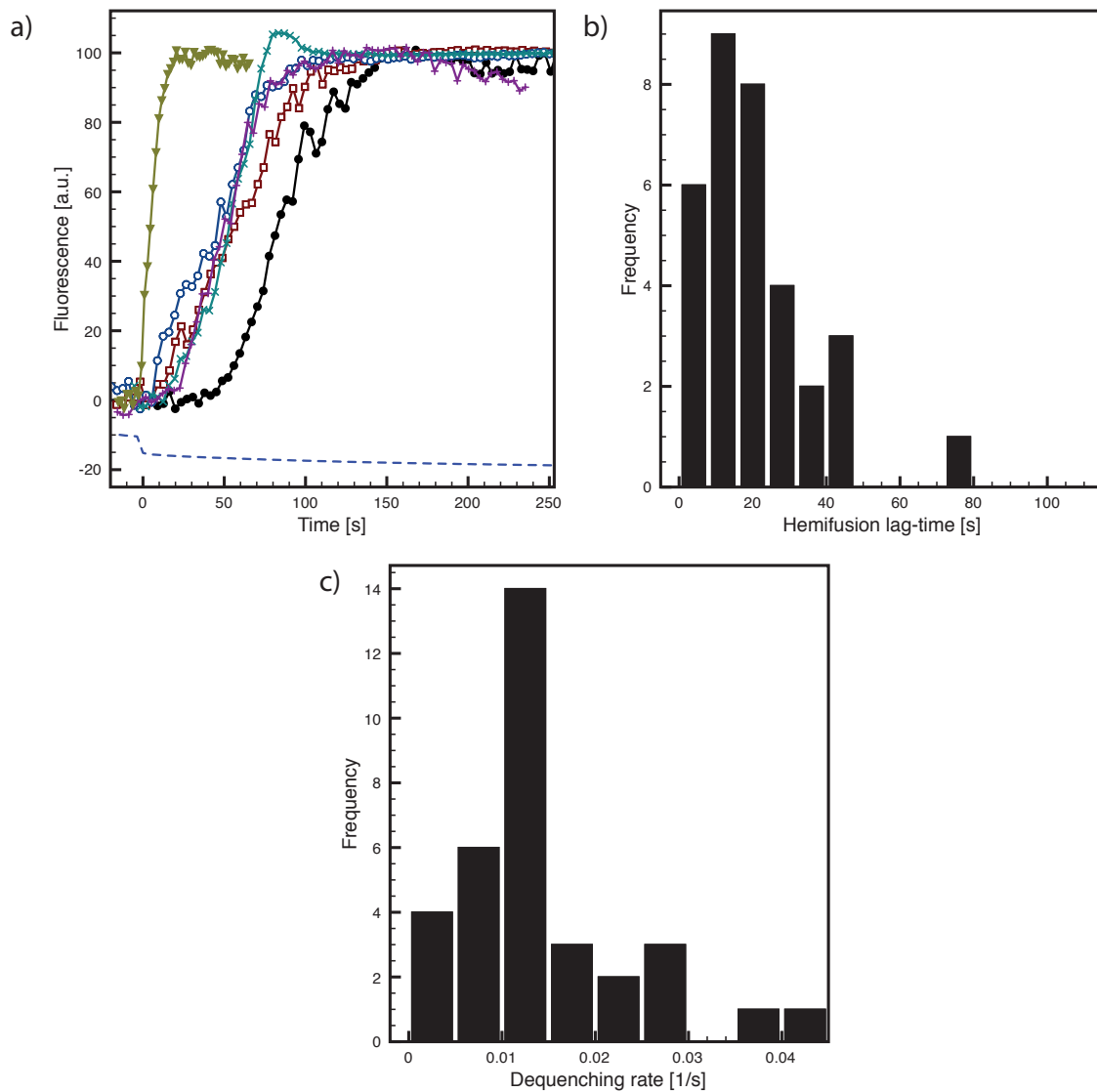


Figure 6.6: R18 dequenching of single virus particles. a) Normalized R18 fluorescence traces of single vaccinia virions obtained with the experimental setup described in Figure 6.4. The dashed line is the fluorescence of microcontact printed BSA-FITC and thus corresponds to the pH. The time of the pH drop was set as $t = 0$ s b) Lag-time distribution and c) dequenching rate of all measured virus particles ($n = 33$).

influenza A virus, VSV, or Semliki Forrest virus [200–202]. In many cases, however, lag phases at optimal fusion conditions were short and could only be accurately observed using specifically designed stopped-flow experiments or when hemifusion was slowed down at non-physiological temperatures or sub-optimal pH. The lag phase was interpreted as the time needed for changes in the quarternary structure, and conformation of the fusion proteins to allow for fusion [203].

When single fusion events of R18-labelled influenza A virus particles with SLBs were monitored microscopically [103], it became apparent that single virus fusion lag times were heterogeneous. Bulk fusion kinetics obscured this heterogeneity and the observed lag phases in such experiments only represented the time it took the first virions to undergo hemifusion. No single particle fusion experiments have been performed with VACV MVs. The lag times determined for VACV MV fusion at 37 °C in this study are slightly longer than those obtained for influenza A virus fusion at 23 °C. In the case of influenza fusion, the lag phases are temperature dependent, with the shortest lag occurring at 37 °C [200]. Comparatively, the lag phases of VACV MV fusion were surprisingly long. The length and heterogeneity of the lag phases may reflect the complexity of the fusion process, which may involve up to 11 viral components of the entry/fusion complex as well as two proteins that presumably inhibit fusion until they dissociate from the EFC at acidic pH [185, 204].

In contrast, the rate of R18 dequenching was found to be more homogeneous (see Figure 6.6 c). This may be explained by the fact that the dequenching rate mainly depends on the diffusion of R18 dye into the cell membrane and therefore has similar kinetics for all virus particles.

6.3.4 Acidification of EGFP-containing cores

In all experiments it was observed that the EGFP fluorescence inside the core quickly decreased after the pH in the microfluidic device was lowered (see Figure 6.7 a). This decrease was followed by an increase of R18 fluorescence, i.e. hemifusion. In some cases, EGFP fluorescence recovered later (see also Figure 6.7 b and c).

The GFP variant used, EGFP, is pH sensitive with an apparent pK_a of 6.15 and the loss in fluorescence intensity at acidic pH is reversible down to a pH of 5.0 [205]. The reduced fluorescence intensity of EGFP-A5 after the pH drop can thus be correlated to a reduced pH in the viral core. Nevertheless, the observed EGFP quenching in the core was surprising because the lipid bilayer surrounding the viral core was expected to be a highly impermeable barrier for protons.

Low pH-mediated quenching of palmitoylated YFP in the interior of avian sarcoma and leukemia virus (ASLV) had been observed in acid-induced fusion experiments before [206]. However, a drop of YFP fluorescence was, in this case, only observed in a fraction of the particles. The authors speculated that those virus particles exhibited membrane defects, contained proton channels, or transmitted protons through an unknown mechanism. That acidification of the virus interior was only observed in a minority of the particles, supports membrane defects as the most likely explanation. In our experiments, however, EGFP fluorescence dropped in every core. It is unlikely that all labeled MVs exhibited membrane defects as EGFP quenching was in many cases followed by successful fusion. Labeled MV

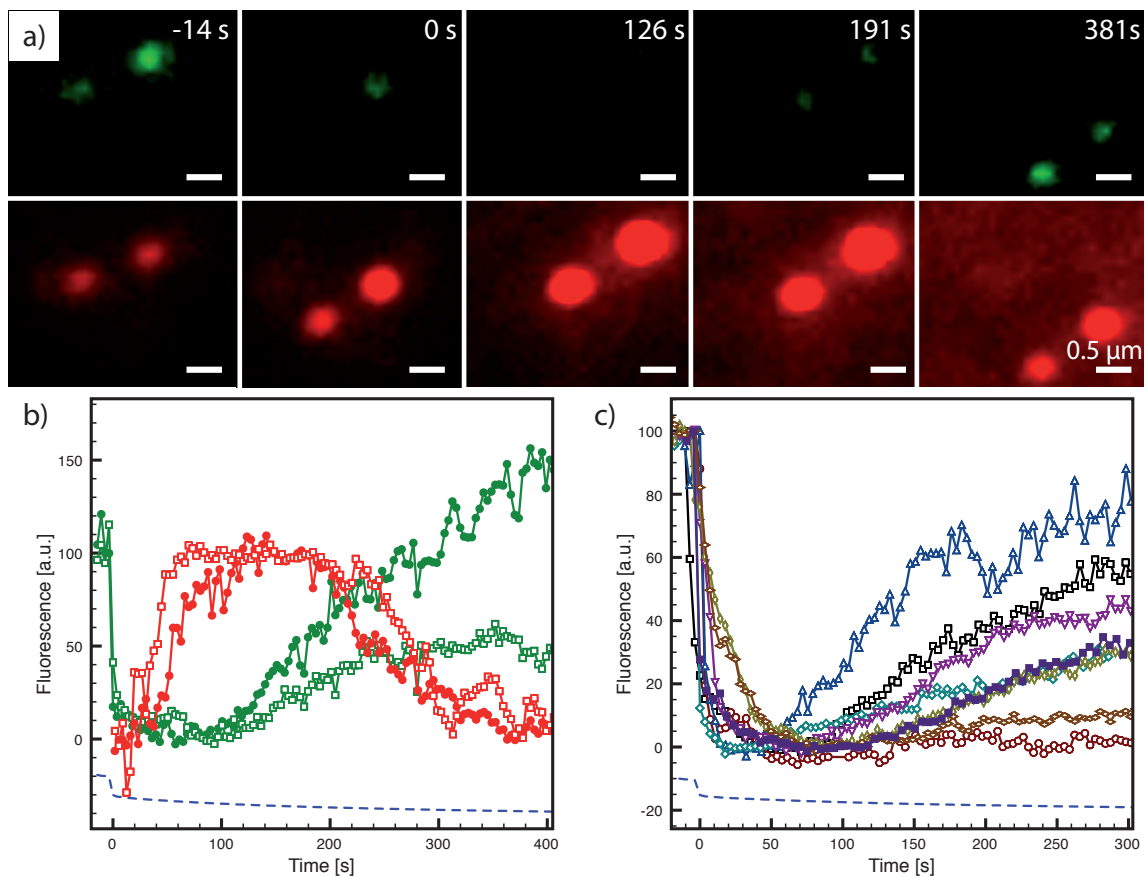


Figure 6.7: GFP recovery after fusion pore opening. a) Time-series of two virions fusing with the plasma membrane, obtained with the experimental setup described in Figure 6.4. The EGFP-A5 signal (top row) quickly decreased after the pH drop at time zero, but recovered after approximately 100 s. The R18 signal (lower row) augmented during hemifusion, reached a maximum at 120 s, and decreased again later, presumably because the dye was diluted into the plasma membrane. Virus particles moved laterally with the cells, suggesting that they were not bound to the surface of the chip. b) Normalized fluorescence traces (red: R18, green: EGFP) of the left virus particle in a. c) Representative normalized fluorescence curves of EGFP-A5 fluorescence after pH decrease. Fluorescence recovered in some virions, while others remained quenched. Dashed lines in both graphs represent the fluorescence of the pH sensor BSA-FITC and indicate when the pH was lowered.

preparations furthermore were as infectious as unlabeled MVs purified in parallel, ruling out the possibility that membrane labeling compromised the integrity of the viral membranes (data not shown). Since R18 fluorescence did not decrease upon the pH drop, it could be excluded that loss of EGFP fluorescence was caused by a movement of the viral particle out of the focal plane. It is therefore hypothesized that VACV MV membrane contains proton channels that can transmit protons into the virus interior along a concentration gradient.

6.3.5 pH-dependent EGFP fluorescence of immobilized MVs

To further investigate core acidification, an additional experiment to measure the pH-dependent fluorescence of many virus particles simultaneously was designed. The same microfluidic device as before was used, but did not block the surfaces with BSA. WR EGFP-A5 MVs were then introduced into the device and incubated at room temperature to allow binding to the glass bottom through electrostatic interactions. Binding and acquisition of many virus particles in one focal plane provided several advantages: no MVs could leave the focus plane due to cell movement and buffers could be exchanged more rapidly and multiple times without the risk of losing trapped cells. Since no R18 fluorescence was recorded, EGFP fluorescence could be acquired at a higher frame rate (2 s). Figure 6.8 shows a typical experiment performed with approximately 100 virus particles. As before, BSA-FITC was used as a pH sensor in the microfluidic device. It was observed that the pH drop in the channel coincided with a strong decrease in EGFP-A5 fluorescence in MVs. Since this phenomenon was observed in all virus particles, it is highly unlikely that virions are proton permeable due to defects in the membrane. When the pH in the same microfluidic device was changed back to pH 7.4, EGFP fluorescence increased rapidly. This indicates that the low pH quenching of EGFP is reversible, and that protons can presumably cross the viral membrane in both directions.

6.3.6 Recovery of EGFP-A5 fluorescence after fusion

When EGFP-A5 containing cores were followed over time in single virus fusion experiments, it was repeatedly observed that EGFP fluorescence recovered with some delay after hemifusion. On average, EGFP recovery started after 121 s and reached 36 % of the fluorescence intensity before the pH drop ($n = 8$). Since R18 fluorescence was recorded at the same time and did not exhibit equivalent changes, it can be ruled out that the increase in EGFP fluorescence occurred due to the movement of viral particles into the focal plane. As acid-quenching of EGFP was shown to be reversible, it is likely that EGFP recovery occurred when the pH within the viral core returned to physiological pH. This is expected to happen when viral cores gain access to the host cell cytosol after fusion pore formation. Due to their membrane potential and the energy-dependent transfer of protons against the concentration gradient, cells can presumably sustain a physiological pH despite their acidic surrounding. The cellular cytosol with a volume that is multiple orders of magnitude bigger than that of the virus, may easily buffer the acidic pH in the viral interior. Recovery of EGFP fluorescence would in this case indicate successful fusion pore formation. Consistent with our interpretation, Melikyan *et al.* also used the recovery of YFP fluorescence after fusion pore

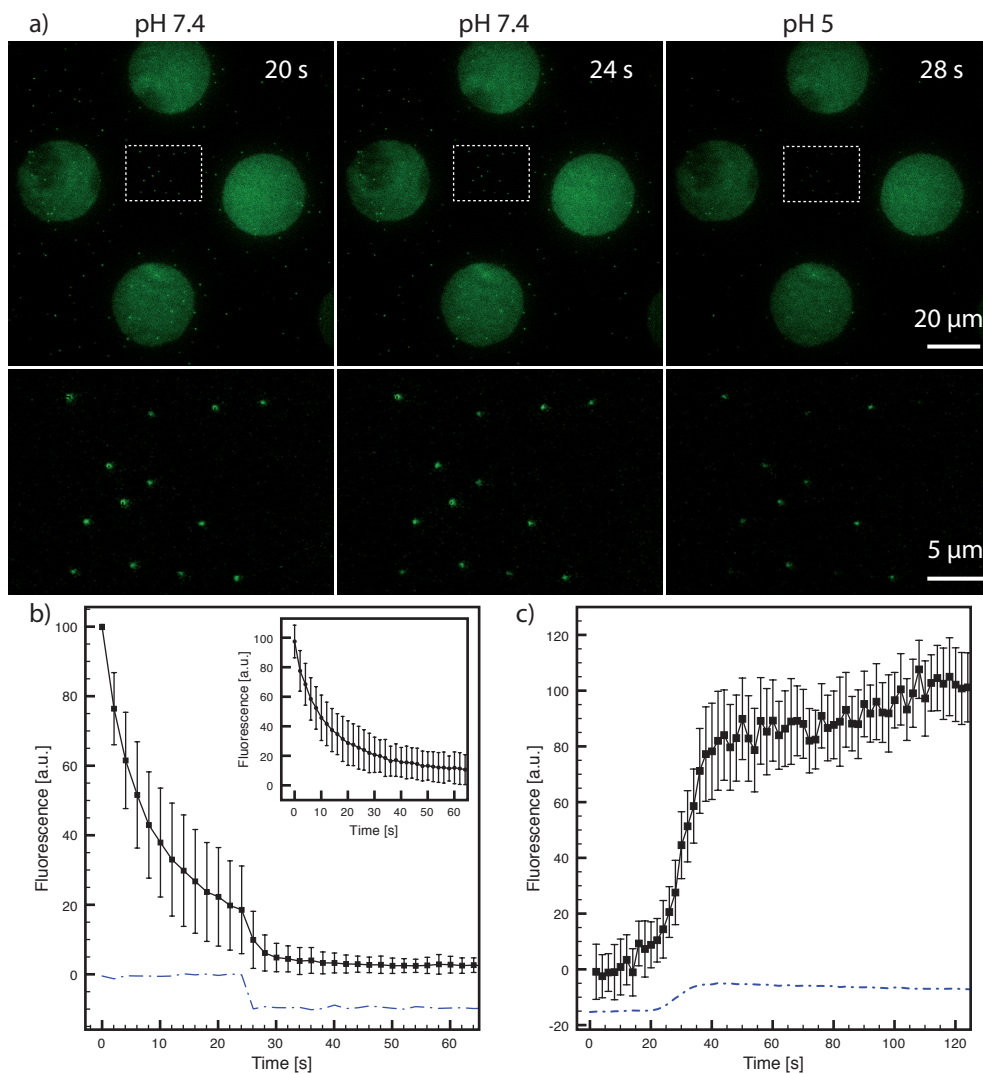


Figure 6.8: EGFP-A5 fluorescence in virions at acidic and neutral pH without fusion. VACV WR EGFP-A5 MVs were bound to the unblocked glass surface of a microfluidic device and recorded by TIRF microscopy, while the pH was changed. a) Time-series of approximately 100 virions during a pH drop from pH 7.4 to pH 5. The dashed rectangles indicate the area of the insets below. The signal of the GFP in the core stayed constant except for photobleaching at pH 7.4 ($t = 20$ s and $t = 24$ s). After the pH drop at $t = 26$ s, the fluorescence of the cores decreased markedly. b) Mean fluorescence and standard deviation of all virions from a). Fluorescence was normalized before calculating the mean. The inset shows a control experiment, in which the pH was kept constant at pH 7.4 and only bleaching occurred. c) Mean fluorescence and standard deviations of virions during a buffer change from pH 5 to pH 7.4. Neutralization of pH in the core led to an increase of the signal.

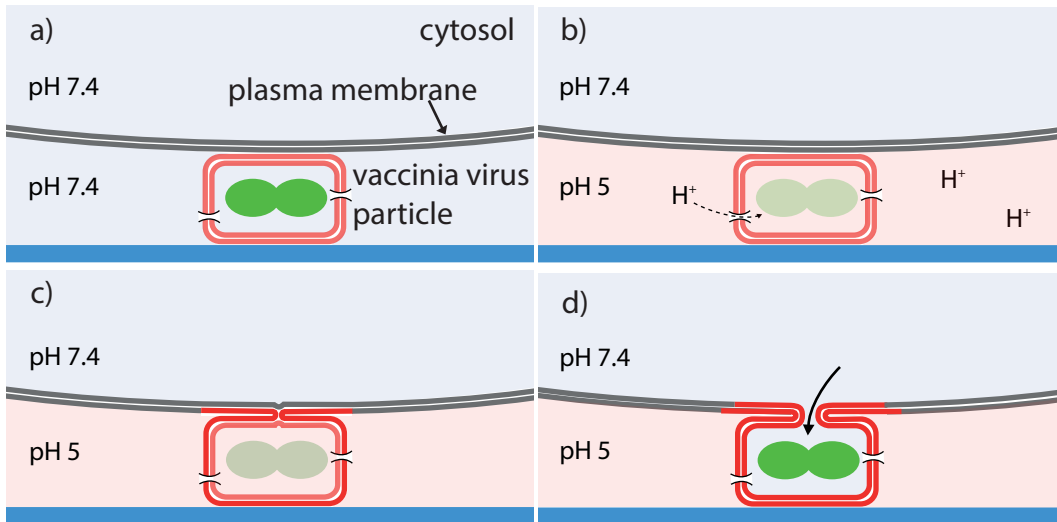


Figure 6.9: Model of acid-induced fusion VACV MV with the plasma membrane. a) VACV MVs are bound to the cell at physiological pH. b) When the buffer is exchanged to pH 5, protons enter the virus particle, presumably through proton channels, and quench EGFP fluorescence. c) After a lag time, hemifusion occurs, which is monitored by R18 dequenching. d) Following complete fusion (fusion pore opening), the interior of the virus is buffered by the cell cytosol, leading to the recovery of EGFP fluorescence.

formation as a marker for content mixing in their ASLV fusion experiments [206].

Taken together, the data suggests EGFP fluorescence in the core is quenched by pH 5 buffers because the viral interior is acidified. EGFP fluorescence recovers over time, presumably after fusion pore formation and content mixing with the host cell cytosol (Figure 6.9). If this model is true, EGFP quenching and recovery should also be detectable in bulk fusion experiments. Furthermore, EGFP recovery would only be expected to occur when fusion takes place. To test this, we used R18-labelled WR EGFP-A5 MVs for bulk fusion experiments in a fluorescence spectrophotometer in which both R18 and EGFP fluorescence of bound virions could be detected (see Figure 6.10). As in single virus fusion experiments, bulk EGFP-A5 fluorescence intensity immediately dropped when the pH in the cuvette was lowered to 5.0; R18 dequenching and thus hemifusion formation directly followed acidification as described earlier. As seen in the single virus experiments, EGFP fluorescence recovered with time after hemifusion, reaching about 20 % of its intensity before low pH treatment. This is in line with the herein described single virus fusion experiments, in which EGFP fluorescence was recovered in a fraction of the observed MVs. When MVs were pretreated with the neutralizing antibody 7D11 prior to binding in parallel experiments, EGFP-A5 fluorescence decreased upon low pH-treatment as in the untreated controls. However, neither R18 dequenching nor EGFP recovery could be observed in the sample. This confirms that 7D11 blocks hemifusion and that EGFP recovery depends on hemifusion formation. This suggests that EGFP recovery is most likely a consequence of fusion pore formation.

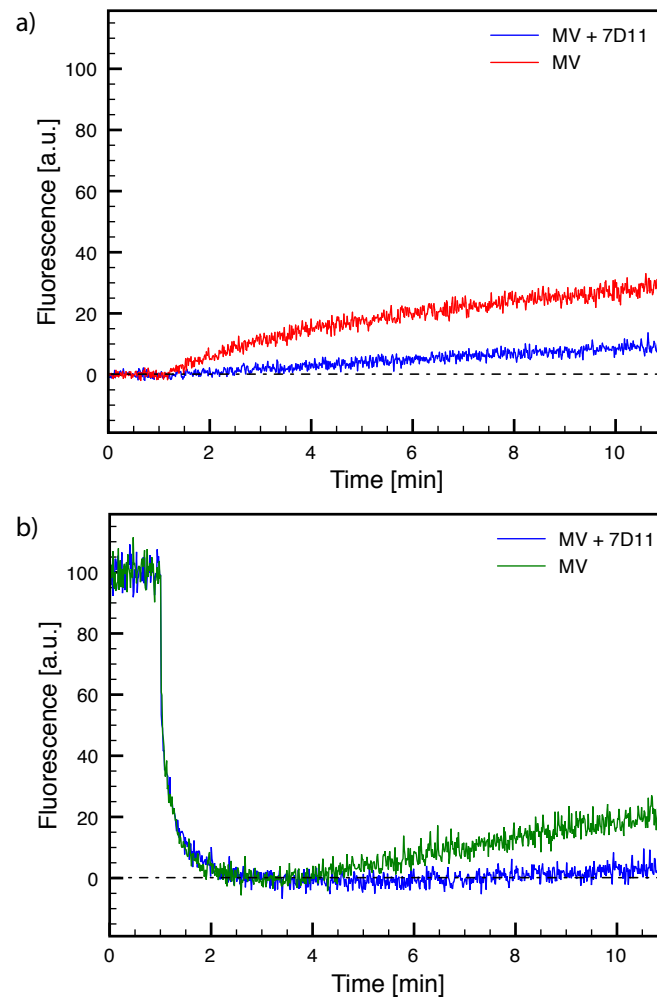


Figure 6.10: Bulk fusion experiments. R18-labelled WR EGFP-A5 MVs were incubated for 1 h at 37 °C in the absence or presence of 100 $\mu\text{g}/\text{ml}$ 7D11 and bound to HeLa S3 cells in the cold. The cell-virus suspension was added to warm PBS at $t = 0$ min and R18 (a) and EGFP (b) fluorescence measured. The pH was lowered to pH 5.0 by addition of MES buffer at $t = 1$ min and fluorescence recorded for 10 min.

6.4 Discussion

An experimental setup to visualize single, acid-induced VACV fusion events at the plasma membrane was established. This permits the quantification of single virus fusion kinetics and couples the measurement of hemifusion to microscopic observation of virus or cell components, exemplified by a fluorescent viral core protein in this study.

In contrast to similar setups described previously [103], fusion with biological membranes rather than non-physiological lipid mixtures was analyzed. This may lead to more relevant results and is particularly helpful for analysis of virus fusion events for which the binding and fusion requirements are unknown. Furthermore, the analyzed fusion was directly coupled to a genuine infection, which we could verify by the detection of virus-encoded reporter genes (data not shown). In principle, this setup can therefore be applied to study fusion of any enveloped virus for which fusion with the plasma membrane occurs naturally or can be triggered artificially. Furthermore, the microfluidic device could be adapted to similar types of experiments, where e.g. the pH drop is more rapidly initiated under no-flow conditions using caged protons [104], or where pH gradients are applied.

In this study, VACV MVs were used as an example of a complex enveloped virus for which the fusion step is poorly characterized. Information on single virus fusion events was not available. Fusion in general had only been studied in bulk experiments under conditions in which fusion happened asynchronously without distinguishing between fusion in endocytic vesicles or at the plasma membrane [197, 198]. While it is possible that different triggers induce MV fusion, it is widely accepted that cell-bound MVs of strain WR can be artificially fused with the plasma membrane by low pH treatment. Using artificially triggered fusion, it is ensured that all detected virus particles receive the signal for fusion at the same time. Observed heterogeneities in fusion under control or perturbed conditions can therefore directly be attributed to the fusion process itself. Using both bulk and single fusion experiments, we confirmed acid-induced fusion of WR MVs. Single fusion experiments allowed to extend the information on MV fusion by revealing variable lag time between acidification and hemifusion.

Using the additional information obtained by observing fusion microscopically, it was found that viral cores were acidified with the surrounding buffers and neutralized with some delay after the measured hemifusion, as deduced from the acid-labile fluorescence of the core protein EGFP-A5. The respective changes in EGFP fluorescence could be confirmed in bulk fusion experiments. In this case, single fusion experiments acted as a discovery tool that inspired bulk experiments that would not have been done otherwise. It is postulated that proton channels in the MV membrane allow the transport of protons into the viral interior, and that the pH is elevated again after fusion pore formation (see Figure 6.9). In this case, EGFP-A5 fluorescence could then be used as a marker for content mixing. The postulated proton channel in the viral membrane would also transmit protons into the viral interior during acidification of MV-containing endocytic vesicles, where acidification may prepare the virus core for activation or uncoating. Further experiments are necessary to confirm the existence and identity of the postulated proton channels in the VACV MV membrane.

The established system allows for the visualization of several important steps of VACV MV fusion: acidification of viral cores, hemifusion, and content mixing. This setup may therefore

help to investigate the VACV MV fusion process more thoroughly, and more importantly distinguish which perturbations directly affect fusion rather than e.g. endocytosis. Most of the EFC components and associated proteins have in a recent study been shown to be required for hemifusion, while the absence of A28, L1, or L5 only affected later steps, such as early gene expression or the localization of cores in the cytosol [198]. An experimental setup with a genuine content mixing marker may help to elucidate the exact role of these proteins. In contrast to Laliberte *et al.* [198], it was found that the neutralizing anti-L1 antibody 7D11 efficiently blocked hemifusion at sufficient concentrations. However, this may be explained by the different experimental conditions, since e.g. fusion was artificially induced in our experiments. Of note, fusion of R18-labelled MVs with small unilamellar vesicles could not be blocked with 7D11 (data not shown), suggesting an indirect role of L1 in fusion or steric hindrance of fusion by 7D11. The here described system could furthermore help to solve the ongoing controversy regarding the fusion inhibitory dimer A25/A26 in the context of pH-dependent or independent fusion of MVs of VACV strains WR and IHD-J, respectively [204, 207].

6.5 Conclusion

A platform was set up that allows for microscopy-based observation and quantification of single viral fusion events at the plasma membrane. As shown for VACV MVs, microscopic analysis of hemifusion can be combined with the detection of other fluorescent signals, e.g. content markers. This approach has already led to the novel finding that VACV MV membranes are proton permeable, presumably due to a yet unidentified proton channel.

7 Conclusions and outlook

In this thesis, the use of microfluidic devices for lipid membrane studies was presented. As discussed before, microfluidic technology allows to control fluids much more precisely compared to bulk assays, which is especially advantageous in kinetic studies.

First, protocols were developed to integrate lipid membranes into microdevices. Liposomes were chosen over suspended and supported bilayers due to their ease of production and the many available protocols for their analysis. In order to use liposomes inside microfluidic chips, immobilization strategies were either newly developed (see chapter 3) or existing techniques improved (see chapter 4). The newly developed protocol for immobilization of various liposomes and living organisms by cholesterol linkers was shown to be useful for long-term studies where automated imaging requires fixed positioning, and where repeated additions of chemical agents and washing steps are needed. Of particular interest is that the surrounding fluid can be rapidly exchanged. Hence, kinetic studies can be performed with a high time resolution, which was also demonstrated in chapter (5) where liposomes were fused with cells. The other immobilization strategy was based on tagged liposomes. The method described by Stamou *et al.* was improved by enclosing the immobilized vesicles inside a microfluidic channel, which allowed rapid fluid exchange.

The integration of lipid membranes by liposome immobilization was applied first to the measurement of permeation coefficients of tetracyclines into vesicles. It was shown that the measurement of permeation coefficients with microfluidic devices requires only very small volumes and short measuring times. The major strength of this approach is the ability to reliably resemble the *in vivo* situation since the drug concentration is kept constant and no unstirred water layer is present, which makes data analysis much more easier. The main drawback of this system is that the detection assay can only be employed for tetracyclines, which form fluorescent complexes with Europium. This limits the applicability of the whole system. By using a different assay the importance of the method can be greatly increased. One possibility is the use of pH indicators inside the liposomes, like carboxyfluorescein or HPTS [89]. Since most drugs change the pH after they passed the membrane as a neutral molecule, this would be broadly applicable.

The protocol to immobilize liposomes by cholesterol linkers was applied for studies on liposome-cell fusion. Negatively charged pH-sensitive liposomes were used because of their ability to fuse at low pH. A microfluidic device was then developed that facilitates the fusion of a small set of liposomes with single cells. This was accomplished by the co-immobilization of both fusion partners on top of each other. This approach circumvented the need to attach liposomes to the cell membrane prior to changing the environment to a fusion buffer and allowed the fast supply of a fusion trigger. Liposome-cell fusion was successfully verified with a dequenching assay and an enzymatic assay, where β -galactosidase is delivered into the cytosol. These studies can help to reproducibly test for lipofection efficiency, which

could ultimately lead to novel, cell-targeting therapeutic strategies. Furthermore, the setup could also be used to deliver minute amounts of enzymes into single cells, possible in a microarray format. To achieve this, liposomes with different contents need to be arrayed, possibly by using valves, in microfluidic devices before cells are introduced.

Additionally to the results presented with liposomes, an experimental setup to visualize single, acid-induced VACV fusion events at the plasma membrane was established. Due to the lack of information how vaccinia virions bind to cell membranes, no artificial system could be developed and cells needed to be used. Thereby, in contrast to similar setups described previously [103], fusion with biological membranes rather than non-physiological lipid mixtures was analyzed. This leads to more relevant results and is particularly helpful for analysis of virus fusion events for which the binding and fusion requirements are unknown. In principle, this setup can therefore be applied to study fusion of any enveloped virus for which fusion with the plasma membrane occurs naturally or can be triggered artificially. The presented results that were obtained with vaccinia virus particles were explained by the existence of a proton channel in the membrane of the virus. Further experiments are necessary to confirm this existence and identity of the postulated proton channels. However, this task is not straightforward as proton channel inhibitors are not readily available due to the small size of a proton. The established system allows for the visualization of several important steps of vaccinia virus fusion: acidification of viral cores, hemifusion, and content mixing. This setup may therefore help to investigate the fusion process more thoroughly, and more importantly distinguish which perturbations directly affect fusion rather than e.g. endocytosis. Furthermore, mutation of viruses may help to distinguish which proteins from the entry-fusion-complex are needed for fusion at low pH, and which ones have different functions. Additionally, biophysical studies like pH dependence or temperature dependence would yield insight into the mechanism of fusion and may help to understand the process.

The platforms presented in this thesis can be utilized in future projects to study a multitude of membrane properties. Especially the use and immobilization of native vesicles is very interesting. This type of vesicle cannot be easily tagged and the immobilization protocol described in chapter 3 is therefore the only reliable tethering approach available. Compared to artificial liposomes, native vesicles have the advantage that membrane proteins of interest can be simply over-expressed in transfected cell lines to increase their copy number in the membrane. The described procedure for blebbing the cells and immobilizing these 'minimal cells' circumvents the need to transfer these membrane proteins into tagged liposomes. This greatly simplifies binding experiments, as well as transport assays such as the study of PgP-transporters, which are under current investigation in the group of Prof. Dittrich. Additionally, studies on G-protein-coupled receptors (GPCRs) would be of high interest. GPCRs are the transducers of the cell membrane, basically translating external physical and chemical stimuli to an appropriate response inside the cell. Although they therefore represent a great drug target and screening of ligands is needed, no microfluidic implementation has been reported yet. By over-expressing the desired GPCR in cells, followed by blebbing of vesicles and their immobilization in microfluidic devices, a screening platform for ligands would be quickly established. Alternatively, another way could be used to bring membranes with GPCRs in microdevices. It was shown that cells can be grown on micrometer-sized beads and that the disruption of these cells leaves only the attached membrane, available

for studying GPCRs in the membrane [208]. With the techniques presented in this thesis to immobilize cells in traps, particles can also be trapped and arrayed. Therefore, it should be straightforward to implement assays for testing GPCRs on beads into microfluidic devices. This would allow rapid fluid exchange and would require less sample.

Another intriguing application of the platforms presented herein is to study effects of shear stress and other mechanical influences on lipid membranes and mechanosensitive membrane proteins. It is known that certain membrane proteins and even lipids are influenced by mechanical stimuli [209]. Hence, mechanobiology is an emerging research field where external mechanical stimuli are delivered to cells and responses are recorded [210]. However, although these whole cell studies are very important to understand the complete cell response, single molecule studies are essential to understand the underlying biophysics. These experiments have usually been performed in a BLM without microfluidics, for example to study the behavior of the epithelial Na^{2+} channel (ENaC) [211]. The control over pressures and flow rates (the external mechanical stimuli), the ease of membrane integration and the possibility for parallelization make the microfluidic devices presented in this thesis highly suited for these studies.

Furthermore, the protocols and platforms could be used to enhance the functionality of artificial cells. It was shown that cells traps can also be used to trap GUVs (data not shown), which are often used as cell models, at predefined locations. Hence, it is feasible to bring GUVs together with SUVs in the same manner as it was shown in chapter 5 for cells. Molecules and proteins can then be introduced into the GUVs by fusion, thereby adding certain functions to the GUV. Since the production of GUVs is usually limited to certain buffers and molecules that can be introduced into the interior and the membrane this could be a general approach to accomplish modifications of the GUV.

In summary, the platforms presented here are highly suitable for fundamental studies on membrane transport, and well as for screening of molecules in high-throughput experiments.

Bibliography

- [1] A Jesorka and O Orwar. Liposomes: Technologies and Analytical Applications. *Annual Review Of Analytical Chemistry*, 1:801–832, 2008.
- [2] AD Bangham, MM Standish, and JC Watkins. Diffusion of univalent ions across the lamellae of swollen phospholipids. *Journal of Molecular Biology*, 13(1):238–252, 1965.
- [3] VP Torchilin. Recent advances with liposomes as pharmaceutical carriers. *Nature Reviews Drug Discovery*, 4(2):145–160, 2005.
- [4] SF Fenz and K Sengupta. Giant vesicles as cell models. *Integrative Biology*, 4:982–995, 2012.
- [5] KA Edwards and AJ Baeumner. Liposomes in analyses. *Talanta*, 68(5):1421–1431, 2006.
- [6] KA Edwards, OR Bolduc, and AJ Baeumner. Miniaturized bioanalytical systems: enhanced performance through liposomes. *Current Opinion In Chemical Biology*, 16(3-4):444–452, 2012.
- [7] R Blumenthal, MJ Clague, SR Durell, and RM Epanand. Membrane fusion. *Chemical Reviews*, 103(1):53–69, 2003.
- [8] SK Wiedmer, ML Riekkola, and MS Jussila. Phospholipids and liposomes in liquid chromatographic and capillary electromigration techniques. *TrAC Trends in Analytical Chemistry*, 23(8):562–582, 2004.
- [9] D Peer, JM Karp, S Hong, OC Farokhzad, R Margalit, and R Langer. Nanocarriers as an emerging platform for cancer therapy. *Nature Nanotechnology*, 2(12):751–760, 2007.
- [10] K Sugano, M Kansy, P Artursson, A Avdeef, S Bendels, L Di, GF Ecker, B Faller, H Fischer, G Gerebtzoff, H Lennernaes, and F Senner. Coexistence of passive and carrier-mediated processes in drug transport. *Nature Reviews Drug Discovery*, 9(8):597–614, 2010.
- [11] SD Kraemer, D Lombardi, A Primorac, AV Thomae, and H Wunderli-Allenspach. Lipid-Bilayer Permeation of Drug-Like Compounds. *Chemistry & Biodiversity*, 6(11):1900–1916, 2009.
- [12] CA Lipinski, F Lombardo, BW Dominy, and PJ Feeney. Experimental and computational approaches to estimate solubility and permeability in drug discovery and development settings. *Advanced Drug Delivery Reviews*, 64:4–17, 2012.

- [13] B Alberts. *Molecular biology of the cell*. Reference edition. Garland Pub, 5th edition, 2008.
- [14] SM Saparov, YN Antonenko, and P Pohl. A new model of weak acid permeation through membranes revisited: does Overton still rule? *Biophysical Journal*, 90(11): L86–8, 2006.
- [15] A Walter and J Gutknecht. Monocarboxylic acid permeation through lipid bilayer membranes. *The Journal of membrane biology*, 77(3):255–264, 1984.
- [16] JMA Grime, MA Edwards, NC Rudd, and PR Unwin. Quantitative visualization of passive transport across bilayer lipid membranes. *Proceedings Of The National Academy Of Sciences Of The United States Of America*, 105(38):14277–14282, 2008.
- [17] AV Thomae, H Wunderli-Allenspach, and SD Kramer. Permeation of aromatic carboxylic acids across lipid bilayers: The pH-partition hypothesis revisited. *Biophysical Journal*, 89(3):1802–1811, 2005.
- [18] M Kansy, F Senner, and K Gubernator. Physicochemical high throughput screening: Parallel artificial membrane permeation assay in the description of passive absorption processes. *Journal Of Medicinal Chemistry*, 41(7):1007–1010, 1998.
- [19] T Korjamo, A T Heikkinen, and J Monkkonen. Analysis of Unstirred Water Layer in In Vitro Permeability Experiments. *Journal of Pharmaceutical Sciences*, 98(12): 4469–4479, 2009.
- [20] ME Haque, TJ McIntosh, and BR Lentz. Influence of lipid composition on physical properties and peg-mediated fusion of curved and uncurved model membrane vesicles: "nature's own" fusogenic lipid bilayer. *Biochemistry*, 40(14):4340–4348, 2001.
- [21] BR Lentz. PEG as a tool to gain insight into membrane fusion. *European Biophysics Journal With Biophysics Letters*, 36(4-5):315–326, 2007.
- [22] D Hoekstra and N Düzgünes. Lipid mixing assays to determine fusion in liposome systems. *Methods In Enzymology*, 220:15–32, 1993.
- [23] N Düzgünes and J Wilschut. Fusion assays monitoring intermixing of aqueous contents. *Methods In Enzymology*, 220:3–14, 1993.
- [24] J Nikolaus, JM Warner, B O'Shaughnessy, and A Herrmann. The pathway to membrane fusion through hemifusion. *Current Topics in Membranes*, 68:1–32, 2011.
- [25] LV Chernomordik and MM Kozlov. Mechanics of membrane fusion. *Nature Structural & Molecular Biology*, 15(7):675–683, 2008.
- [26] L Chernomordik, A Chanturiya, J Green, and J Zimmerberg. The hemifusion intermediate and its conversion to complete fusion: regulation by membrane composition. *Biophysical Journal*, 69(3):922–929, 1995.

-
- [27] LV Chernomordik and MM Kozlov. Protein-lipid interplay in fusion and fission of biological membranes. *Annual Review of Biochemistry*, 72:175–207, 2003.
- [28] J Marra and J Israelachvili. Direct measurements of forces between phosphatidylcholine and phosphatidylethanolamine bilayers in aqueous electrolyte solutions. *Biochemistry*, 24(17):4608–4618, 1985.
- [29] H Karanth and RSR Murthy. pH-sensitive liposomes—principle and application in cancer therapy. *The Journal of Pharmacy and Pharmacology*, 59(4):469–483, 2007.
- [30] MB Yatvin, W Kreutz, BA Horwitz, and M Shinitzky. pH-sensitive liposomes: possible clinical implications. *Science*, 210(4475):1253–1255, 1980.
- [31] RM Straubinger. pH-sensitive liposomes for delivery of macromolecules into cytoplasm of cultured cells. *Methods In Enzymology*, 221:361–376, 1993.
- [32] J Connor, MB Yatvin, and L Huang. pH-sensitive liposomes: acid-induced liposome fusion. *Proceedings Of The National Academy Of Sciences Of The United States Of America*, 81(6):1715–1718, 1984.
- [33] H Ellens, J Bentz, and FC Szoka. pH-induced destabilization of phosphatidylethanolamine-containing liposomes: role of bilayer contact. *Biochemistry*, 23(7):1532–1538, 1984.
- [34] N Düzgünes, RM Straubinger, PA Baldwin, DS Friend, and D Papahadjopoulos. Proton-induced fusion of oleic acid-phosphatidylethanolamine liposomes. *Biochemistry*, 24(13):3091–3098, 1985.
- [35] R Jahn and RH Scheller. SNAREs—engines for membrane fusion. *Nature Reviews. Molecular cell biology*, 7(9):631–643, 2006.
- [36] E Karatekin, J Di Giovanni, C Iborra, J Coleman, B O’Shaughnessy, M Seagar, and JE Rothman. A fast, single-vesicle fusion assay mimics physiological SNARE requirements. *Proceedings Of The National Academy Of Sciences Of The United States Of America*, 107(8):3517–3521, 2010.
- [37] SC Harrison. Viral membrane fusion. *Nature Structural & Molecular Biology*, 15(7):690–698, 2008.
- [38] D Hoekstra, T de Boer, K Klappe, and J Wilschut. Fluorescence method for measuring the kinetics of fusion between biological membranes. *Biochemistry*, 23(24):5675–5681, 1984.
- [39] M J Clague, C Schoch, L Zech, and R Blumenthal. Gating kinetics of pH-activated membrane-fusion of vesicular stomatitis-virus with cells - stopped-flow measurements by dequenching of octadecylrhodamine fluorescence. *Biochemistry*, 29(5):1303–1308, 1990.

- [40] SC Terry, JH Jerman, and JB Angell. A gas chromatographic air analyzer fabricated on a silicon wafer. *IEEE Transactions on Electron Devices*, 26(12):1880–1886, 1979.
- [41] A Manz, N Graber, and HM Widmer. Miniaturized total chemical analysis systems: A novel concept for chemical sensing. *Sensors and Actuators B-Chemical*, 1(1-6):244–248, 1990.
- [42] DJ Harrison, K Fluri, K Seiler, Z Fan, CS Effenhauser, and A Manz. Micromachining a miniaturized capillary electrophoresis-based chemical analysis system on a chip. *Science*, 261(5123):895–897, 1993.
- [43] P Wilding, MA Shoffner, and LJ Kricka. PCR in a silicon microstructure. *Clinical Chemistry*, 40(9):1815–1818, 1994.
- [44] AY Fu, C Spence, A Scherer, FH Arnold, and SR Quake. A microfabricated fluorescence-activated cell sorter. *Nature Biotechnology*, 17(11):1109–1111, 1999.
- [45] DC Duffy, JC McDonald, OJA Schueller, and GM Whitesides. Rapid prototyping of microfluidic systems in poly(dimethylsiloxane). *Analytical Chemistry*, 70(23):4974–4984, 1998.
- [46] JI Park, A Saffari, S Kumar, A Günther, and E Kumacheva. Microfluidic synthesis of polymer and inorganic particulate materials. *Annual Review of Materials Research*, 40:415–443, 2010.
- [47] Y Song, J Hormes, and CSSR Kumar. Microfluidic synthesis of nanomaterials. *Small*, 4(6):698–711, 2008.
- [48] E Kjeang, N Djilali, and D Sinton. Microfluidic fuel cells: A review. *Journal Of Power Sources*, 186(2):353–369, 2009.
- [49] CD Chin, V Linder, and SK Sia. Commercialization of microfluidic point-of-care diagnostic devices. *Lab On A Chip*, 12(12):2118–2134, 2012.
- [50] J El-Ali, PK Sorger, and KF Jensen. Cells on chips. *Nature*, 442(7101):403–411, 2006.
- [51] X Mu, W Zheng, J Sun, W Zhang, and X Jiang. Microfluidics for Manipulating Cells. *Small*, 9(1):9–21, 2012.
- [52] T Squires and S Quake. Microfluidics: Fluid physics at the nanoliter scale. *Reviews of Modern Physics*, 77(3):977–1026, 2005.
- [53] AD Howard, G McAllister, SD Feighner, Q Liu, RP Nargund, LH Van der Ploeg, and AA Patchett. Orphan G-protein-coupled receptors and natural ligand discovery. *Trends in Pharmacological Sciences*, 22(3):132–140, 2001.
- [54] H Suzuki and S Takeuchi. Microtechnologies for membrane protein studies. *Analytical And Bioanalytical Chemistry*, 391(8):2695–2702, 2008.

-
- [55] SM Christensen and D Stamou. Surface-based lipid vesicle reactor systems: fabrication and applications. *Soft Matter*, 3(7):828–836, 2007.
- [56] SM Christensen and DG Stamou. Sensing-Applications of Surface-Based Single Vesicle Arrays. *Sensors*, 10(12):11352–11368, 2010.
- [57] D Stamou, C Duschl, E Delamarche, and H Vogel. Self-Assembled Microarrays of Attoliter Molecular Vessels. *Angewandte Chemie International ed.*, 42(45):5580–5583, 2003.
- [58] S Svedhem, I Pfeiffer, C Larsson, C Wingren, C Borrebaeck, and F Höök. Patterns of DNA-labeled and scFv-antibody-carrying lipid vesicles directed by material-specific immobilization of DNA and supported lipid bilayer formation on an Au/SiO₂ template. *Chembiochem*, 4(4):339–343, 2003.
- [59] C Yoshina-Ishii, GP Miller, ML Kraft, ET Kool, and SG Boxer. General method for modification of liposomes for encoded assembly on supported bilayers. *Journal Of The American Chemical Society*, 127(5):1356–1357, 2005.
- [60] T Stora, Z Dienes, H Vogel, and C Duschl. Histidine-Tagged Amphiphiles for the Reversible Formation of Lipid Bilayer Aggregates on Chelator-Functionalized Gold Surfaces. *Langmuir*, 16(12):5471–5478, 2000.
- [61] ND Kalyankar, MK Sharma, SV Vaidya, D Calhoun, C Maldarelli, A Couzis, and L Gilchrist. Arraying of intact liposomes into chemically functionalized microwells. *Langmuir*, 22(12):5403–5411, 2006.
- [62] MR Dusseiller, B Niederberger, B Städler, D Falconnet, M Textor, and J Vörös. A novel crossed microfluidic device for the precise positioning of proteins and vesicles. *Lab On A Chip*, 5(12):1387, 2005.
- [63] DC Tan, IPM Wijaya, M Andreasson-Ochsner, EN Vasina, M Nallani, W Hunziker, and E-K Sinner. A novel microfluidics-based method for probing weak protein–protein interactions. *Lab On A Chip*, 12(15):2726, 2012.
- [64] P Mueller, DO Rudin, HT Tien, and WC Wescott. Reconstitution of cell membrane structure in vitro and its transformation into an excitable system. *Nature*, 194:979–980, 1962.
- [65] A Janshoff and C Steinem. Transport across artificial membranes-an analytical perspective. *Analytical And Bioanalytical Chemistry*, 385(3):433–451, 2006.
- [66] H Suzuki, K Tabata, Y Kato-Yamada, H Noji, and S Takeuchi. Planar lipid bilayer reconstitution with a micro-fluidic system. *Lab On A Chip*, 4(5):502–505, 2004.
- [67] H Suzuki, KV Tabata, H Noji, and S Takeuchi. Electrophysiological recordings of single ion channels in planar lipid bilayers using a polymethyl methacrylate microfluidic chip. *Biosensors & Bioelectronics*, 22(6):1111–1115, 2007.

- [68] M Zagnoni, ME Sandison, and H Morgan. Microfluidic array platform for simultaneous lipid bilayer membrane formation. *Biosensors & Bioelectronics*, 24(5):1235–1240, 2009.
- [69] M Zagnoni, ME Sandison, P Marius, AG Lee, and H Morgan. Controlled delivery of proteins into bilayer lipid membranes on chip. *Lab On A Chip*, 7(9):1176–1183, 2007.
- [70] X Han, A Studer, H Sehr, I Geissbühler, M Di Berardino, FK Winkler, and LX Tiefenauer. Nanopore Arrays for Stable and Functional Free-Standing Lipid Bilayers. *Advanced Materials*, 19(24):4466–4470, 2007.
- [71] R Kawano, T Osaki, H Sasaki, and S Takeuchi. A Polymer-Based Nanopore-Integrated Microfluidic Device for Generating Stable Bilayer Lipid Membranes. *Small*, 6(19):2100–2104, 2010.
- [72] R Kawano, T Osaki, H Sasaki, M Takinoue, S Yoshizawa, and S Takeuchi. Rapid detection of a cocaine-binding aptamer using biological nanopores on a chip. *Journal Of The American Chemical Society*, 133(22):8474–8477, 2011.
- [73] K Funakoshi, H Suzuki, and S Takeuchi. Lipid bilayer formation by contacting monolayers in a microfluidic device for membrane protein analysis. *Analytical Chemistry*, 78(24):8169–8174, 2006.
- [74] N Malmstadt, MA Nash, RF Purnell, and JJ Schmidt. Automated formation of lipid-bilayer membranes in a microfluidic device. *Nano Letters*, 6(9):1961–1965, 2006.
- [75] CE Stanley, KS Elvira, XZ Niu, AD Gee, O Ces, JB Edel, and AJ Demello. A microfluidic approach for high-throughput droplet interface bilayer (DIB) formation. *Chemical Communications*, 46(10):1620–1622, 2010.
- [76] S Ota, H Suzuki, and S Takeuchi. Microfluidic lipid membrane formation on microchamber arrays. *Lab On A Chip*, 11(15):2485–2487, 2011.
- [77] LK Tamm and HM McConnell. Supported phospholipid bilayers. *Biophysical Journal*, 47(1):105–113, 1985.
- [78] ET Castellana and PS Cremer. Solid supported lipid bilayers: From biophysical studies to sensor design. *Surface Science Reports*, 61(10):429–444, 2006.
- [79] E Reimhult and K Kumar. Membrane biosensor platforms using nano- and microporous supports. *Trends in Biotechnology*, 26(2):82–89, 2008.
- [80] CH Nielsen. Biomimetic membranes for sensor and separation applications. *Analytical And Bioanalytical Chemistry*, 395(3):697–718, 2009.
- [81] Maria Sundh, Sofia Svedhem, and Duncan S Sutherland. Influence of phase separating lipids on supported lipid bilayer formation at SiO₂ surfaces. *Physical chemistry chemical physics : PCCP*, 12(2):453–460, 2009.

-
- [82] M Tanaka and E Sackmann. Polymer-supported membranes as models of the cell surface. *Nature*, 437(7059):656–663, 2005.
- [83] JT Groves, N Ulman, and SG Boxer. Micropatterning fluid lipid bilayers on solid supports. *Science*, 275(5300):651–653, 1997.
- [84] L Kam and SG Boxer. Spatially selective manipulation of supported lipid bilayers by laminar flow: Steps toward biomembrane microfluidics. *Langmuir*, 19(5):1624–1631, 2003.
- [85] T Yang, S Jung, H Mao, and PS Cremer. Fabrication of Phospholipid Bilayer-Coated Microchannels for On-Chip Immunoassays. *Analytical Chemistry*, 73(2):165–169, 2001.
- [86] C Hamai, T Yang, S Kataoka, PS Cremer, and SM Musser. Effect of Average Phospholipid Curvature on Supported Bilayer Formation on Glass by Vesicle Fusion. *Biophysical Journal*, 90(4):1241–1248, 2006.
- [87] CL Kuyper, JS Kuo, SA Mutch, and DT Chiu. Proton permeation into single vesicles occurs via a sequential two-step mechanism and is heterogeneous. *Journal Of The American Chemical Society*, 128(10):3233–3240, 2006.
- [88] S Li, P Hu, and N Malmstadt. Confocal Imaging to Quantify Passive Transport across Biomimetic Lipid Membranes. *Analytical Chemistry*, 82(18):7766–7771, 2010.
- [89] S Li, P C Hu, and N Malmstadt. Imaging Molecular Transport across Lipid Bilayers. *Biophysical Journal*, 101(3):700–708, 2011.
- [90] G Ohlsson, SR Tabaei, J Beech, J Kvassman, U Johanson, P Kjellbom, JO Tegenfeldt, and F Höök. Solute transport on the sub 100 ms scale across the lipid bilayer membrane of individual proteoliposomes. *Lab On A Chip*, 12(22):4635–4643, 2012.
- [91] G Favero, L Campanella, S Cavallo, A D’Annibale, M Perrella, E Mattei, and T Ferri. Glutamate Receptor Incorporated in a Mixed Hybrid Bilayer Lipid Membrane Array, as a Sensing Element of a Biosensor Working under Flowing Conditions. *Journal Of The American Chemical Society*, 127(22):8103–8111, 2005.
- [92] C Shao, B Sun, M Colombini, and DL Devoe. Rapid microfluidic perfusion enabling kinetic studies of lipid ion channels in a bilayer lipid membrane chip. *Annals of Biomedical Engineering*, 39(8):2242–2251, 2011.
- [93] LJ Siskind, A Davoody, N Lewin, S Marshall, and M Colombini. Enlargement and Contracture of C2-Ceramide Channels. *Biophysical Journal*, 85(3):1560–1575, 2003.
- [94] M Brändén, S Dahlin, and F Höök. Label-free measurements of molecular transport across liposome membranes using evanescent-wave sensing. *ChemPhysChem*, 9(17):2480–2485, 2008.

- [95] H Sasaki, R Kawano, T Osaki, K Kamiya, and S Takeuchi. Single-vesicle estimation of ATP-binding cassette transporters in microfluidic channels. *Lab On A Chip*, 12(4):702–704, 2012.
- [96] H Jung, AD Robison, and PS Cremer. Multivalent ligand–receptor binding on supported lipid bilayers. *Journal of Structural Biology*, 168(1):90–94, 2009.
- [97] T Yang, OK Baryshnikova, H Mao, MA Holden, and PS Cremer. Investigations of bivalent antibody binding on fluid-supported phospholipid membranes: the effect of hapten density. *Journal Of The American Chemical Society*, 125(16):4779–4784, 2003.
- [98] J Shi, T Yang, S Kataoka, Y Zhang, AJ Diaz, and PS Cremer. GM 1 Clustering Inhibits Cholera Toxin Binding in Supported Phospholipid Membranes. *Journal Of The American Chemical Society*, 129(18):5954–5961, 2007.
- [99] H Jung, T Yang, MD Lasagna, J Shi, GD Reinhart, and PS Cremer. Impact of Hapten Presentation on Antibody Binding at Lipid Membrane Interfaces. *Biophysical Journal*, 94(8):3094–3103, 2008.
- [100] ED Goluch, AW Shaw, SG Sligar, and C Liu. Microfluidic patterning of nanodisc lipid bilayers and multiplexed analysis of protein interaction. *Lab On A Chip*, 8(10):1723, 2008.
- [101] DJ Estes and M Mayer. Giant liposomes in physiological buffer using electroformation in a flow chamber. *Biochimica Et Biophysica Acta*, 1712(2):152–160, 2005.
- [102] DJ Estes, SR Lopez, AO Fuller, and M Mayer. Triggering and visualizing the aggregation and fusion of lipid membranes in microfluidic chambers. *Biophysical Journal*, 91(1):233–243, 2006.
- [103] DL Floyd, JR Ragains, JJ Skehel, SC Harrison, and AM van Oijen. Single-particle kinetics of influenza virus membrane fusion. *Proceedings Of The National Academy Of Sciences Of The United States Of America*, 105(40):15382–15387, 2008.
- [104] DA Costello, DW Lee, J Drewes, KA Vasquez, K Kisler, U Wiesner, L Pollack, GR Whittaker, and S Daniel. Influenza virus-membrane fusion triggered by proton uncaging for single particle studies of fusion kinetics. *Analytical Chemistry*, 84(20):8480–8489, 2012.
- [105] H Mao, T Yang, and PS Cremer. A microfluidic device with a linear temperature gradient for parallel and combinatorial measurements. *Journal Of The American Chemical Society*, 124(16):4432–4435, 2002.
- [106] L Chao and S Daniel. Measuring the partitioning kinetics of membrane biomolecules using patterned two-phase coexistent lipid bilayers. *Journal Of The American Chemical Society*, 133(39):15635–15643, 2011.
- [107] LM Borland, S Kottegoda, KS Phillips, and NL Allbritton. Chemical analysis of single cells. *Annual Review of Analytical Chemistry*, 1:191–227, 2008.

-
- [108] N Fertig, RH Blick, and JC Behrends. Whole cell patch clamp recording performed on a planar glass chip. *Biophysical Journal*, 82(6):3056–3062, 2002.
- [109] C Farre and N Fertig. HTS techniques for patch clamp-based ion channel screening – advances and economy. *Expert Opinion on Drug Discovery*, 7(6):515–524, 2012.
- [110] C Ionescu-Zanetti, RM Shaw, J Seo, Y-N Jan, LY Jan, and LP Lee. Mammalian electrophysiology on a microfluidic platform. *Proceedings Of The National Academy Of Sciences Of The United States Of America*, 102(26):9112–9117, 2005.
- [111] H Kimura, T Yamamoto, H Sakai, Y Sakai, and T Fujii. An integrated microfluidic system for long-term perfusion culture and on-line monitoring of intestinal tissue models. *Lab On A Chip*, 8(5):741–746, 2008.
- [112] EWK Young, MWL Watson, S Srigunapalan, AR Wheeler, and CA Simmons. Technique for Real-Time Measurements of Endothelial Permeability in a Microfluidic Membrane Chip Using Laser-Induced Fluorescence Detection. *Analytical Chemistry*, 82(3):808–816, 2010.
- [113] JH Yeon and J Park. Drug permeability assay using microhole-trapped cells in a microfluidic device. *Analytical Chemistry*, 81(5):1944–1951, 2009.
- [114] G Tresset and S Takeuchi. A microfluidic device for electrofusion of biological vesicles. *Biomedical Microdevices*, 6(3):213–218, 2004.
- [115] J Wang and C Lu. Microfluidic cell fusion under continuous direct current voltage. *Applied Physics Letters*, 89(23):234102, 2006.
- [116] TC Bakker Schut, YM Kraan, W Barlag, L de Leij, BG de Grooth, and J Greve. Selective electrofusion of conjugated cells in flow. *Biophysical Journal*, 65(2):568–572, 1993.
- [117] AM Skelley, O Kirak, H Suh, R Jaenisch, and J Voldman. Microfluidic control of cell pairing and fusion. *Nature Methods*, 6(2):147–152, 2009.
- [118] HN Joensson, ML Samuels, ER Brouzes, M Medkova, M Uhlén, DR Link, and H Andersson-Svahn. Detection and analysis of low-abundance cell-surface biomarkers using enzymatic amplification in microfluidic droplets. *Angewandte Chemie International ed.*, 48(14):2518–2521, 2009.
- [119] J Wang, B Fei, RL Geahlen, and C Lu. Quantitative analysis of protein translocations by microfluidic total internal reflection fluorescence flow cytometry. *Lab On A Chip*, 10(20):2673–2679, 2010.
- [120] D Qin, YN Xia, and GM Whitesides. Rapid prototyping of complex structures with feature sizes larger than 20 μm . *Advanced Materials*, 8(11), 1996.
- [121] A Bernard, E Delamarche, H Schmid, B Michel, HR Bosshard, and H Biebuyck. Printing patterns of proteins. *Langmuir*, 14(9):2225–2229, 1998.

- [122] A Khademhosseini, KY Suh, S Jon, G Eng, J Yeh, G-J Chen, and R Langer. A soft lithographic approach to fabricate patterned microfluidic channels. *Analytical Chemistry*, 76(13):3675–3681, 2004.
- [123] LD Mayer, MJ Hope, and PR Cullis. Vesicles of variable sizes produced by a rapid extrusion procedure. *Biochimica Et Biophysica Acta*, 858(1):161–168, 1986.
- [124] D Falconnet, G Csucs, HM Grandin, and M Textor. Surface engineering approaches to micropattern surfaces for cell-based assays. *Biomaterials*, 27(16):3044–3063, 2006.
- [125] D Di Carlo, LY Wu, and LP Lee. Dynamic single cell culture array. *Lab On A Chip*, 6(11):1445–1449, 2006.
- [126] SS Lee, IA Vizcarra, DHEW Huberts, LP Lee, and M Heinemann. Whole lifespan microscopic observation of budding yeast aging through a microfluidic dissection platform. *Proceedings Of The National Academy Of Sciences Of The United States Of America*, 109(13):4916–4920, 2012.
- [127] M-C Kim, BC Isenberg, J Sutin, A Meller, JY Wong, and CM Klapperich. Programmed trapping of individual bacteria using micrometre-size sieves. *Lab On A Chip*, 11(6):1089–1095, 2011.
- [128] B Stadler, D Falconnet, I Pfeiffer, F Höök, and J Vörös. Micropatterning of DNA-tagged vesicles. *Langmuir*, 20(26):11348–11354, 2004.
- [129] SB Sato, K Ishii, A Makino, K Iwabuchi, A Yamaji-Hasegawa, Y Senoh, I Nagaoka, H Sakuraba, and T Kobayashi. Distribution and transport of cholesterol-rich membrane domains monitored by a membrane-impermeant fluorescent polyethylene glycol-derivatized cholesterol. *The Journal of biological chemistry*, 279(22):23790–23796, 2004.
- [130] RD Lovchik, F Bianco, M Matteoli, and E Delamarche. Controlled deposition of cells in sealed microfluidics using flow velocity boundaries. *Lab On A Chip*, 9(10):1395–1402, 2009.
- [131] J Mercer and A Helenius. Vaccinia virus uses macropinocytosis and apoptotic mimicry to enter host cells. *Science*, 320(5875):531–535, 2008.
- [132] H Pick, EL Schmid, A-P Tairi, E Ilegems, R Hovius, and H Vogel. Investigating cellular signaling reactions in single attoliter vesicles. *Journal Of The American Chemical Society*, 127(9):2908–2912, 2005.
- [133] MI Angelova and DS Dimitrov. Liposome Electroformation. *Faraday Discussions*, 81, 1986.
- [134] C Dietrich, LA Bagatolli, ZN Volovyk, NL Thompson, M Levi, K Jacobson, and E Gratton. Lipid rafts reconstituted in model membranes. *Biophysical Journal*, 80(3):1417–1428, 2001.

-
- [135] GD Eytan. Use of liposomes for reconstitution of biological functions. *Biochimica Et Biophysica Acta*, 694(2):185–202, 1982.
- [136] MK Doeven, JHA Folgering, V Krasnikov, ER Geertsma, G van den Bogaart, and B Poolman. Distribution, lateral mobility and function of membrane proteins incorporated into giant unilamellar vesicles. *Biophysical Journal*, 88(2):1134–1142, 2005.
- [137] P Walde and S Ichikawa. Enzymes inside lipid vesicles: Preparation, reactivity and applications. *Biomolecular Engineering*, 18(4):143–177, 2001.
- [138] T-M Hsin and ES Yeung. Single-molecule reactions in liposomes. *Angewandte Chemie International ed.*, 46(42):8032–8035, 2007.
- [139] SM Nomura, K Tsumoto, T Hamada, K Akiyoshi, Y Nakatani, and K Yoshikawa. Gene expression within cell-sized lipid vesicles. *ChemBioChem*, 4(11):1172–1175, 2003.
- [140] H Wu, AE Oliver, VN Ngassam, CK Yee, AN Parikh, and Y Yeh. Preparation, characterization, and surface immobilization of native vesicles obtained by mechanical extrusion of mammalian cells. *Integrative Biology*, 4(6):685–692, 2012.
- [141] FI Schmidt, CKE Bleck, and J Mercer. Poxvirus host cell entry. *Current Opinion in Virology*, 2(1):20–27, 2012.
- [142] N Ruiz, D Kahne, and TJ Silhavy. Transport of lipopolysaccharide across the cell envelope: the long road of discovery. *Nature Reviews Microbiology*, 7(9):677–683, 2009.
- [143] P Kohut, D Wustner, L Hronska, K Kuchler, I Hapala, and M Valachovic. The role of ABC proteins Aus1p and Pdr11p in the uptake of external sterols in yeast: Dehydroergosterol fluorescence study. *Biochemical and Biophysical Research Communications*, 404(1):233–238, 2011.
- [144] M Argast and CF Beck. Tetracycline diffusion through phospholipid-bilayers and binding to phospholipids. *Antimicrobial Agents And Chemotherapy*, 26(2):263–265, 1984.
- [145] D Schnappinger and W Hillen. Tetracyclines: Antibiotic action, uptake, and resistance mechanisms. *Archives Of Microbiology*, 165(6):359–369, 1996.
- [146] H Nikaido and DG Thanassi. Penetration of lipophilic agents with multiple protonation sites into bacterial-cells - Tetracyclines and fluoroquinolones as examples. *Antimicrobial Agents And Chemotherapy*, 37(7):1393–1399, 1993.
- [147] I Chopra and M Roberts. Tetracycline antibiotics: Mode of action, applications, molecular biology, and epidemiology of bacterial resistance. *Microbiology And Molecular Biology Reviews*, 65(2), 2001.
- [148] A Avdeef. Physicochemical profiling (solubility, permeability and charge state). *Current topics in medicinal chemistry*, 1(4):277–351, 2001.

- [149] A Avdeef, S Bendels, L Di, B Faller, M Kansy, K Sugano, and Y Yamauchi. PAMPA - Critical factors for better predictions of absorption. *Journal of Pharmaceutical Sciences*, 96(11):2893–2909, 2007.
- [150] D Galinis-Luciani, L Nguyen, and M Yazdanian. Is PAMPA a useful too for discovery? *Journal of Pharmaceutical Sciences*, 96(11):2886–2892, 2007.
- [151] H Lennernäs. Human intestinal permeability. *Journal of Pharmaceutical Sciences*, 87(4):403–410, 1998.
- [152] AM Seddon, D Casey, RV Law, A Gee, RH Templer, and O Ces. Drug interactions with lipid membranes. *Chemical Society Reviews*, 38(9):2509–2519, 2009.
- [153] P E Sum and P Petersen. Synthesis and structure-activity relationship of novel glycycline derivatives leading to the discovery of GAR-936. *Bioorganic & Medicinal Chemistry Letters*, 9(10):1459–1462, 1999.
- [154] KN Agwuh and A MacGowan. Pharmacokinetics and pharmacodynamics of the tetracyclines including glycyclines. *The Journal of antimicrobial chemotherapy*, 58(2):256–265, 2006.
- [155] MG Charest, CD Lerner, JD Brubaker, DR Siege, and AG Myers. A convergent enantioselective route to structurally diverse 6-deoxytetracycline antibiotics. *Science*, 308(5720):395–398, 2005.
- [156] M Bally, K Bailey, K Sugihara, D Grieshaber, J Voeroes, and B Städler. Liposome and Lipid Bilayer Arrays Towards Biosensing Applications. *Small*, 6(22):2481–2497, 2010.
- [157] GR Bartlett. Phosphorus assay in column chromatography. *The Journal of biological chemistry*, 234(3):466–468, 1959.
- [158] S Paula, AG Volkov, and DW Deamer. Permeation of halide anions through phospholipid bilayers occurs by the solubility-diffusion mechanism. *Biophysical Journal*, 74(1):319–327, 1998.
- [159] T Teorell and E Stenhagen. Universal buffer over the pH range 2.0 to 12.0. *Biochem Z*, 1938.
- [160] GT Peres, S Rath, and FG Reyes Reyes. A HPLC with fluorescence detection method for the determination of tetracyclines residues and evaluation of their stability in honey. *Food Control*, 21(5):620–625, 2010.
- [161] SV Eliseeva and JCG Buenzli. Lanthanide luminescence for functional materials and bio-sciences. *Chemical Society Reviews*, 39(1):189–227, 2010.
- [162] AN Grasso, LDS Teixeira, ND Vieira, and LC Courrol. Optical Properties of Metacycline, Oxytetracycline and Chlortetracycline Europium Complexes in the Presence of Hydrogen Peroxide. *Journal of Fluorescence*, 19(4):715–721, 2009.

- [163] M Saiki and FW Lima. Determination of stability-constants for complexes of rare-earth elements and tetracycline. *Journal Of Radioanalytical Chemistry*, 36(2):435–450, 1977.
- [164] MR Gilmartin, J McLaren, and J Schacht. Confounding factors in lanthanide ion probe spectrofluorometric assay of aminoglycoside antibiotics. *Analytical Biochemistry*, 283(1):116–119, 2000.
- [165] IV Tetko, J Gasteiger, R Todeschini, A Mauri, D Livingstone, P Ertl, VA Palyulin, EV Radchenko, NS Zefirov, AS Makarenko, VY Tanchuk, and VV Prokopenko. Virtual computational chemistry laboratory—design and description. *Journal of computer-aided molecular design*, 19(6):453–463, 2005.
- [166] IH Pitman. Pro-drugs of amides, imides, and amines. *Medicinal Research Reviews*, 1(2):189–214, 1981.
- [167] H Bundgaard and M Johansen. Prodrugs as Drug Delivery Systems .4. N-Mannich Bases as Potential Novel Prodrugs for Amides, Ureides, Amines, and Other Nh-Acidic Compounds. *Journal of Pharmaceutical Sciences*, 69(1):44–46, 1980.
- [168] AV Thomae, T Koch, C Panse, H Wunderli-Allenspach, and SD Krämer. Comparing the lipid membrane affinity and permeation of drug-like acids: the intriguing effects of cholesterol and charged lipids. *Pharmaceutical research*, 24(8):1457–1472, 2007.
- [169] D D Lasic. *Liposomes: from physics to applications* . Elsevier Science Publishers B.V.: Amsterdam, The Netherlands, 1993.
- [170] CJ Thomas and A Surolia. Kinetics of the interaction of endotoxin with polymyxin B and its analogs: a surface plasmon resonance analysis. *Febs Letters*, 445(2-3):420–424, 1999.
- [171] DC Drummond, M Zignani, and J Leroux. Current status of pH-sensitive liposomes in drug delivery. *Progress In Lipid Research*, 39(5):409–460, 2000.
- [172] RM Straubinger, K Hong, DS Friend, and D Papahadjopoulos. Endocytosis of liposomes and intracellular fate of encapsulated molecules: encounter with a low pH compartment after internalization in coated vesicles. *Cell*, 32(4):1069–1079, 1983.
- [173] RM Straubinger, N Düzgünes, and D Papahadjopoulos. pH-sensitive liposomes mediate cytoplasmic delivery of encapsulated macromolecules. *Febs Letters*, 179(1):148–154, 1985.
- [174] K Eyer, P Kuhn, C Hanke, and PS Dittrich. A microchamber array for single cell isolation and analysis of intracellular biomolecules. *Lab On A Chip*, 12(4):765–772, 2012.
- [175] P Ghosh, X Yang, R Arvizo, Z-J Zhu, SS Agasti, Z Mo, and VM Rotello. Intracellular delivery of a membrane-impermeable enzyme in active form using functionalized gold nanoparticles. *Journal Of The American Chemical Society*, 132(8):2642–2645, 2010.

- [176] JW Holland, C Hui, PR Cullis, and TD Madden. Poly(ethylene glycol)–lipid conjugates regulate the calcium-induced fusion of liposomes composed of phosphatidylethanolamine and phosphatidylserine. *Biochemistry*, 35(8):2618–2624, 1996.
- [177] R Blumenthal, SA Gallo, M Viard, Y Raviv, and A Puri. Fluorescent lipid probes in the study of viral membrane fusion. *Chemistry and Physics of Lipids*, 116(1-2):39–55, 2002.
- [178] N Düzgünes, TM Allen, J Fedor, and D Papahadjopoulos. Lipid mixing during membrane aggregation and fusion - why fusion assays disagree. *Biochemistry*, 26(25):8435–8442, 1987.
- [179] S Hamann, JF Kiilgaard, T Litman, FJ Alvarez-Leefmans, BR Winther, and T Zeuthen. Measurement of Cell Volume Changes by Fluorescence Self-Quenching. *Analytical And Bioanalytical Chemistry*, 12(2):139–145, 2002.
- [180] SD Patil, DG Rhodes, and DJ Burgess. Biophysical characterization of anionic lipoplexes. *Biochimica Et Biophysica Acta*, 1711(1):1–11, 2005.
- [181] GP Dimri, X Lee, G Basile, M Acosta, G Scott, C Roskelley, EE Medrano, M Linskens, I Rubelj, and O Pereira-Smith. A biomarker that identifies senescent human cells in culture and in aging skin in vivo. *Proceedings Of The National Academy Of Sciences Of The United States Of America*, 92(20):9363–9367, 1995.
- [182] DJ Kurz, S Decary, Y Hong, and JD Erusalimsky. Senescence-associated (beta)-galactosidase reflects an increase in lysosomal mass during replicative ageing of human endothelial cells. *Journal of Cell Science*, 113 (Pt 20):3613–3622, 2000.
- [183] M Marsh and A Helenius. Virus entry: open sesame. *Cell*, 124(4):729–740, 2006.
- [184] G Campadelli-Fiume, L Menotti, E Avitabile, and T Gianni. Viral and cellular contributions to herpes simplex virus entry into the cell. *Current Opinion in Virology*, 2(1):28–36, 2012.
- [185] B Moss. Poxvirus cell entry: how many proteins does it take? *Viruses*, 4(5):688–707, 2012.
- [186] CT Wild, DC Shugars, TK Greenwell, CB McDanal, and TJ Matthews. Peptides corresponding to a predictive alpha-helical domain of human immunodeficiency virus type 1 gp41 are potent inhibitors of virus infection. *Proceedings Of The National Academy Of Sciences Of The United States Of America*, 91(21):9770–9774, 1994.
- [187] NR Collins, RW Holz, and J Zimmerberg. *Comprehensive Biophysics*. Elsevier, Amsterdam, May 2012.
- [188] KI Damon. *Fields Virology*. Lippincott Williams & Wilkins, 2013.

-
- [189] AC Townsley, AS Weisberg, TR Wagenaar, and B Moss. Vaccinia virus entry into cells via a low-pH-dependent endosomal pathway. *Journal of Virology*, 80(18):8899–8908, 2006.
- [190] SC Gong, CF Lai, and M Esteban. Vaccinia virus induces cell fusion at acid pH and this activity is mediated by the N-terminus of the 14-kDa virus envelope protein. *Virology*, 178(1):81–91, 1990.
- [191] HK Johannsdottir, R Mancini, J Kartenbeck, L Amato, and A Helenius. Host cell factors and functions involved in vesicular stomatitis virus entry. *Journal of Virology*, 83(1):440–453, 2009.
- [192] MA Walling and JRE Shepard. Cellular heterogeneity and live cell arrays. *Chemical Society Reviews*, 40(7):4049–4076, 2011.
- [193] DG Spiller, CD Wood, DA Rand, and MRH White. Measurement of single-cell dynamics. *Nature*, 465(7299):736–745, 2010.
- [194] P Stiefel, FI Schmidt, P Dörig, P Behr, T Zambelli, JA Vorholt, and J Mercer. Cooperative vaccinia infection demonstrated at the single-cell level using FluidFM. *Nano Letters*, 12(8):4219–4227, 2012.
- [195] EJ Wolffe, S Vijaya, and B Moss. A myristylated membrane protein encoded by the vaccinia virus L1R open reading frame is the target of potent neutralizing monoclonal antibodies. *Virology*, 211(1):53–63, 1995.
- [196] FI Schmidt, CKE Bleck, A Helenius, and J Mercer. Vaccinia extracellular virions enter cells by macropinocytosis and acid-activated membrane rupture. *Embo Journal*, 30(17):3647–3661, 2011.
- [197] RW Doms, R Blumenthal, and B Moss. Fusion of intra- and extracellular forms of vaccinia virus with the cell membrane. *Journal of Virology*, 64(10):4884–4892, 1990.
- [198] JP Laliberte, AS Weisberg, and B Moss. The Membrane Fusion Step of Vaccinia Virus Entry Is Cooperatively Mediated by Multiple Viral Proteins and. *Plos Pathogens*, 7(12):e1002446, 2011.
- [199] J Mercer, S Knébel, FI Schmidt, J Crouse, C Burkard, and A Helenius. Vaccinia virus strains use distinct forms of macropinocytosis for host-cell entry. *Proceedings Of The National Academy Of Sciences Of The United States Of America*, 107(20):9346–9351, 2010.
- [200] T Stegmann, JM White, and A Helenius. Intermediates in influenza induced membrane fusion. *Embo Journal*, 9(13):4231–4241, 1990.
- [201] MJ Clague, C Schoch, L Zech, and R Blumenthal. Gating kinetics of pH-activated membrane fusion of vesicular stomatitis virus with cells: stopped-flow measurements by dequenching of octadecylrhodamine fluorescence. *Biochemistry*, 29(5):1303–1308, 1990.

- [202] R Bron, J M Wahlberg, H Garoff, and J Wilschut. Membrane fusion of Semliki Forest virus in a model system: correlation between fusion kinetics and structural changes in the envelope glycoprotein. *Embo Journal*, 12(2):693–701, 1993.
- [203] FM Hughson. Structural characterization of viral fusion proteins. *Current Biology*, 5(3):265–274, 1995.
- [204] SJ Chang, YX Chang, R Izmailyan, YL Tang, and W Chang. Vaccinia virus A25 and A26 proteins are fusion suppressors for mature virions and determine strain-specific virus entry pathways into HeLa, CHO-K1, and L cells. *Journal of Virology*, 84(17):8422–8432, 2010.
- [205] J Llopis, JM McCaffery, A Miyawaki, MG Farquhar, and RY Tsien. Measurement of cytosolic, mitochondrial, and Golgi pH in single living cells with green fluorescent proteins. *Proceedings Of The National Academy Of Sciences Of The United States Of America*, 95(12):6803–6808, 1998.
- [206] GB Melikyan, RJO Barnard, LG Abrahamyan, W Mothes, and JAT Young. Imaging individual retroviral fusion events: from hemifusion to pore formation and growth. *Proceedings Of The National Academy Of Sciences Of The United States Of America*, 102(24):8728–8733, 2005.
- [207] Z Bengali, PS Satheshkumar, and B Moss. Orthopoxvirus species and strain differences in cell entry. *Virology*, 433(2):506–512, 2012.
- [208] S Roizard, C Danelon, G Hassaïne, J Piguet, K Schulze, R Hovius, R Tampé, and H Vogel. Activation of G-Protein-Coupled Receptors in Cell-Derived Plasma Membranes Supported on Porous Beads. *Journal Of The American Chemical Society*, 133(42):16868–16874, 2011.
- [209] R Phillips, T Ursell, P Wiggins, and P Sens. Emerging roles for lipids in shaping membrane-protein function. *Nature Reviews Microbiology*, 459(7245):379–385, 2009.
- [210] F Kurth, K Eyer, A Franco-Obregón, and PS Dittrich. A new mechanobiological era: microfluidic pathways to apply and sense forces at the cellular level. *Current Opinion In Chemical Biology*, 16(3-4):400–408, 2012.
- [211] MS Awayda, II Ismailov, BK Berdiev, and DJ Benos. A cloned renal epithelial Na⁺ channel protein displays stretch activation in planar lipid bilayers. *The American Journal of Physiology*, 268(6 Pt 1), 1995.

Acknowledgments

First, I would like to thank Prof. Petra Dittrich for the possibility to perform the research for this thesis in her group. I am especially thankful for all the scientific freedom and trust I was given. Petra allowed me to follow my own little projects and interests in the lab, all of which helped me to gain a broad understanding of my research field.

I am very happy and thankful that Prof. Peter Walde co-examined this thesis on rather short notice, but with a lot of interest and enthusiasm.

Research is not a one-man-show, but a team endeavor. Many people helped me in the projects discussed in this thesis and in other projects. I am especially grateful to the help of Stefanie Krämer for discussions regarding permeability and the possibility to use equipment in her lab, Vincent Foster for measuring the lipid content in my lipid suspensions, Florian Schmidt for everything virus-related and great team work, Jason Mercer and Ari Helenius for discussions in the vaccinia virus project, Richard Obexer for the preparation of the GFP-labelled bacteria, Sara Fornera for applying one of my microchips in a very nice project, Jens Möller for introducing me to the MAPL process and Suse Dröscher for being my FIRST mentor.

Thankfully, I received much support from the whole Dittrich group. I thank everyone who worked in the group during my PhD time. It was always a really nice atmosphere and lots of fun! Especially the Friday evenings in the Bistro will never be forgotten. Special thanks go to those I worked probably closest with: Klaus (don't worry, I will still call you and ask you for help when I'm not sure how to do some biochemistry), Tom (for proofreading and entertainment), Dario and Josep (for sharing interesting projects with me in their respective fields of research), Ben (for introducing me to the lab in the beginning) and my students Steffen and Friedrich (for being independent researchers who didn't need a lot of help).

I am also very grateful for all the work and help from Christoph, Christian and Heinz. It will be very tough for me to work with other people in mechanical/electrical workshops somewhere else, because I will expect the same standard of work.

Last but not least, I would like to thank my family. Sara was always on my side during the last three years and she definitely supported me a lot. I also like to thank Vincent because let me get some sleep in most of the nights.

Curriculum vitae

Personal data

Name Phillip Kuhn
Birth December 22th 1982 in Hamburg, Germany
Citizenship German
e-mail phillip.kuhn@org.chem.ethz.ch

Current position

since 09/2009 PhD candidate in the laboratory of Prof. Petra S. Dittrich
Department of Chemistry and Applied Biosciences
ETH Zurich, Zurich, Switzerland

Education

10/2003–7/2009 Diploma in microsystems technology, Albert-Ludwigs-University Freiburg,
Germany
06/2002 Abitur, Hölderlin-Gymnasium, Lauffen a.N., Germany

Research experience

01–07/2009 Diploma thesis with of Prof. Dr. Zengerle (Lab for MEMS applications)
HSG-IMIT and IMTEK
Freiburg, Germany
05–07/2008 Internship in the Advanced Systems Group
Roche Diagnostics
Rotkreuz, Switzerland
11/2007–05/2008 Visit in the research groups of Dr. Joshua Edel and Dr. Tim Albrecht
Institute for Biomedical Engineering, Imperial College
London, UK
2004–2007 Part-time work in the group of Prof. Gerald Urban (Lab of sensors)
IMTEK, Albert-Ludwigs University Freiburg
Freiburg, Germany

Publications

1. Schmidt, F.I.*, **Kuhn, P.*** Mercer, J., Dittrich, P. S. Single virus fusion experiments reveal proton influx into vaccinia virions and hemifusion lag times. Submitted
2. Eyer, K., Stratz, S., **Kuhn, P.**, Kuster, S.K., Dittrich, P. S. Implementing enzyme linked immunosorbent assays on a microfluidic chip to quantify intracellular proteins and metabolites in single cells. *Analytical Chemistry*, online
3. Robinson, T., **Kuhn, P.**, Eyer, K., Dittrich, P. S. Microfluidic trapping of giant unilamellar vesicles to study membrane channel transport. Submitted
4. **Kuhn, P.**, Robinson, T., Eyer, K., Schmidt, F.I., Mercer, J., Dittrich, P. S. (2012) A facile protocol for the immobilization of vesicles, virus particles, bacteria and yeast cells. *Integrative Biology*, 4(12), 1550-1555
5. Eyer, K.*, **Kuhn, P.***, Hanke, C., Dittrich, P. S. (2012). A microchamber array for single cell isolation and analysis of intracellular biomolecules. *Lab on a Chip*, 12(4), 765-772.
6. Fornera, S., **Kuhn, P.**, Lombardi, D., Schluter, A., Dittrich, P., Walde, P. (2012). Sequential Immobilization of Enzymes in Microfluidic Channels for Cascade Reactions. *ChemPlusChem*, 77, 98-101.
7. Stadler, J., Schmid, T., Opilik, L., **Kuhn, P.**, Dittrich, P. S., Zenobi, R. (2011). Tip-enhanced Raman spectroscopic imaging of patterned thiol monolayers. *Beilstein Journal of Nanotechnology*, 2(1), 509-515.
8. **Kuhn, P.**, Eyer, K., Allner, S., Lombardi, D., Dittrich, P. S. (2011). A Microfluidic Vesicle Screening Platform: Monitoring the Lipid Membrane Permeability of Tetracyclines. *Analytical Chemistry*, 83(23), 8877-8885.
9. **Kuhn, P.**, Puigmarti-Luis, J., Imaz, I., Maspocho, D., Dittrich, P. S. (2011). Controlling the length and location of in situ formed nanowires by means of microfluidic tools. *Lab on a Chip*, 11(4), 753-757.
10. Ayub, M., Ivanov, A., Hong, J., **Kuhn, P.**, Instuli, E., Edel, J. B., Albrecht, T. (2010). Precise electrochemical fabrication of sub-20 nm solid-state nanopores for single-molecule biosensing. *Journal of physics: Condensed matter*, 22(45).
11. **Kuhn P.**, Dittrich P.S., Physical Chemistry 2009: Cells in the Microchip, *Nachrichten aus der Chemie*, 58 (3), 314-317 (2010).

* contributed equally